Isogeometric Analysis: Approximation, stability and error estimates for h-refined meshes

Y. Bazilevs*, L. Beirão da Veiga†, J.A. Cottrell*, T.J.R. Hughes*, G. Sangalli♮

*The University of Texas at Austin
Institute for Computational Engineering and Sciences
1 University Station C0200
Austin, TX 78712-0027, U.S.A.

†Dipartimento di Matematica "F.Enriques"
Università di Milano
Via Saldini 50, 20133 Milano, Italy

♮Dipartimento di Matematica "F. Casorati"
Università di Pavia
Via Ferrata 1, 27100 Pavia, Italy

Abstract

We begin the mathematical study of Isogeometric Analysis based on NURBS (non-uniform rational B-splines.) Isogeometric Analysis is a generalization of classical Finite Element Analysis (FEA) which possesses improved properties. For example, NURBS are capable of more precise geometric representation of complex objects and, in particular, can exactly represent many commonly engineered shapes, such as cylinders, spheres and tori. Isogeometric Analysis also simplifies mesh refinement because the geometry is fixed at the coarsest level of refinement and is unchanged throughout the refinement process. This eliminates geometrical errors and the necessity of linking the refinement procedure to a CAD representation of the geometry, as in classical FEA. In this work we study approximation and stability properties in the context of h-refinement. We develop approximation estimates based on a new Bramble-Hilbert lemma in so-called "bent" Sobolev spaces appropriate for NURBS approximations and we establish inverse estimates similar to ones for finite elements. We apply the theoretical results to several cases of interest including elasticity, isotropic incompressible elasticity and Stokes flow, and advection-diffusion, and perform numerical tests which corroborate the mathematical results. We also perform numerical calculations that involve hypotheses outside our theory and these suggest that there are many other interesting mathematical properties of Isogeometric Analysis yet to be proved.

Keywords: B-splines; NURBS; finite elements; approximation; error estimates; inverse estimates; stability; elliptic boundary value problems; elasticity; incompressibility; Stokes flow; advection-diffusion; h-refinement.

Contents

1 Introduction

Isogeometric Analysis based on NURBS (non-uniform rational B-splines) was introduced in [25, 13]. The objectives of Isogeometric Analysis are to generalize and improve upon Finite Element Analysis (FEA) in the following ways: 1) To provide more accurate modeling of complex geometries and to exactly represent common engineering shapes such as circles, cylinders, spheres, ellipsoids, etc.; 2) To fix exact geometries at the coarsest level of discretization and eliminate geometrical errors *ab initio*; 3) To vastly simplify mesh refinement of complex industrial geometries by eliminating the necessity to communicate with the CAD description of geometry; 4) To provide systematic refinement procedures, including classical h- and p-refinements analogues, and to develop a new "k-refinement" procedure that increases the smoothness almost everywhere of element functions beyond the standard C^0-continuity of finite elements and exhibits improved accuracy and efficiency compared with classical p-refinement. The references [25, 13] provide a comprehensive introduction to the main ideas and procedures, and computational verification of its veracity and potential. In a sense, Isogeometric Analysis is a superset of FEA. Standard h- and p-methods can be reproduced, but Isogeometric Analysis includes directions and possibilities not available in standard FEA. Some of these have been explored in [25, 13] and many others identified. At the same time, Isogeometric Analysis has many features in common with FEA, in particular, it invokes the isoparametric concept in which dependent variables and the geometry share the same basis functions. We note that, despite the geometry being fixed at the coarsest level of discretization, the mesh, and the corresponding basis, can be refined and order-elevated while maintaining the original exact geometry. The isoparametric concept possesses important properties relevant to the analysis of structures (see [25, 23]) and the Lagrangian description of continuous media for which the geometry and mesh need to be updated by the displacement field.

In this paper we initiate the mathematical study of Isogeometric Analysis with NURBS as a basis. We focus on h-refinement. In Section 2 we briefly introduce the B-spline polynomials and NURBS, focusing only on issues necessary for subsequent developments. For background, the interested reader may consult standard references, such as Rogers [33], Piegl and Tiller [32], and Farin [16]. The geometry of the mapping between a d-cube in the parametric space (d is the number of space dimensions) and its image in physical space requires the introduction of concepts and spaces not utilized in standard FEA. The reason for this is that when the continuity of the interpolant is sufficiently high, one cannot stay in a single element and invoke a standard Bramble-Hilbert estimate. A notion of "support extension" is necessitated, but produces the following complication: If we assume a function u is of class H^m in the support extension in the physical domain, its pull-back by the geometrical mapping is no longer an H^m-function in the support extension in the parametric domain. Rather, it is of class H^m on the supports of individual elements comprising the support extension in the parametric domain, but with reduced regularity across the internal element boundaries. This new non-standard space is a Hilbert space, and its approximation properties are key to our developments. It may be thought of as intermediate in continuity between standard Sobolev spaces and the "broken" Sobolev spaces utilized in the analysis of Discontinuous Galerkin Methods [3, 31]. For this reason we refer to these new spaces as "bent" Sobolev spaces.

In Section 3 we establish the approximation properties of NURBS within so-called "patches" that is, d-cubes in the parametric domain and their images in physical space under the geometric mapping. The union of patches in physical space comprises the geometry. We begin by establishing a new Bramble-Hilbert lemma that utilizes the concept of support extension developed in Section 2 and expresses how functions in bent Sobolev spaces, involving the regularity constraints of B-

spline spaces, are approximated by B-splines. This result enables us to overcome the difficulties previously mentioned, and we feel it may be of interest in its own right. NURBS are projective transformations of B-splines (Farin [16]) and their approximation properties are established with the aid of the new Bramble-Hilbert lemma. These results depend crucially on the specific structure of NURBS basis functions engendered by the projective transformation. The approximation results are generalized to include strongly imposed Dirichlet boundary data. In Section 4, we establish inverse inequalities for NURBS. These are required, for example, in the convergence analysis of Stabilized Methods. Our results in Sections 3 and 4 are developed for a single patch. However, they may be generalized in a straightforward way to geometries composed of multiple patches by standard techniques. (The assembly of arrays for multiple compatible patches is analogous to the assembly of individual elements in FEA.) Consequently, our subsequent applications to physical problems may be viewed as pertinent to the multiple patch case in addition, of course, to the single patch case.

In Section 5 we apply the results obtained in Sections 3 and 4 to obtain error estimates for problems of interest. We begin with linear elasticity theory. This is a standard symmetric, positive-definite, elliptic problem for which a minimum principle exists and optimal error estimates follow directly from the approximation results. Next we consider stabilized formulations of incompressible and almost incompressible isotropic elasticity. Here, in order to obtain stability and error estimates, we require both the new approximation result and inverse estimates for NURBS. As is usual for Stabilized Methods, these results pertain to a wide variety of displacement and pressure interpolatory combinations. We follow these developments with the more technically challenging case of inf-sup (i.e., Babuška-Brezzi, or BB) stable Galerkin methods. We focus on the case of C^0-continuous interpolations across element boundaries and, in particular, on the case of the displacement field one order higher than the pressure. (When we speak of "order" of a NURBS basis, we are thinking of the polynomial order of their B-spline progenitors.) This case is somewhat analogous to known BB-stable finite elements (see, e.g, Brezzi-Fortin [8]). However, geometric aspects of NURBS and Isogeometric Analysis provide new analytical challenges. In Isogeometric Analysis, the exact geometry is fixed patch-wise by the coarsest mesh and maintained, along with its parameterization, throughout h-refinement. This is a distinguishing feature of Isogeometric Analysis and one not shared by FEA. To facilitate analysis, the notion of a "vertex mesh" is introduced, which may be thought of as a coarsening of the "control net" or "control mesh" of NURBS theory. NURBS are not interpolatory and so the coefficients of basis functions (i.e, "control points," or "generalized coordinates") in the geometrical mapping do not lie on the geometry and thus do not have a direct physical interpretation. The control net is the piece-wise multilinear interpolant of the control points. In three dimensions it is a mesh of trilinear hexahedral elements. At the coarsest level of discretization it is often quite distinct from the exact geometry. However, as the mesh is h-refined, the control mesh converges to the physical mesh. (In a sense, use of low-order finite elements may be viewed as performing analysis on a particular control mesh rather than an actual geometry.) The theoretical analysis of mixed Galerkin methods for the incompressible problem presented herein utilizes the concept of the vertex mesh. We are able to prove inf-sup stability and establish quasi-optimal error estimates by employing the approximation results for NURBS. In our final application, we consider Stabilized Methods for scalar advection-diffusion. Utilizing standard arguments, along with the new approximation results and inverse estimates, we establish stability and error estimates analogous to those for finite elements.

In Section 6 we present several numerical calculations to test the mathematical results. In all cases that fall within the hypotheses of the mathematical results, the computed error estimates were found to be consistent with theory. We also tested some cases that do not satisfy our

hypotheses. For example, in the analysis of a linear elastic boundary-value problem for a plate with a circular hole, the geometrical mapping utilized is singular at one corner point of the domain. (This was a choice, not a necessity.) Consequently, the hypotheses of our theory are not satisfied. Nevertheless, optimal rates of convergence were still obtained. In other examples, concerning incompressible elastic analysis by the mixed Galerkin method, we tested displacement-pressure combinations that were smoother than C^0 across element boundaries. Recall, our mathematical results for the BB-stable theory are only applicable in the C^0 case. In particular, we tested cubic displacements combined with quadratic pressure, but both C^1-continuous across element interfaces. In the examples presented, and some others not shown, we found this combination to be stable and optimally convergent. We conjecture that for additional smoothness, beyond C^0, across element interfaces, elements of this type, with displacements one order higher than pressure, are mathematically stable and optimally convergent. We did not investigate pressures that are discontinuous across element boundaries, but, inspired by the spectral element work of Maday, Patera, and Ronquist [29], and others, we conjecture that for pressure two orders lower than displacements, error estimates suboptimal by one order can be proven. We did study Stabilized Methods and mixed Galerkin methods on the driven cavity Stokes flow problem. (The equations of Stokes flow are form-identical to the equations of isotropic incompressible elasticity.) The solution of the driven cavity possesses pressure singularities and represents a stringent stability test. All Stabilized Methods, and mixed Galerkin methods with displacement (i.e., velocity in this case) one order higher than pressure, proved stable. On the other hand, equal-order interpolations for mixed Galerkin methods were manifestly unstable. Finally, we numerically verified error estimates for Stabilized Methods for an advection-diffusion problem with a boundary layer. By excising the boundary layer domain, we demonstrated optimal "interior estimates" for unresolved cases.

2 Preliminaries

In what follows, let $d \geq 2$ be the dimension of the physical domain of interest. Throughout the analysis, we will make use of the classical Lebesgue spaces $L^p(\Omega)$, endowed with the norm $\|\cdot\|_{L^p(\Omega)}$, where $\Omega \subset \mathbb{R}^d$ is a generic open domain, and $1 \leq p \leq \infty$. We also will need the Sobolev spaces $W^{k,p}(\Omega)$, for k a positive integer and $1 \leq p \leq \infty$, endowed with the usual norm $\|\cdot\|_{W^{k,p}(\Omega)}$ and seminorm $|\cdot|_{W^{k,p}(\Omega)}$, see [1] for details. For the Hilbert spaces $W^{k,2}(\Omega)$ we will switch to the notation $H^k(\Omega)$, and, accordingly, $\|\cdot\|_{H^k(\Omega)}$ and $|\cdot|_{H^k(\Omega)}$ will be used for their norms and seminorms, respectively. We set $H^0(\Omega) := L^2(\Omega)$, and

$$\|\cdot\|_{H^0(\Omega)} \equiv |\cdot|_{H^0(\Omega)} := \|\cdot\|_{L^2(\Omega)}.$$

The spaces of continuous functions on Ω with k^{th}-order continuous derivatives will be denoted by $C^k(\Omega)$.

The rest of this section will be devoted to the introduction of the univariate and the multivariate (tensor product) B-spline basis functions and related spaces, the NURBS (*non-uniform rational B-spline*) basis functions, function space, and the NURBS geometrical map $\mathbf{F}$. This presentation is quite brief and notationally oriented[1]; a more complete introduction to NURBS and isogeometric analysis can be found in [25].

[1]Be aware that some of the notation and terminology contained here is different from that of [25]. Care should be exercised in comparing the two.

2.1 Univariate splines

For any α, $1 \le \alpha \le d$, given positive integers m_α and n_α, we introduce the (ordered) knot vector

$$\Xi_\alpha := \{0 = \xi_{1,\alpha}, \xi_{2,\alpha}, \ldots, \xi_{n_\alpha+m_\alpha,\alpha} = 1\}, \tag{1}$$

where we allow repetition of knots, that is, we only assume $\xi_{1,\alpha} \le \xi_{2,\alpha} \le \ldots \le \xi_{n_\alpha+m_\alpha,\alpha}$. We assume the Ξ_α's are *open* knot vectors, that is, the first m_α as well as the last m_α knots are repeated (see [25, §2.1]).

Through the iterative procedure detailed in [34, Theorem 4.15] or in [25, §2.2] one constructs m_α-order B-spline basis functions, which are piecewise polynomials of degree $p_\alpha := m_\alpha - 1$ on the subdivision (1)[2]. If a knot $\xi_{i,\alpha}$ is not repeated, then the B-spline basis functions have $p_\alpha - 1$ continuous derivatives at $\xi_{i,\alpha}$. In general, at a knot $\xi_{i,\alpha}$ repeated k times, with $1 \le k \le p_\alpha + 1$, the B-spline basis functions have $p_\alpha - k$ continuous derivatives, where $p_\alpha - k = -1$ is allowed and stands for a discontinuity. The B-splines basis functions are denoted by $B_{i,\alpha}$, for $i = 1, \ldots, n_\alpha$; each $B_{i,\alpha}$ is non-negative and supported in $(\xi_{i,\alpha}, \xi_{i+m_\alpha,\alpha})$. The interval $(\xi_{i,\alpha}, \xi_{i+1,\alpha})$ is referred to as a knot span. The B-spline basis functions constitute a partition of unity, namely,

$$\sum_{i=1}^{n_\alpha} B_{i,\alpha} = 1 \tag{2}$$

A typical example is presented in Figure 1. The space of *splines* is denoted by

$$\mathcal{S}_\alpha \equiv \mathcal{S}(\Xi_\alpha, p_\alpha) := \text{span}\{B_{i,\alpha}\}_{i=1,\ldots,n_\alpha}. \tag{3}$$

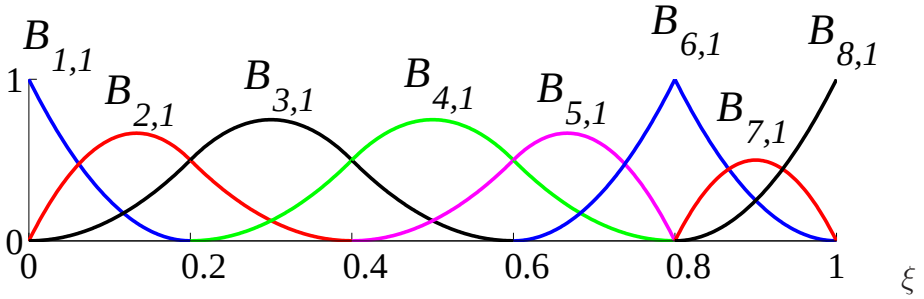

Figure 1: Example of a quadratic ($p_1 = 2$) B-spline basis in one dimension derived from the knot vector $\Xi = \{0, 0, 0, 0.2, 0.4, 0.6, 0.8, 0.8, 1, 1, 1\}$. Note that due to the open knot vector (i.e., the first and last knots are repeated $p_1 + 1$ times), the first and last basis functions are interpolatory (i.e., they take on the value 1 at the first and last knots). The continuity at interior knots ξ_i is $C^{p_1-m_i}$, where m_i is the number of repetitions of knot ξ_i. For example, only the interior knot 0.8 is repeated, and the continuity there is $C^{p_1-2} = C^0$. At the other knots the continuity is $C^{p_1-1} = C^1$, the maximal continuity of quadratic B-splines.

[2]We adhere to the terminology in which the "degree" of a quadratic, cubic, quartic, etc., polynomial is 2, 3, 4, etc., respectively, and the corresponding "order" is 3, 4, 5, etc., respectively. This is not the the usual terminology used in the finite element literature, but is frequently used in the splines literature. In [25, 13] we use the finite element terminology to emphasize the similarities with finite elements.

2.2 Multivariate tensor product splines

Assume that d knot vectors Ξ_α, with $1 \le \alpha \le d$, are given. Let $(0,1)^d \subset \mathbb{R}^d$ be an open *parametric domain*, referred to as a *patch*. Associated with the knot vectors Ξ_α there is a *mesh* $\mathcal{Q}$, that is, a partition of $(0,1)^d$ into d-dimensional open knot spans, or elements,

$$\mathcal{Q} \equiv \mathcal{Q}(\Xi_1, \ldots, \Xi_d) := \left\{ Q = \otimes_{\alpha=1}^{d} (\xi_{i_\alpha,\alpha}, \xi_{i_\alpha+1,\alpha}) |\, Q \neq \emptyset, m_\alpha \le i_\alpha \le n_\alpha - 1 \right\}. \tag{4}$$

We denote by h_Q the diameter of the element $Q \in \mathcal{Q}$.

The tensor product B-spline basis functions are defined as

$$B_{i_1 \ldots i_d} := B_{i_1,1} \otimes \ldots \otimes B_{i_d,d}; \tag{5}$$

The tensor-product spline space $\mathcal{S}$ is:

$$\mathcal{S} \equiv \mathcal{S}(\Xi_1, \ldots, \Xi_d; p_1, \ldots, p_d) := \otimes_{\alpha=1}^{d} \mathcal{S}(\Xi_\alpha, p_\alpha) = \text{span}\{B_{i_1 \ldots i_d}\}_{i_1=1,\ldots,i_d=1}^{n_1,\ldots,n_d}. \tag{6}$$

To a (non empty) element $Q = \otimes_{\alpha=1}^{d} (\xi_{i_\alpha,\alpha}, \xi_{i_\alpha+1,\alpha}) \in \mathcal{Q}$, we associate $\tilde{Q} \subset (0,1)^d$ defined as

$$\tilde{Q} := \otimes_{\alpha=1}^{d} (\xi_{i_\alpha - m_\alpha + 1,\alpha}, \xi_{i_\alpha + m_\alpha,\alpha}). \tag{7}$$

The set $\tilde{Q}$ will be referred to as the *support extension* of Q, since it is the union of the supports of basis functions whose support intersects Q. An illustration of support extensions is presented later in Figure 3.

The functions in $\mathcal{S}$ are piecewise polynomials of degree p_α in the α coordinate. The regularity of each d-dimensional basis function $B_{i_1 \ldots i_d}$ across the element boundaries depends on the regularity of the one-dimensional basis functions $B_{i_\alpha,\alpha}$, for $1 \le \alpha \le d$, at the corresponding knots. Given two adjacent elements Q_1 and Q_2 we denote by m_{Q_1,Q_2} the number of continuous derivatives across their common $(d-1)$-dimensional face $\partial Q_1 \cap \partial Q_2$; $m_{Q_1,Q_2} = -1$ is associated with a discontinuity. For the subsequent analysis, we introduce the following *"bent" Sobolev space* of order $m \in \mathbb{N}$

$$\mathcal{H}^m := \left\{ \begin{array}{l} v \in L^2((0,1)^d) \text{ such that} \\ \\ v_{|Q} \in H^m(Q), \forall Q \in \mathcal{Q}, \text{ and} \\ \\ \boldsymbol{\nabla}^k (v_{|Q_1}) = \boldsymbol{\nabla}^k (v_{|Q_2}) \text{ on } \partial Q_1 \cap \partial Q_2, \\ \forall k \in \mathbb{N} \text{ with } 0 \le k \le \min\{m_{Q_1,Q_2}, m-1\} \\ \forall Q_1, Q_2 \text{ with } \partial Q_1 \cap \partial Q_2 \neq \emptyset \end{array} \right\}; \tag{8}$$

where $\boldsymbol{\nabla}^k$ denotes the (k-linear) k^{th}-order partial derivative operator, while $\boldsymbol{\nabla}^0 v = v$. This is a well-defined Hilbert space, endowed with the seminorms

$$|v|_{\mathcal{H}^i}^2 := \sum_{Q \in \mathcal{Q}} |v|_{H^i(Q)}^2, \qquad 0 \le i \le m \tag{9}$$

and norm

$$\|v\|_{\mathcal{H}^m}^2 := \sum_{i=0}^{m} |v|_{\mathcal{H}^i}^2. \tag{10}$$

Indeed, the trace of $\boldsymbol{\nabla}^k v$ is well defined on $\partial Q_1 \cap \partial Q_2$, for $0 \leq k \leq \min\{m_{Q_1,Q_2}, m-1\}$ (see [1]). We also need the restriction of $\mathcal{H}^m$ to a given support extension $\tilde{Q}$, which is denoted by $\mathcal{H}^m(\tilde{Q}) := \{v_{|\tilde{Q}} | v \in \mathcal{H}^m\}$, and endowed with the seminorm and norm

$$|v|^2_{\mathcal{H}^i(\tilde{Q})} := \sum_{\substack{Q' \in \mathcal{Q} \\ Q' \cap \tilde{Q} \neq \emptyset}} |v|^2_{H^i(Q')} \qquad \text{and} \qquad \|v\|^2_{\mathcal{H}^m(\tilde{Q})} := \sum_{i=0}^{m} |v|^2_{\mathcal{H}^i(\tilde{Q})}. \tag{11}$$

The bent Sobolev spaces are intermediate in continuity between standard Sobolev spaces and so-called "broken" Sobolev spaces [31] utilized in the analysis of discontinuous Galerkin methods.

2.3 NURBS and the geometry of the physical domain

We associate to each of the tensor-product B-spline basis functions $B_{i_1 \ldots i_d}$ a strictly positive constant *weight* $w_{i_1 \ldots i_d}$ and a *control point* $\mathbf{C}_{i_1 \ldots i_d} \in \mathbb{R}^d$; we also introduce the *weighting function*

$$w := \sum_{i_1=1,\ldots,i_d=1}^{n_1,\ldots,n_d} w_{i_1 \ldots i_d} B_{i_1 \ldots i_d}, \tag{12}$$

which, due to the partition of unity and non-negativity properties of B-spline bases, is strictly greater than zero and is smooth on each element, along with its reciprocal. The NURBS basis functions on the patch $(0,1)^d$ are defined by a projective transformation (see Farin [16]):

$$R_{i_1 \ldots i_d} = \frac{w_{i_1 \ldots i_d} B_{i_1 \ldots i_d}}{w}, \tag{13}$$

and, accordingly, the NURBS space on the patch, denoted by $\mathcal{N}$, is

$$\mathcal{N} \equiv \mathcal{N}(\Xi_1, \ldots, \Xi_d; p_1, \ldots, p_d; w) := \text{span}\{R_{i_1 \ldots i_d}\}_{i_1=1,\ldots,i_d=1}^{n_1,\ldots,n_d}. \tag{14}$$

The NURBS geometrical map $\mathbf{F}$ is given by

$$\mathbf{F} = \sum_{i_1=1,\ldots,i_d=1}^{n_1,\ldots,n_d} \mathbf{C}_{i_1 \ldots i_d} R_{i_1 \ldots i_d}; \tag{15}$$

$\mathbf{F}$ is a parameterization of the physical domain Ω of interest (see [25]), that is,

$$\mathbf{F} : (0,1)^d \to \Omega.$$

We assume that $\mathbf{F}$ is invertible, with smooth inverse, on each element $Q \in \mathcal{Q}$.

Finally, each element $Q \in \mathcal{Q}$ is mapped into an element

$$K = \mathbf{F}(Q) := \{\mathbf{F}(\xi) | \xi \in Q\}, \tag{16}$$

and analogously $\tilde{Q}$, the support extension of Q, is mapped into

$$\tilde{K} = \mathbf{F}(\tilde{Q}). \tag{17}$$

We then introduce the mesh $\mathcal{K}$ in the physical domain Ω

$$\mathcal{K} := \{K = \mathbf{F}(Q) |\, Q \in \mathcal{Q}\}, \tag{18}$$

and the space $\mathcal{V}$ of NURBS on Ω (which is the *push-forward* of the space $\mathcal{N}$ of NURBS on the patch)

$$\mathcal{V} \equiv \mathcal{V}(p_1, \ldots, p_\alpha) := \text{span}\{R_{i_1 \ldots i_d} \circ \mathbf{F}^{-1}\}_{i_1=1,\ldots,i_d=1}^{n_1,\ldots,n_d} \tag{19}$$

NURBS are capable of representing all conic sections, such as circles and ellipses, and consequently cylinders, spheres, tori, ellipsoids, are also exactly representable. See [25, 13] and the standard texts [33, 32, 16] for examples.

3 Approximation properties of the NURBS space

We consider now a family of meshes $\{\mathcal{Q}_h\}_h$ on $(0,1)^d$, where each $\mathcal{Q}_h$ is defined as in Section 2.2, and h denotes the family index, representing the global mesh size

$$h = \max\{h_Q | Q \in \mathcal{Q}_h\}.$$

The family of meshes is assumed to be *shape regular*, that is, the ratio between the smallest edge of $Q \in \mathcal{Q}_h$ and its diameter h_Q is bounded, uniformly with respect to Q and h. This implies that the mesh is *locally quasi-uniform*—the ratio of the sizes of two neighboring elements is uniformly bounded. Following the construction in the previous section, associated with the family of meshes $\{\mathcal{Q}_h\}_h$ we introduce the families of meshes on the physical domain $\{\mathcal{K}_h\}_h$, and the spaces $\{\mathcal{S}_h\}_h$, $\{\mathcal{N}_h\}_h$, $\{\mathcal{V}_h\}_h$, and $\{\mathcal{H}_h^m\}_h$ endowed with their respective norms.

In practical applications, the geometry of the physical domain Ω is frequently described on a mesh of relatively few elements, while the computation of an approximate solution to the problem is performed on a refined mesh (fine enough to achieve desired accuracy). Therefore, we assume that there is a *coarsest mesh* $\mathcal{Q}_{h_0}$ in the family $\{\mathcal{Q}_h\}_h$, of which all the other meshes are a refinement, and that the description of the geometry is fixed at the level of $\mathcal{Q}_{h_0}$. This means that the weighting function w of (12) and the geometrical map $\mathbf{F}$ in (15) are assigned in $\mathcal{S}_{h_0}$ and $(\mathcal{N}_{h_0})^d$, respectively, and are the same for every h. When the mesh and the spaces are refined (see [25, §2.4] for details on the refinement procedures), the weights $w_{i_1 \ldots i_d}$ are selected so that w stays fixed (see [25, equation (6)]); in a similar way, the control points $\mathbf{C}_{i_1 \ldots i_d}$ are adjusted such that $\mathbf{F}$ remains unchanged. Thus the geometry *and* its parameterization are held fixed in the refinement process. See Figure 2 for an illustration of this idea.

In what follows, we will denote by C a positive, *dimensionless* constant, possibly different at each occurrence, which depends only on the space dimension d, on the polynomial degrees $p_\alpha,\ \alpha = 1, 2, ..., d$, and on the shape regularity of the mesh family $\{\mathcal{Q}_h\}_h$. Observe that the p_α are considered fixed, since we only address h-refinement in this paper (see [25, §2.4], [13]). We will denote by C_{shape} another positive, dimensionless constant, possibly different at each occurrence, which may also depend on the geometry of Ω but still *not* on h. Specifically, C_{shape} depends on the *shape* of Ω, but not on its *size*; therefore C_{shape} is by assumption homogeneous of order 0 with respect to w and $\boldsymbol{\nabla}\mathbf{F}$, where $\boldsymbol{\nabla}\mathbf{F}$ is the matrix of partial derivatives of the coordinate components of $\mathbf{F}$, that is, C_{shape} is invariant if w and $\boldsymbol{\nabla}\mathbf{F}$ are scaled by a multiplicative factor. Actually, C_{shape} only depends on the dimensionless functions $w/\|w\|_{L^\infty(\Omega)}$ and $\boldsymbol{\nabla}\mathbf{F}/\|\boldsymbol{\nabla}\mathbf{F}\|_{L^\infty(\Omega)}$. Furthermore, if C_{shape} appears in a *local* estimate, then it depends only on the local values of w and $\boldsymbol{\nabla}\mathbf{F}$.

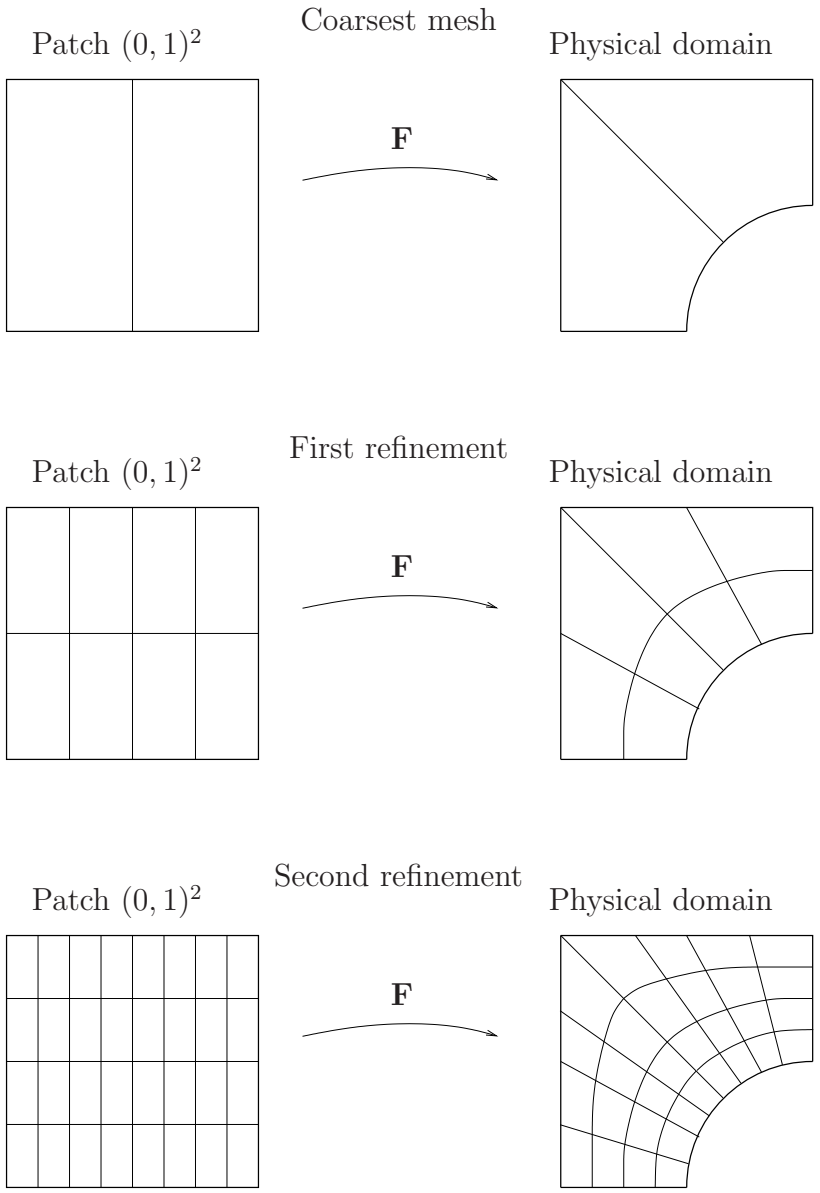

Figure 2: h-refinement with NURBS. In this illustration a NURBS patch is mapped onto a quarter of a square domain with a circular hole in physical space. The minimum degree NURBS required to exactly represent the geometry is quadratic. The open knot vectors are $\Xi_1 = \{0, 0, 0, 0.5, 1, 1, 1\}$ and $\Xi_2 = \{0, 0, 0, 1, 1, 1\}$, as illustrated. (For further details of the construction, see [25].) The exact geometry is represented at the coarsest level of discretization, and it and its parameterization are unchanged during refinement. In particular, the geometrical map $\mathbf{F}$ and the weighting function w are unchanged during refinement. In the figure, the refinement is performed uniformly, but this is not necessary.

3.1 Approximation with splines on a patch in the parametric domain

Our first lemma states the local approximation properties of the spline space $\mathcal{S}_h$. It is an extension of the classical result (see Bramble and Hilbert [7]). Our estimate involves bent Sobolev seminorms and spaces (8)–(9), which will be needed, in the following sections, when dealing with NURBS on the parametric and physical domains. Let p be defined as

$$p := \min_{1\leq\alpha\leq d}\{p_\alpha\}. \tag{20}$$

Lemma 3.1. *Let k and l be integer indices with $0 \leq k \leq l \leq p+1$. Given $Q \in \mathcal{Q}_h$, $\tilde{Q}$ as in (7), $v \in \mathcal{H}^l_h$, there exists an $s \in \mathcal{S}_h$ such that*

$$|v-s|_{\mathcal{H}^k_h(\tilde{Q})} \leq C h_Q^{l-k} |v|_{\mathcal{H}^l_h(\tilde{Q})}. \tag{21}$$

Proof. Consider an element $Q \in \mathcal{Q}_h$ and its corresponding support extension $\tilde{Q}$. The number of elements Q' forming the support extension $\tilde{Q}$ and the degree of regularity of the functions in $\mathcal{S}_h$ or $\mathcal{H}^l_h$ across the internal element boundaries in $\tilde{Q}$ may vary, according to the multiplicities of knots in the underlying knot vectors (see Section 2.2). Nevertheless, it is clear that there is only a finite number of *patterns* for all the possible support extensions $\tilde{Q}$ of any mesh of the family $\{\mathcal{Q}_h\}_h$, and the maximum number of them depends only on p_α and on the space dimension d. It is not restrictive, therefore, to prove (21) for a particular $\tilde{Q}$, with the constant C appearing in (21) independent of the size of elements forming $\tilde{Q}$.

For the proof, we associate to $\tilde{Q}$ a reference support extension $\hat{Q}$ through a piecewise affine map $\mathbf{G} : \hat{Q} \to \tilde{Q}$ such that each element $Q' \in \tilde{Q}$ is the image of a hypercube $\mathbf{G}^{-1}(Q')$ which has unit edge length, where $\mathbf{G}^{-1}(Q') := \{\mathbf{G}^{-1}(\xi) | \xi \in Q'\}$ (see Figure 3).

Let $\hat{\mathcal{H}}^m_{\mathbf{c}}$ be the pullback of $\mathcal{H}^m_h(\tilde{Q})$ through $\mathbf{G}$

$$\hat{\mathcal{H}}^m_{\mathbf{c}} := \left\{ \hat{v} | \hat{v} = v \circ \mathbf{G},\, v \in \mathcal{H}^m_h(\tilde{Q}) \right\}, \tag{22}$$

where $\mathbf{c}$ is a vector of positive real numbers with the following meaning: assume that we have an ordering of the internal boundaries e of the elements in $\tilde{Q}$ (e consists of $d-1$-dimensional hypercubes, that is, line segments for $d=2$ or rectangles for $d=3$) and a corresponding ordering on the internal boundaries $\hat{e}$ in $\hat{Q}$. Also, define on each e and $\hat{e}$ a unique normal direction $\mathbf{n}_e$ and $\mathbf{n}_{\hat{e}}$. If e is shared between the two adjacent elements Q_1 and Q_2 belonging to $\tilde{Q}$, then, by construction, a function $v \in \mathcal{H}^m_h(\tilde{Q})$ has *matching* normal derivatives on e, up to the order $\min\{m_{Q_1,Q_2}, m-1\}$ (see definition (8))

$$\frac{\partial^i}{\partial \mathbf{n}_e^i}\left(v_{|Q_1}\right) = \frac{\partial^i}{\partial \mathbf{n}_e^i}\left(v_{|Q_2}\right) \qquad \text{on } e = \partial Q_1 \cap \partial Q_2, \quad 0 \leq i \leq \min\{m_{Q_1,Q_2}, m-1\}. \tag{23}$$

When $i=0$, the equality above expresses continuity of v across $\partial Q_1 \cap \partial Q_2$. For the pullback $\hat{v} = v \circ \mathbf{G}$, condition (23) is equivalent to

$$\frac{\partial^i}{\partial \mathbf{n}_{\hat{e}}^i}\left(\hat{v}_{|\mathbf{G}^{-1}(Q_1)}\right) = (c_e)^i \frac{\partial^i}{\partial \mathbf{n}_{\hat{e}}^i}\left(\hat{v}_{|\mathbf{G}^{-1}(Q_2)}\right) \qquad \text{on } \hat{e} = \mathbf{G}^{-1}(e), \quad 0 \leq i \leq \min\{m_{Q_1,Q_2}, m-1\}, \tag{24}$$

where the constant c_e equals the ratio of the lengths of the two elements Q_1 and Q_2 in the direction of $\mathbf{n}_e$. The vector $\mathbf{c}$ collects all of these coefficients. Since all of the meshes are (uniformly) shape

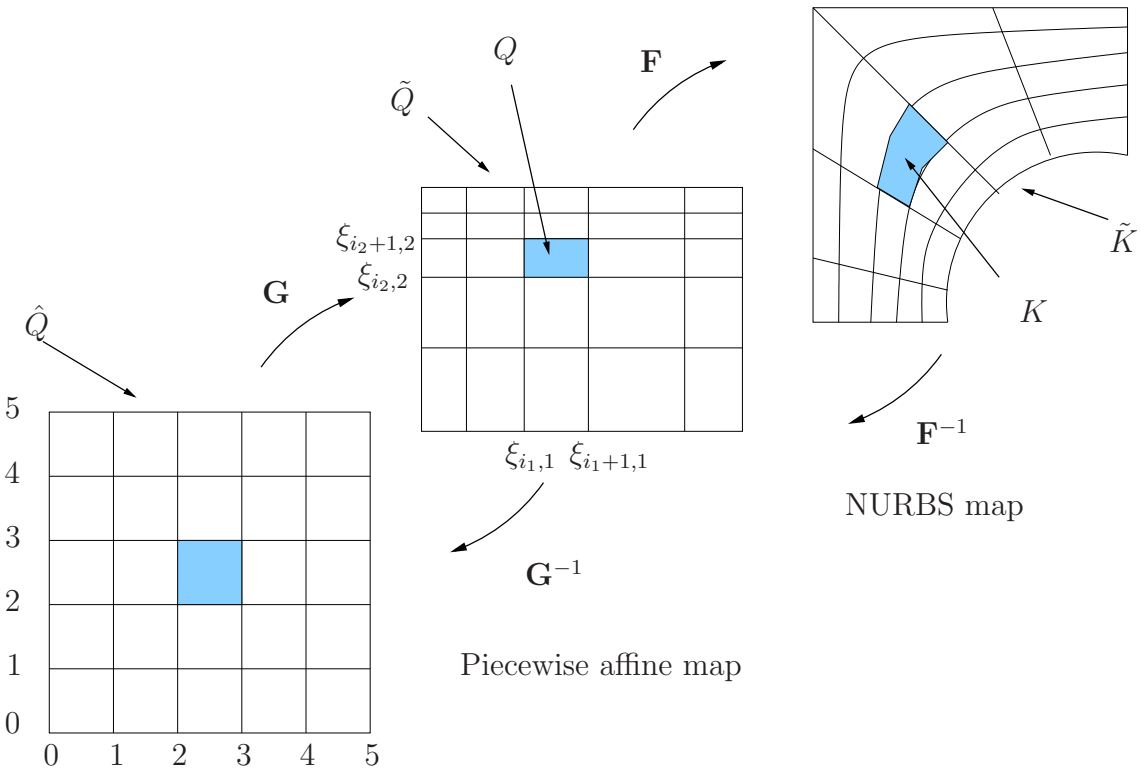

Figure 3: Depiction of the support extensions $\tilde{K}$, $\tilde{Q}$, and corresponding $\hat{Q}$. For non-repeated knots, the case illustrated would conform to quadratic B-splines or NURBS (i.e., $p_\alpha = 2$). Quadratic splines and NURBS have support over three knot spans in each direction. That is, each basis function is supported by a 3×3 mesh of elements. The support extensions are confined to individual patches in the multipatch case, assuming the patches are adjoined in C^0-continuous fashion.

regular and locally quasi-uniform, the coefficients c_e belong to a compact set bounded away from 0. Together with the space $\hat{\mathcal{H}}^m_{\mathbf{c}}$, we introduce the usual broken Sobolev space of order m

$$\hat{\mathcal{H}}^m := \left\{ \hat{v} \mid \hat{v} = v \circ \mathbf{G},\, v_{|Q'} \in H^m(Q'), \forall Q' \text{ with } Q' \cap \tilde{Q} \neq \emptyset \right\}, \tag{25}$$

for which no conditions on the derivatives on the internal boundaries are assumed. We have $\hat{\mathcal{H}}^m_{\mathbf{c}} \subset \hat{\mathcal{H}}^m$, for any $\mathbf{c}$. We define on $\hat{\mathcal{H}}^m$ the seminorms and norm

$$|\hat{v}|^2_{\hat{\mathcal{H}}^i} := \sum_{\substack{Q' \in \mathcal{Q}_h \\ Q' \cap \tilde{Q} \neq \emptyset}} |\hat{v}|^2_{H^i(\mathbf{G}^{-1}(Q'))}, \quad 0 \leq i \leq m, \qquad \text{and} \qquad \|\hat{v}\|^2_{\hat{\mathcal{H}}^m} := \sum_{i=0}^{m} |\hat{v}|^2_{\hat{\mathcal{H}}^i}, \tag{26}$$

and we recall that

$$\|\hat{v}\|^2_{\hat{\mathcal{H}}^m} \leq C \left(\|\hat{v}\|^2_{L^2(\hat{Q})} + |\hat{v}|^2_{\hat{\mathcal{H}}^m} \right), \qquad \forall \hat{v} \in \hat{\mathcal{H}}^m. \tag{27}$$

Let $\hat{\mathcal{P}}$ represent the set of piecewise polynomial functions of degree at most $l-1$ on $\hat{Q}$, that is, the set of functions that are polynomials of the prescribed degree on each element forming $\hat{Q}$, and define $\hat{\mathcal{P}}_{\mathbf{c}} := \hat{\mathcal{P}} \cap \hat{\mathcal{H}}^l_{\mathbf{c}}$. Observe that

$$\hat{\mathcal{P}}_{\mathbf{c}} \subset \{ \hat{v} \mid \hat{v} = v \circ \mathbf{G},\, v \in \mathcal{S}_h \}. \tag{28}$$

By (27), (28), usual scaling arguments, and since $k \leq l$, in order to prove (21) it is then sufficient to find, given $\hat{v} \in \hat{\mathcal{H}}^l_{\mathbf{c}}$, a suitable $\hat{s} \in \hat{\mathcal{P}}_{\mathbf{c}}$ such that

$$\|\hat{v} - \hat{s}\|_{L^2(\hat{Q})} + |\hat{v} - \hat{s}|_{\hat{\mathcal{H}}^l} \leq C|\hat{v}|_{\hat{\mathcal{H}}^l}, \tag{29}$$

with C independent of $\hat{v}$ and $\mathbf{c}$. Let $\hat{\Pi}_{\mathbf{c}} : \hat{\mathcal{H}}^l \to \hat{\mathcal{P}}_{\mathbf{c}}$ be the $L^2(\hat{Q})$-projection onto the space $\hat{\mathcal{P}}_{\mathbf{c}}$. We prove that (29) holds true for $\hat{s} := \hat{\Pi}_{\mathbf{c}}\hat{v}$, that is we are going to show that

$$\|\hat{v} - \hat{\Pi}_{\mathbf{c}}\hat{v}\|_{L^2(\hat{Q})} + |\hat{v} - \hat{\Pi}_{\mathbf{c}}\hat{v}|_{\hat{\mathcal{H}}^l} \leq C|\hat{v}|_{\hat{\mathcal{H}}^l}, \qquad \forall \hat{v} \in \hat{\mathcal{H}}^l_{\mathbf{c}}, \tag{30}$$

uniformly with respect to $\mathbf{c}$.

We prove (30) by contradiction. Because

$$|\hat{\Pi}_{\mathbf{c}}\hat{v}|_{\hat{\mathcal{H}}^l} = 0, \qquad \forall \hat{v} \in \hat{\mathcal{H}}^l, \, \forall \mathbf{c}, \tag{31}$$

assuming that (30) is false implies the existence of a sequence $\{\mathbf{c}_j\}_{j\in\mathbb{N}}$ of vectors and a sequence $\{\hat{v}_j\}_{j\in\mathbb{N}}$ of functions in $\hat{\mathcal{H}}^l_{\mathbf{c}_j}$ such that

$$\|\hat{v}_j - \hat{\Pi}_{\mathbf{c}_j}\hat{v}_j\|_{L^2(\hat{Q})} = 1, \tag{32}$$

and

$$|\hat{v}_j|_{\hat{\mathcal{H}}^l} = 1/j. \tag{33}$$

As discussed above, the components of $\mathbf{c}_j$ are in a compact set; therefore it is not restrictive to assume that the sequence $\{\mathbf{c}_j\}_{j\in\mathbb{N}}$ converges towards a limit $\mathbf{c}_\infty$ (i.e., the components of $\mathbf{c}_j$ converge to the corresponding components of $\mathbf{c}_\infty$).

Recall that the space $\hat{\mathcal{H}}^l$ is compactly embedded into $L^2(\hat{Q})$. Therefore, defining $\hat{\eta}_j := \hat{v}_j - \hat{\Pi}_{\mathbf{c}_j}\hat{v}_j$, since $\|\hat{\eta}_j\|_{\hat{\mathcal{H}}^l} \leq C\|\hat{v}_j - \hat{\Pi}_{\mathbf{c}_j}\hat{v}_j\|_{L^2(\hat{Q})} + C|\hat{v}_j|_{\hat{\mathcal{H}}^l(\hat{Q})}$ is uniformly bounded, it is not restrictive to assume that the functions $\hat{\eta}_j$ converge towards a limit $\hat{\eta}_\infty$ in $L^2(\hat{Q})$. By (31) and (33), $\{\hat{\eta}_j\}_{j\in\mathbb{N}}$ is also a Cauchy sequence in $\hat{\mathcal{H}}^l$, hence $\hat{\eta}_j \to \hat{\eta}_\infty$ in $\hat{\mathcal{H}}^l$. Therefore

$$|\hat{\eta}_\infty|_{\hat{\mathcal{H}}^l} = \lim_{j\to\infty} |\hat{\eta}_j|_{\hat{\mathcal{H}}^l} = 0,$$

that is,

$$\hat{\eta}_\infty \in \hat{\mathcal{P}}. \tag{34}$$

In fact, since $\hat{\eta}_j \in \hat{\mathcal{H}}^l_{\mathbf{c}_j}$, it is easy to see that the conditions of (24) pass to the limit, yielding $\hat{\eta}_\infty \in \hat{\mathcal{H}}^l_{\mathbf{c}_\infty}$. This means that $\hat{\eta}_\infty \in \hat{\mathcal{P}}_{\mathbf{c}_\infty}$, and

$$\hat{\eta}_\infty = \hat{\Pi}_{\mathbf{c}_\infty}\hat{\eta}_\infty. \tag{35}$$

We have

$$\begin{aligned}\|\hat{\Pi}_{\mathbf{c}_\infty}\hat{\eta}_\infty\|_{L^2(\hat{Q})} &\leq \left\|\hat{\Pi}_{\mathbf{c}_\infty}\hat{\eta}_\infty - \hat{\Pi}_{\mathbf{c}_j}\hat{\eta}_\infty\right\|_{L^2(\hat{Q})} + \left\|\hat{\Pi}_{\mathbf{c}_j}\hat{\eta}_\infty - \hat{\Pi}_{\mathbf{c}_j}\hat{\eta}_j\right\|_{L^2(\hat{Q})} + \|\hat{\Pi}_{\mathbf{c}_j}\hat{\eta}_j\|_{L^2(\hat{Q})} \\ &= I + II + III.\end{aligned}$$

It is easy to see that $I \to 0$ when $j \to \infty$; indeed, we can have bases for $\mathcal{P}_{\mathbf{c}_j}$ that converge to a basis for $\mathcal{P}_{\mathbf{c}_\infty}$. Moreover, since $\hat{\Pi}_{\mathbf{c}_j}$ is uniformly bounded, $II = \|\hat{\Pi}_{\mathbf{c}_j}(\hat{\eta}_\infty - \hat{\eta}_j)\|_{L^2(\hat{Q})} \leq \|\hat{\eta}_\infty - \hat{\eta}_j\|_{L^2(\hat{Q})} \to 0$. Clearly, $III = 0$. Thus, $\hat{\Pi}_{\mathbf{c}_\infty}\hat{\eta}_\infty = 0$, and so by (35), we finally get

$$\hat{\eta}_\infty = 0, \tag{36}$$

which is in contradiction with (32), which implies

$$\|\hat{\eta}_\infty\|_{L^2(\hat{Q})} = \lim_{j\to\infty} \|\hat{\eta}_j\|_{L^2(\hat{Q})} = 1.$$

This proves (30). □

In [34, Chapter 12] a projector on the spline space $\mathcal{S}_h$ is introduced. The projector, here denoted by $\Pi_{\mathcal{S}_h}$, with the present notation is written as

$$\Pi_{\mathcal{S}_h} v := \sum_{i_1=1,\dots,i_d=1}^{n_1,\dots,n_d} (\lambda_{i_1\dots i_d} v)\, B_{i_1\dots i_d}, \qquad \forall v \in L^2((0,1)^d) \tag{37}$$

where the $\lambda_{i_1\dots i_d}$ are *dual* basis functionals, that is,

$$\begin{aligned} &\lambda_{j_1\dots j_d} B_{i_1\dots i_d} = 1 \quad \text{if } j_\alpha = i_\alpha,\ \forall 1 \le \alpha \le d, \\ &\lambda_{j_1\dots j_d} B_{i_1\dots i_d} = 0 \quad \text{otherwise.} \end{aligned}$$

From [34, Chapter 12], the functionals $\lambda_{i_1\dots i_d}$ can be represented by functions with local support. This induces local stability properties on $\Pi_{\mathcal{S}_h}$. We summarize the previous properties in the following result, proved in [34, Theorem 12.6]:

Lemma 3.2. *We have*

$$\Pi_{\mathcal{S}_h} s = s, \qquad \forall s \in \mathcal{S}_h \ \textit{(spline preserving)}, \tag{38}$$

$$\|\Pi_{\mathcal{S}_h} v\|_{L^2(Q)} \le C \|v\|_{L^2(\tilde{Q})}, \qquad \forall v \in L^2((0,1)^d), \forall Q \in \mathcal{Q}_h \ \textit{(stability)}. \tag{39}$$

Lemma 3.3. *Let $\Pi_{\mathcal{S}_h} : L^2((0,1)^d) \to \mathcal{S}_h$ satisfy (38) and (39), and $0 \le k \le l \le p+1$; then for all $Q \in \mathcal{Q}_h$*

$$|v - \Pi_{\mathcal{S}_h} v|_{H^k(Q)} \le C h_Q^{l-k} |v|_{\mathcal{H}^l(\tilde{Q})}, \qquad \forall v \in \mathcal{H}_h^l(\tilde{Q}) \cap L^2((0,1)^d). \tag{40}$$

Proof. Let s be as in Lemma 3.1; then, using (38),

$$\begin{aligned} |v - \Pi_{\mathcal{S}_h} v|_{H^k(Q)} &= |v - s + \Pi_{\mathcal{S}_h}(v - s)|_{H^k(Q)} \\ &\le |v - s|_{H^k(Q)} + |\Pi_{\mathcal{S}_h}(v - s)|_{H^k(Q)} \\ &= I + II. \end{aligned}$$

Using (21) we get straightforwardly

$$I \le C h_Q^{l-k} |v|_{\mathcal{H}_h^l(\tilde{Q})}.$$

The usual inverse inequality for polynomials yields

$$|\Pi_{\mathcal{S}_h}(v - s)|_{H^k(Q)} \le C h_Q^{-k} \|\Pi_{\mathcal{S}_h}(v - s)\|_{L^2(Q)},$$

whence, making use of (39) and (21), we get

$$II \le C h_Q^{-k} \|v - s\|_{L^2(\tilde{Q})} \le C h_Q^{l-k} |v|_{\mathcal{H}_h^l(\tilde{Q})}.$$

□

3.2 Approximation with NURBS on a patch in the parametric domain

In this section we derive the approximation properties of the NURBS space on the patch $(0,1)^d$. We define the projector $\Pi_{\mathcal{N}_h} : L^2((0,1)^d) \to \mathcal{N}_h$ as

$$\Pi_{\mathcal{N}_h} v := \frac{\Pi_{\mathcal{S}_h}(wv)}{w}, \qquad \forall v \in L^2((0,1)^d), \tag{41}$$

where w is defined by (12).

Lemma 3.4. *Let k and l be integer indices with $0 \le k \le l \le p+1$; we have*

$$|v - \Pi_{\mathcal{N}_h} v|_{H^k(Q)} \le C_{shape} h_Q^{l-k} \|v\|_{\mathcal{H}_h^l(\tilde{Q})}, \qquad \forall v \in \mathcal{H}_h^l, \forall Q \in \mathcal{Q}_h \tag{42}$$

Proof. Recalling that $w \in \mathcal{S}_{h_0} \subset \mathcal{S}_h$, it follows easily that, if $v \in \mathcal{H}^l(\tilde{Q})$, then also $wv \in \mathcal{H}^l(\tilde{Q})$. Therefore, making use of the definition (41), the Hölder inequality, and (40), we have

$$\begin{aligned}
|v - \Pi_{\mathcal{N}_h} v|_{H^k(Q)} &= \left| \frac{1}{w} \left(wv - \Pi_{\mathcal{S}_h} wv \right) \right|_{H^k(Q)} \\
&\le C \sum_{i=0}^{k} \left| \frac{1}{w} \right|_{W^{i,\infty}(Q)} |wv - \Pi_{\mathcal{S}_h} wv|_{H^{k-i}(Q)} \\
&\le C h_Q^{l-k} \sum_{i=0}^{k} \left| \frac{1}{w} \right|_{W^{i,\infty}(Q)} |wv|_{\mathcal{H}_h^{l-i}(\tilde{Q})} \\
&\le C h_Q^{l-k} \sum_{i=0}^{k} \left| \frac{1}{w} \right|_{W^{i,\infty}(Q)} \sum_{j=0}^{l-i} \sum_{\substack{Q' \in \mathcal{Q}_h \\ Q' \cap \tilde{Q} \neq \emptyset}} |w|_{W^{j,\infty}(Q')} \, |v|_{H^{l-(i+j)}(Q')} \, .
\end{aligned}$$

Since $0 \le i + j \le l$ in the last summations, we get (42), with a constant C_{shape} that depends on $|1/w|_{W^{i,\infty}(Q)} |w|_{W^{j,\infty}(Q')}$, that is, only depends on the weight function w and its reciprocal $1/w$ on $\tilde{Q}$, and is uniformly bounded with respect to the mesh size. □

3.3 Approximation with NURBS in the physical domain

The following lemma gives estimates for the change of variable from the patch to the physical domain.

Lemma 3.5. *Let m be a non-negative integer, $Q \in \mathcal{Q}_h$ and $K = \mathbf{F}(Q)$. For all functions $v \in H^m(K)$, it holds that*

$$|v \circ \mathbf{F}|_{H^m(Q)} \le C_{shape} \, \| \det \boldsymbol{\nabla} \mathbf{F}^{-1} \|_{L^\infty(K)}^{1/2} \sum_{j=0}^{m} \| \boldsymbol{\nabla} \mathbf{F} \|_{L^\infty(Q)}^{j} |v|_{H^j(K)} \tag{43}$$

$$|v|_{H^m(K)} \le C_{shape} \, \| \det \boldsymbol{\nabla} \mathbf{F} \|_{L^\infty(Q)}^{1/2} \, \| \boldsymbol{\nabla} \mathbf{F} \|_{L^\infty(Q)}^{-m} \sum_{j=0}^{m} |v \circ \mathbf{F}|_{H^j(Q)} \tag{44}$$

Proof. We will address the case $m \ge 1$, the case $m = 0$ being trivial. We start by introducing the function

$$\check{\mathbf{F}} = \frac{\mathbf{F}}{\| \boldsymbol{\nabla} \mathbf{F} \|_{L^\infty(Q)}} \; : \; Q \to \check{K} \tag{45}$$

A direct derivation gives

$$\boldsymbol{\nabla}^k \mathbf{F} = \|\boldsymbol{\nabla}\mathbf{F}\|_{L^\infty(Q)} \boldsymbol{\nabla}^k \check{\mathbf{F}} \tag{46}$$

where here and in what follows k indicates an integer with $1 \leq k \leq m$. From (46) we get

$$\|\boldsymbol{\nabla}^k \mathbf{F}\|_{L^\infty(Q)} \leq \|\boldsymbol{\nabla}\mathbf{F}\|_{L^\infty(Q)} \|\boldsymbol{\nabla}^k \check{\mathbf{F}}\|_{L^\infty(Q)}. \tag{47}$$

Let now ξ be any point in Q and $x = \mathbf{F}(\xi)$. We then have by definition

$$x = \|\boldsymbol{\nabla}\mathbf{F}\|_{L^\infty(Q)} \check{\mathbf{F}}(\xi), \tag{48}$$

$$\xi = \check{\mathbf{F}}^{-1}\left(\frac{x}{\|\boldsymbol{\nabla}\mathbf{F}\|_{L^\infty(Q)}}\right). \tag{49}$$

As a consequence we have

$$\mathbf{F}^{-1}(x) = \xi = \check{\mathbf{F}}^{-1}\left(\frac{x}{\|\boldsymbol{\nabla}\mathbf{F}\|_{L^\infty(Q)}}\right). \tag{50}$$

which, by derivation, gives

$$\boldsymbol{\nabla}^k \mathbf{F}^{-1}(x) = \boldsymbol{\nabla}^k \check{\mathbf{F}}^{-1}\left(\frac{x}{\|\boldsymbol{\nabla}\mathbf{F}\|_{L^\infty(Q)}}\right) \|\boldsymbol{\nabla}\mathbf{F}\|^{-k}_{L^\infty(Q)}. \tag{51}$$

Taking the L^∞ norm, identity (51) gives

$$\|\boldsymbol{\nabla}^k \mathbf{F}^{-1}\|_{L^\infty(K)} \leq \|\boldsymbol{\nabla}^k \check{\mathbf{F}}^{-1}\|_{L^\infty(\check{K})} \|\boldsymbol{\nabla}\mathbf{F}\|^{-k}_{L^\infty(Q)}. \tag{52}$$

By Lemma 3 in [11], there exists a constant C depending only on m such that, for all $\xi \in Q$,

$$\|\boldsymbol{\nabla}^m (v \circ \mathbf{F})(\xi)\| \leq C \sum_{j=1}^{m} \|\boldsymbol{\nabla}^j v(x)\| \sum_{\mathbf{i} \in I(j,m)} \|\boldsymbol{\nabla}\mathbf{F}(\xi)\|^{i_1} \|\boldsymbol{\nabla}^2 \mathbf{F}(\xi)\|^{i_2} ... \|\boldsymbol{\nabla}^m \mathbf{F}(\xi)\|^{i_m}, \tag{53}$$

where

$$I(j,m) = \{\mathbf{i} = (i_1, i_2, ..., i_m) \in \mathbb{N}^m \ : \ i_1 + i_2 + ... + i_m = j, \ i_1 + 2i_2 + ... + m i_m = m\}. \tag{54}$$

A change of variables, bound (53) and the Hölder inequality give

$$|v \circ \mathbf{F}|_{H^m(Q)} \leq C \| \det \boldsymbol{\nabla}\mathbf{F}^{-1}\|^{1/2}_{L^\infty(K)} \sum_{j=1}^{m} |v|_{H^j(K)} \sum_{\mathbf{i} \in I(j,m)} \|\boldsymbol{\nabla}\mathbf{F}\|^{i_1}_{L^\infty(Q)} \|\boldsymbol{\nabla}^2 \mathbf{F}\|^{i_2}_{L^\infty(Q)} ... \|\boldsymbol{\nabla}^m \mathbf{F}\|^{i_m}_{L^\infty(Q)}. \tag{55}$$

Using (47) and recalling (54), the above bound easily gives

$$\begin{aligned} |v \circ \mathbf{F}|_{H^m(Q)} &\leq C \| \det \boldsymbol{\nabla}\mathbf{F}^{-1}\|^{1/2}_{L^\infty(K)} \sum_{j=1}^{m} |v|_{H^j(K)} \|\boldsymbol{\nabla}\mathbf{F}\|^{j}_{L^\infty(Q)} \\ &\quad \cdot \sum_{\mathbf{i} \in I(j,m)} \|\boldsymbol{\nabla}\check{\mathbf{F}}\|^{i_1}_{L^\infty(Q)} \|\boldsymbol{\nabla}^2 \check{\mathbf{F}}\|^{i_2}_{L^\infty(Q)} ... \|\boldsymbol{\nabla}^m \check{\mathbf{F}}\|^{i_m}_{L^\infty(Q)} \\ &\leq C'(m, \|\boldsymbol{\nabla}\check{\mathbf{F}}\|_{W^{m,\infty}(Q)}) \, \| \det \boldsymbol{\nabla}\mathbf{F}^{-1}\|^{1/2}_{L^\infty(K)} \sum_{j=1}^{m} \|\boldsymbol{\nabla}\mathbf{F}\|^{j}_{L^\infty(Q)} |v|_{H^j(K)}. \end{aligned} \tag{56}$$

Applying Lemma 3 of [11] to the inverse function $\mathbf{F}^{-1}$, similar arguments give

$$|v|_{H^m(K)} \leq$$
$$C\|\det \boldsymbol{\nabla}\mathbf{F}\|^{1/2}_{L^\infty(Q)} \sum_{j=1}^{m} |v\circ\mathbf{F}|_{H^j(Q)} \sum_{\mathbf{i}\in I(j,m)} \|\boldsymbol{\nabla}\mathbf{F}^{-1}\|^{i_1}_{L^\infty(K)} \|\boldsymbol{\nabla}^2\mathbf{F}^{-1}\|^{i_2}_{L^\infty(K)} \cdots \|\boldsymbol{\nabla}^m\mathbf{F}^{-1}\|^{i_m}_{L^\infty(K)}.$$

Applying (52) to bound (57), following the same steps as already performed in (56) it finally follows that

$$|v|_{H^m(K)} \leq C''(m, \|\boldsymbol{\nabla}\check{\mathbf{F}}^{-1}\|_{W^{m,\infty}(\check{K})}) \, \|\det \boldsymbol{\nabla}\mathbf{F}\|^{1/2}_{L^\infty(Q)} \, \|\boldsymbol{\nabla}\mathbf{F}\|^{-m}_{L^\infty(Q)} \sum_{j=1}^{m} |v\circ\mathbf{F}|_{H^j(Q)}. \tag{57}$$

Bounds (43) and (44) are proven, provided we show that C' and C'' behave as *shape* dependent constants C_{shape} (see Section 3). From the above calculations it immediately follows that C' and C'' are continuous functions of $\|\boldsymbol{\nabla}\check{\mathbf{F}}\|_{W^{m,\infty}(Q)}$ and $\|\boldsymbol{\nabla}\check{\mathbf{F}}^{-1}\|_{W^{m,\infty}(\check{K})}$, respectively. Observe that $\boldsymbol{\nabla}\check{\mathbf{F}}$ and $\boldsymbol{\nabla}\check{\mathbf{F}}^{-1}$ are 0-homogeneous with respect to $\boldsymbol{\nabla}\mathbf{F}$, and so are C' and C''. Furthermore, from (46) and (51)

$$\|\boldsymbol{\nabla}\check{\mathbf{F}}\|_{W^{m,\infty}(Q)} = \frac{\|\boldsymbol{\nabla}\mathbf{F}\|_{W^{m,\infty}(Q)}}{\|\boldsymbol{\nabla}\mathbf{F}\|_{L^\infty(Q)}} \leq \|\boldsymbol{\nabla}\mathbf{F}\|_{W^{m,\infty}(Q)} \inf_{x\in K} \|\boldsymbol{\nabla}\mathbf{F}^{-1}(x)\| \tag{58}$$

$$\|\boldsymbol{\nabla}\check{\mathbf{F}}^{-1}\|_{W^{m,\infty}(\check{K})} \leq \sum_{j=0}^{m} \|\boldsymbol{\nabla}^j\mathbf{F}^{-1}\|_{L^\infty(K)} \|\boldsymbol{\nabla}\mathbf{F}\|^j_{L^\infty(Q)}; \tag{59}$$

recalling that the NURBS map $\mathbf{F}$ is fixed, uniform boundedness with respect to the mesh-size easily follows.

□

We define the projector $\Pi_{\mathcal{V}_h} : L^2(\Omega) \to \mathcal{V}_h$ as

$$\Pi_{\mathcal{V}_h} v := (\Pi_{\mathcal{N}_h}(v\circ\mathbf{F}))\circ\mathbf{F}^{-1}, \qquad \forall v \in L^2(\Omega). \tag{60}$$

We refer to (60) as the push-forward of the NURBS projector. It is defined in Figure 4 and its approximation properties are stated in the next result.

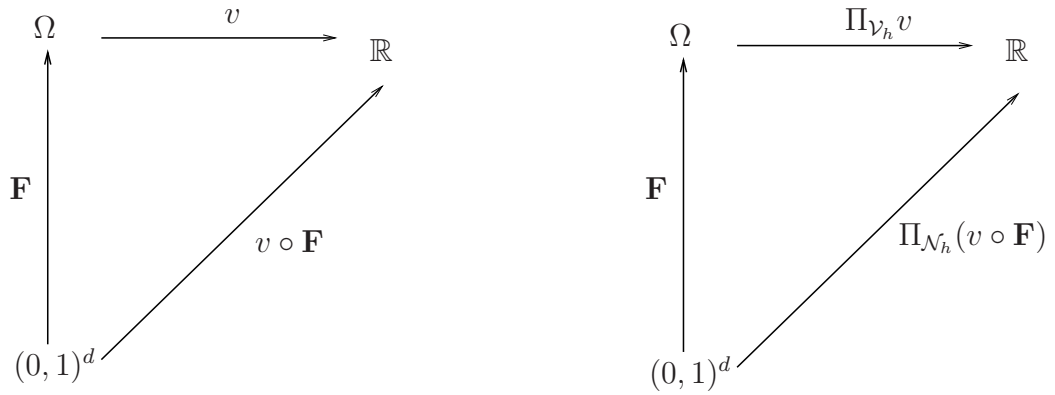

Figure 4: $\Pi_{\mathcal{V}_h} v$ is the push-forward of the NURBS projector $\Pi_{\mathcal{N}_h}(v\circ\mathbf{F})$, where $v \in L^2(\Omega)$ and $v\circ\mathbf{F} \in L^2((0,1)^d)$.

Theorem 3.1. *Let k and l be integer indices with $0 \le k \le l \le p+1$; let $Q \in \mathcal{Q}_h$, $K = \mathbf{F}(Q)$, $\tilde{Q}$ and $\tilde{K}$ as in (7) and (17), respectively; we have*

$$|v - \Pi_{\mathcal{V}_h} v|_{H^k(K)} \le C_{shape} h_K^{l-k} \sum_{i=0}^{l} \|\boldsymbol{\nabla}\mathbf{F}\|_{L^\infty(\tilde{Q})}^{i-l} |v|_{H^i(\tilde{K})}, \qquad \forall v \in L^2(\Omega) \cap H^l(\tilde{K}), \tag{61}$$

where h_K is the element size in the physical domain defined as

$$h_K = \|\boldsymbol{\nabla}\mathbf{F}\|_{L^\infty(Q)} h_Q. \tag{62}$$

Proof. Using (60), and then (44), we have

$$\begin{aligned} |v - \Pi_{\mathcal{V}_h} v|_{H^k(K)} &= |v - (\Pi_{\mathcal{N}_h}(v \circ \mathbf{F})) \circ \mathbf{F}^{-1}|_{H^k(K)} \\ &\le C_{shape} \|\det \boldsymbol{\nabla}\mathbf{F}\|_{L^\infty(Q)}^{1/2} \|\boldsymbol{\nabla}\mathbf{F}\|_{L^\infty(Q)}^{-k} \sum_{i=0}^{k} |v \circ \mathbf{F} - \Pi_{\mathcal{N}_h}(v \circ \mathbf{F})|_{H^i(Q)} \end{aligned} \tag{63}$$

Notice that since $v \in H^l(\tilde{K})$, we have $v \circ \mathbf{F} \in \mathcal{H}_h^l(\tilde{Q})$ and we can use the estimate of (42) on each term $|v \circ \mathbf{F} - \Pi_{\mathcal{N}_h}(v \circ \mathbf{F})|_{H^i(Q)}$, obtaining

$$\begin{aligned} |v \circ \mathbf{F} - \Pi_{\mathcal{N}_h}(v \circ \mathbf{F})|_{H^i(Q)} &\le C_{shape} h_Q^{l-k} \|v \circ \mathbf{F}\|_{\mathcal{H}_h^{l+i-k}(\tilde{Q})} \\ &\le C_{shape} h_Q^{l-k} \sum_{j=0}^{l+i-k} |v \circ \mathbf{F}|_{\mathcal{H}_h^j(\tilde{Q})}. \end{aligned} \tag{64}$$

Since $0 \le i \le k$ in (63) and $0 \le j \le l+i-k$ in (64), the two sums over the indices collapse into one and we have

$$\begin{aligned} |v - \Pi_{\mathcal{V}_h} v|_{H^k(K)} &\le C_{shape} \|\det \boldsymbol{\nabla}\mathbf{F}\|_{L^\infty(Q)}^{1/2} \|\boldsymbol{\nabla}\mathbf{F}\|_{L^\infty(Q)}^{-k} h_Q^{l-k} \sum_{i=0}^{l} |v \circ \mathbf{F}|_{\mathcal{H}_h^i(\tilde{Q})} \\ &= C_{shape} \|\det \boldsymbol{\nabla}\mathbf{F}\|_{L^\infty(Q)}^{1/2} \|\boldsymbol{\nabla}\mathbf{F}\|_{L^\infty(Q)}^{-k} h_Q^{l-k} \sum_{i=0}^{l} \sum_{\substack{Q' \in \mathcal{Q}_h \\ Q' \cap \tilde{Q} \neq \emptyset}} |v \circ \mathbf{F}|_{H^i(Q')}. \end{aligned} \tag{65}$$

Using (43) on each term $|v \circ \mathbf{F}|_{\mathcal{H}_h^i(Q')}$ of the last summation of (65) we get

$$|v \circ \mathbf{F}|_{H^i(Q')} \le C_{shape} \|\det \boldsymbol{\nabla}\mathbf{F}^{-1}\|_{L^\infty(K')}^{1/2} \sum_{j=0}^{i} \|\boldsymbol{\nabla}\mathbf{F}\|_{L^\infty(Q')}^{j} |v|_{H^j(K')}, \tag{66}$$

where, as before, $\mathbf{F}(Q') = K'$. From (65) and (66), since $0 \le i \le l$ and $0 \le j \le i$, by coalescing the double summation onto a single sum, we have

$$\begin{aligned} |v - \Pi_{\mathcal{V}_h} v|_{H^k(K)} &\le C_{shape} \|\boldsymbol{\nabla}\mathbf{F}\|_{L^\infty(Q)}^{-k} h_Q^{l-k} \sum_{i=0}^{l} \sum_{\substack{K' \in \mathcal{K}_h \\ K' \cap \tilde{K} \neq \emptyset}} \|\boldsymbol{\nabla}\mathbf{F}\|_{L^\infty(Q')}^{i} |v|_{H^i(K')} \\ &\le C_{shape} \|\boldsymbol{\nabla}\mathbf{F}\|_{L^\infty(\tilde{Q})}^{-k} h_Q^{l-k} \sum_{i=0}^{l} \|\boldsymbol{\nabla}\mathbf{F}\|_{L^\infty(\tilde{Q})}^{i} |v|_{H^i(\tilde{K})}, \end{aligned} \tag{67}$$

where we also used $\|\det \boldsymbol{\nabla}\mathbf{F}\|^{1/2}_{L^\infty(Q)}\|\det \boldsymbol{\nabla}\mathbf{F}^{-1}\|^{1/2}_{L^\infty(K)} \leq C_{shape}$. Multiplying and dividing the right-hand side of (67) by $\|\boldsymbol{\nabla}\mathbf{F}\|^l_{L^\infty(\tilde{Q})}$, and using the definition of the element size in the physical domain (62) we obtain

$$|v - \Pi_{\mathcal{V}_h} v|_{H^k(K)} \leq C_{shape} \frac{\|\boldsymbol{\nabla}\mathbf{F}\|^{l-k}_{L^\infty(\tilde{Q})}}{\|\boldsymbol{\nabla}\mathbf{F}\|^{l-k}_{L^\infty(Q)}} h_K^{l-k} \sum_{i=0}^{l} \|\boldsymbol{\nabla}\mathbf{F}\|^{i-l}_{L^\infty(\tilde{Q})} |v|_{H^i(\tilde{K})}. \tag{68}$$

Subsuming the fraction in the above inequality into C_{shape}, we finally get (61). □

As a corollary we have the global error estimate stated below.

Theorem 3.2. *Let k and l be integer indices with $0 \leq k \leq l \leq p+1$, we have*

$$\sum_{K\in\mathcal{K}_h} |v - \Pi_{\mathcal{V}_h} v|^2_{\mathcal{H}^k_h(K)} \leq C_{shape} \sum_{K\in\mathcal{K}_h} h_K^{2(l-k)} \sum_{i=0}^{l} \|\boldsymbol{\nabla}\mathbf{F}\|^{2(i-l)}_{L^\infty(\mathbf{F}^{-1}(K))} |v|^2_{H^i(K)}, \forall v \in H^l(\Omega). \tag{69}$$

Remark 3.1. *We note from Theorem 3.1 and Theorem 3.2 that the NURBS space $\mathcal{V}_h$ on the physical domain Ω delivers the optimal rate of convergence, as for the classical finite element spaces of degree p. Note that a bound on the k^{th}-order seminorm of the error $v - \Pi_{\mathcal{V}_h} v$ requires a control on the full l^{th}-order norm of v, unlike for finite elements (or splines, as in (40)) where only the l^{th}-order seminorm of v is involved in the right-hand side of the estimate. This is due to the role played by the weighting function w and the geometrical map $\mathbf{F}$.*

Note moreover that the estimates stated in Theorem 3.1 and 3.2 are dimensionally *consistent. Indeed C_{shape} is a dimensionless constant, while both h_K and $\|\boldsymbol{\nabla}\mathbf{F}\|_{L^\infty(\mathbf{F}^{-1}(K))}$ have dimensions of length; the patch $(0,1)^d$ is dimensionless while the physical space Ω is a dimensional space, which implies that $\boldsymbol{\nabla}\mathbf{F}$ has the dimensions of length. The coefficients $\|\boldsymbol{\nabla}\mathbf{F}\|^{i-l}_{L^\infty(\mathbf{F}^{-1}(K)))}$ compensate for the different dimensions of the the seminorms $|v|_{H^i}$ inside the summation of (61) and (69).*

3.4 Spaces with boundary conditions

Dealing with boundary conditions in the variational formulation of continuum mechanics problems requires Sobolev spaces of functions satisfying boundary constraints. The analysis developed in the previous sections can be adapted to this context with only minor modifications, as sketched below.

We focus our attention on the case of Dirichlet boundary conditions for second-order differential operators of the type discussed later in Section 5-6. Let $\partial\Omega$ be the boundary of $\Omega \subset \mathbb{R}^d$, with $d = 2, 3$, and $\Gamma_D \subset \partial\Omega$ the part of the boundary where the Dirichlet conditions hold. Moreover assume, for the sake of simplicity, that Γ_D is the union of element faces (for $d = 3$) or edges (for $d = 2$), and let $\gamma_D = \mathbf{F}^{-1}(\Gamma_D)$. For the purposes of analysis of the numerical methods, we need a projector from $H^k(\Omega)$ into $\mathcal{V}_h$ which preserves the nullity of the traces on Γ_D and with the same approximation properties as stated in Theorem 3.2. Let

$$H^1_{\Gamma_D}(\Omega) = \left\{ v \in H^1(\Omega) \mid v = 0 \text{ on } \Gamma_D \right\},$$

and accordingly

$$H^1_{\gamma_D}((0,1)^d) = \left\{ v \in H^1((0,1)^d) \mid v = 0 \text{ on } \gamma_D \right\},$$

Assume, for the sake of simplicity, that $\mathcal{S}_h \subset C^0((0,1)^d)$. It is easy to verify (see [25] or [34]) that the tensor product B-spline basis functions give

$$\mathcal{S}_h \cap H^1_{\gamma_D}((0,1)^d) = \text{span}\{B_{i_1\dots i_d} \mid B_{i_1\dots i_d} \in H^1_{\gamma_D}((0,1)^d),\, 1 \le i_\alpha \le n_\alpha,\, 1 \le \alpha \le d\}. \tag{70}$$

It seems natural therefore to modify the definition of (37), restricting to such a basis in (70). Therefore we set

$$\Pi^0_{\mathcal{S}_h} v := \sum_{\substack{i_\alpha=1,\dots,n_\alpha \\ B_{i_1\dots i_d}\in H^1_{\gamma_D}((0,1)^d)}} (\lambda_{i_1\dots i_d} v)\, B_{i_1\dots i_d}, \qquad \forall v \in H^1_{\gamma_D}((0,1)^d), \tag{71}$$

where, since (70), $\Pi^0_{\mathcal{S}_h} : H^1_{\gamma_D}((0,1)^d) \to \mathcal{S}_h \cap H^1_{\gamma_D}((0,1)^d)$.

The projectors $\Pi^0_{\mathcal{N}_h} : H^1_{\gamma_D}((0,1)^d) \to \mathcal{N}_h \cap H^1_{\gamma_D}((0,1)^d)$ and $\Pi^0_{\mathcal{V}_h} : H^1_{\Gamma_D}(\Omega) \to \mathcal{V}_h \cap H^1_{\Gamma_D}(\Omega)$ can be defined accordingly:

$$\begin{aligned} \Pi^0_{\mathcal{N}_h} v &:= \frac{\Pi^0_{\mathcal{S}_h}(wv)}{w}, \qquad \forall v \in H^1_{\gamma_D}((0,1)^d), \\ \Pi^0_{\mathcal{V}_h} v &:= \left(\Pi^0_{\mathcal{N}_h}(v \circ \mathbf{F})\right) \circ \mathbf{F}^{-1}, \qquad \forall v \in H^1_{\Gamma_D}(\Omega); \end{aligned}$$

The key tool of our analysis, Lemma 3.1, admits the following extension.

Lemma 3.6. *Let k and l be integer indices with $0 \le k < l \le p+1$ and $l \ge 1$; given $Q \in \mathcal{Q}_h$, $\tilde{Q}$ as in (7), $v \in \mathcal{H}^l_h(\tilde{Q}) \cap H^1_{\gamma_D}((0,1)^d)$, there exists an $s \in \mathcal{S}_h \cap H^1_{\gamma_D}((0,1)^d)$ such that*

$$|v - s|_{\mathcal{H}^k_h(\tilde{Q})} \le C h_Q^{l-k} |v|_{\mathcal{H}^l_h(\tilde{Q})}. \tag{72}$$

The proof is similar. From Lemma 3.6, the rest of the analysis follows in a straight forward manner as in the previous sections, leading to the result below.

Theorem 3.3. *Let k and l be integer indices with $0 \le k < l \le p+1$, we have*

$$\sum_{K\in\mathcal{K}_h} |v - \Pi^0_{\mathcal{V}_h} v|^2_{\mathcal{H}^k_h(K)} \le C_{shape} \sum_{K\in\mathcal{K}_h} h_K^{2(l-k)} \sum_{i=0}^{l} \|\boldsymbol{\nabla}\mathbf{F}\|^{2(i-l)}_{L^\infty(\mathbf{F}^{-1}(K))} |v|^2_{H^i(K)}, \forall v \in H^l(\Omega) \cap H^1_{\Gamma_D}(\Omega). \tag{73}$$

4 Inverse inequalities for NURBS

In this section, we prove some inverse inequalities which resemble the ones for finite elements spaces.

Theorem 4.1. *We have*

$$|v|_{H^2(K)} \le C_{shape} h_K^{-1} |v|_{H^1(K)} \qquad \forall K \in \mathcal{K}_h,\, \forall v \in \mathcal{V}_h, \tag{74}$$

Proof. Lemma 3.5 yields

$$|v|_{H^2(K)} \le C_{shape} \|\det \boldsymbol{\nabla}\mathbf{F}\|^{1/2}_{L^\infty(Q)} \|\boldsymbol{\nabla}\mathbf{F}\|^{-2}_{L^\infty(Q)} \|v \circ \mathbf{F}\|_{H^2(Q)} \tag{75}$$

where, as before, $\mathbf{F}(Q) = K$. Moreover

$$\|v \circ \mathbf{F}\|_{H^2(Q)} \leq C \left\| \frac{1}{w} \right\|_{W^{2,\infty}(Q)} \|w(v \circ \mathbf{F})\|_{H^2(Q)} \tag{76}$$

Since $w(v \circ \mathbf{F})$ is a polynomial of global degree $p_1 \cdot \ldots \cdot p_d$, for a usual inverse inequality we have

$$\|v \circ \mathbf{F}\|_{H^2(Q)} \leq C\, h_Q^{-1} \left\| \frac{1}{w} \right\|_{W^{2,\infty}(Q)} \|w(v \circ \mathbf{F})\|_{H^1(Q)} \tag{77}$$

We now have, again using Lemma 3.5,

$$\begin{aligned} \|w(v \circ \mathbf{F})\|_{H^1(Q)} &\leq C \|w\|_{W^{1,\infty}(Q)} \|v \circ \mathbf{F}\|_{H^1(Q)} \\ &\leq C_{shape} \|w\|_{W^{1,\infty}(Q)} \| \det \boldsymbol{\nabla} \mathbf{F}^{-1} \|^{1/2}_{L^\infty(K)} \sum_{j=0}^{1} \|\boldsymbol{\nabla} \mathbf{F}\|^j_{L^\infty(Q)} |v|_{H^j(K)}. \end{aligned} \tag{78}$$

Joining all of the above bounds, we finally get

$$|v|_{H^2(K)} \leq C_{shape} h_Q^{-1} \sum_{j=0}^{1} \|\boldsymbol{\nabla} \mathbf{F}\|^{j-2}_{L^\infty(Q)} |v|_{H^j(K)} \tag{79}$$

Let now v_K represent the constant function equal to the average of v on K; note that $v_K \in \mathcal{V}_h$. Therefore, applying (79), classical polynomial interpolation results, and recalling that $\|\boldsymbol{\nabla} \mathbf{F}\|^{-1}_{L^\infty(Q)} h_K = h_Q$, it easily follows that

$$\begin{aligned} |v|_{H^2(K)} &= |v - v_K|_{H^2(K)} \\ &\leq C_{shape} h_Q^{-1} \sum_{j=0}^{1} \|\boldsymbol{\nabla} \mathbf{F}\|^{j-2}_{L^\infty(Q)} |v - v_K|_{H^j(K)} \\ &\leq C_{shape} h_K^{-1} |v|_{H^1(K)}. \end{aligned}$$

□

More general inverse inequalities can be easily derived following the approach given above. In particular, the following result holds.

Theorem 4.2. *Let k and l be integer indices with $0 \leq k \leq l$; we have*

$$\|v\|_{H^l(K)} \leq C_{shape}\, h_K^{k-l} \sum_{i=0}^{k} \|\boldsymbol{\nabla} \mathbf{F}\|^{i-k}_{L^\infty(\mathbf{F}^{-1}(K))} |v|_{H^i(K)} \qquad \forall K \in \mathcal{K}_h,\ \forall v \in \mathcal{V}_h. \tag{80}$$

5 Applications to physical problems

In this section we obtain error estimates for NURBS applied to some linear physical problems. The basis of the analyses is the approximation and inverse estimates of the previous sections. After considering classical Galerkin methods for elliptic problems, we consider application of stabilized and BB-stable methods to saddle-point problems, and finally we study stabilized methods for advective-diffusive problems.

5.1 Elasticity

We start by considering the classical two- and three-dimensional linear elastic problem. We assume that the boundary $\partial\Omega$ is decomposed into a Dirichlet part Γ_D and a Neumann part Γ_N; as usual, Γ_D and Γ_N are the unions of element edges (for $d = 2$) and faces (for $d = 3$), respectively. Moreover, let $\mathbf{f} : \Omega \to \mathbb{R}^d$ be the given body force and $\mathbf{g} : \Omega : \Gamma_N \to \mathbb{R}^d$ the given traction on Γ_N.

Then, the mixed boundary-value problem for $\Omega \subset \mathbb{R}^3$, supported on Γ_D and free on Γ_N, reads

$$\begin{cases} \boldsymbol{\nabla} \cdot \mathbb{C}\boldsymbol{\varepsilon}(\mathbf{u}) + \mathbf{f} = \mathbf{0} & \text{in } \Omega \\ \mathbf{u} = \mathbf{0} & \text{on } \Gamma_D \\ \mathbb{C}\boldsymbol{\varepsilon}(\mathbf{u}) \cdot \mathbf{n} = \mathbf{g} & \text{on } \Gamma_N, \end{cases} \tag{81}$$

where $(\boldsymbol{\nabla}\cdot)$ is the divergence, $\mathbf{n}$ is the unit outward normal at each point of the boundary and the fourth-order tensor $\mathbb{C}$ is defined by

$$\mathbb{C}\mathbf{w} = 2\mu \left[\mathbf{w} + \frac{\nu}{1-2\nu} \mathrm{tr}(\mathbf{w})\mathbf{I} \right] \tag{82}$$

for all second-order tensors $\mathbf{w}$, where tr represents the trace operator and $\mu > 0,\ 0 \le \nu < 1/2$ are, respectively, the shear modulus and Poisson's ratio. The case of inhomogeneous Dirichlet data can be reduced to (81) by standard means. The stress, $\boldsymbol{\sigma}$, is given by Hooke's law, $\boldsymbol{\sigma} = \mathbb{C}\boldsymbol{\varepsilon}$.

Assuming for simplicity a regular loading $\mathbf{f} \in [L^2(\Omega)]^d$ and $\mathbf{g} \in [L^2(\Gamma_N)]^d$, we introduce also

$$< \boldsymbol{\psi}, \mathbf{v} >= (\mathbf{f}, \mathbf{v})_\Omega + (\mathbf{g}, \mathbf{v})_{\Gamma_N} \qquad \forall \mathbf{v} \in [H^1(\Omega)]^d, \tag{83}$$

where $(\ ,\ )_\Omega$, $(\ ,\ )_{\Gamma_N}$ indicate, as usual, the L^2 scalar products on Ω and Γ_N, respectively. The variational form of problem (81) then reads: find $\mathbf{u} \in [H^1_{\Gamma_D}(\Omega)]^d$ such that

$$(\mathbb{C}\boldsymbol{\varepsilon}(\mathbf{u}), \boldsymbol{\varepsilon}(\mathbf{v}))_\Omega =< \boldsymbol{\psi}, \mathbf{v} > \qquad \forall \mathbf{v} \in [H^1_{\Gamma_D}(\Omega)]^d \tag{84}$$

As is well known, this is an elliptic problem. In order to solve it using NURBS, we follow the same Galerkin approach adopted for classical finite elements, that is, we restrict the original problem to the finite-dimensional NURBS space: find $\mathbf{u}_h \in V_h$ such that

$$(\mathbb{C}\boldsymbol{\varepsilon}(\mathbf{u}), \boldsymbol{\varepsilon}(\mathbf{v}))_\Omega =< \boldsymbol{\psi}, \mathbf{v} > \qquad \forall \mathbf{v} \in V_h, \tag{85}$$

where

$$V_h = [\mathcal{V}_h]^d \cap [H^1_{\Gamma_D}(\Omega)]^d, \tag{86}$$

with $\mathcal{V}_h$ a NURBS space built as described in the previous sections.

The stability and consistency of the discrete problem (85) follow immediately. Therefore, a classical convergence analysis easily gives

$$|\mathbf{u} - \mathbf{u}_h|_{H^1} \le C(\nu) \inf_{\mathbf{v}_h \in V_h} |\mathbf{u} - \mathbf{v}_h|_{H^1(\Omega)}. \tag{87}$$

As a consequence, the interpolation properties of the past section give the optimal convergence of the method with respect to the norm and degree used: assuming quasi-uniform mesh refinement, $h_K \simeq h$, and $\min_\alpha p_\alpha = k$, $\mathbf{u} \in [H^{k+1}(\Omega)]^d$ we have

$$|\mathbf{u} - \mathbf{u}_h|_{H^1(\Omega)} \le C(\nu, \mathbf{u}) C_{shape} h^k; \tag{88}$$

moreover, assuming the regularity of the problem, i.e.

$$\|\mathbf{u}\|_{H^2(\Omega)} \le C \|\mathbf{f}\|_{L^2(\Omega)} \tag{89}$$

for all $\mathbf{f} \in L^2(\Omega)$, whenever $\mathbf{g} = 0$, the following L^2 estimate easily follows using an Aubin-Niestche argument

$$\|\mathbf{u} - \mathbf{u}_h\|_{L^2(\Omega)} \le C(\nu, \mathbf{u}) C_{shape} h^{k+1}. \tag{90}$$

5.2 Incompressible and almost incompressible isotropic elasticity – stabilized methods

It is well known that the constant C in bound (87) tends to $+\infty$ as the Poisson ratio $\nu \to 1/2$. As it happens for classical finite elements, in such cases the NURBS discretization (85) is expected to give non-satisfactory approximation results. In order to treat both this (almost incompressible) case and the limit (incompressible) case, we rewrite problem (84) in the standard mixed form.

For notation simplicity we now set the shear modulus $2\mu = 1$, and define the positive constant

$$\varepsilon = \frac{1-2\nu}{\nu} \tag{91}$$

The incompressible case is represented by $\varepsilon = 0$.

The mixed variational formulation of (81) then reads: find $(\mathbf{u}, p) \in H^1_{\Gamma_D}(\Omega) \times L^2(\Omega)$ such that

$$\begin{cases} (\boldsymbol{\varepsilon}(\mathbf{u}), \boldsymbol{\varepsilon}(\mathbf{v}))_\Omega - (\boldsymbol{\nabla} \cdot \mathbf{v}, p)_\Omega =< \boldsymbol{\psi}, \mathbf{v} > & \forall \mathbf{v} \in [H^1_{\Gamma_D}(\Omega)]^d \\ (\boldsymbol{\nabla} \cdot \mathbf{u}, q)_\Omega + \varepsilon (p, q)_\Omega = 0 & \forall q \in L^2(\Omega). \end{cases} \tag{92}$$

Throughout this section and the next, we assume that $\Gamma_D \neq \partial\Omega$. If $\Gamma_D = \partial\Omega$ and $\varepsilon = 0$, the space for the pressure needs to be replaced by

$$L^2_0(\Omega) = \left\{ q \in L^2(\Omega) \mid \int_\Omega q = 0 \right\} \tag{93}$$

in order for the problem to have a unique solution.

Whenever $\varepsilon > 0$, the stability of the problem and the good properties of the NURBS space guarantee optimal error bounds for Galerkin's method applied to (92). On the other hand, similarly to classical finite elements, we expect the Galerkin discretization with NURBS to suffer from lack of stability as $\varepsilon \to 0$. In general, unless certain combination of spaces (V_h, P_h) are found (see next section), the approximation properties of the numerical method are well known to deteriorate as $\varepsilon \to 0$; even worse, the limit case $\varepsilon = 0$ can suffer from complete lack of stability and spurious modes. One way to avoid this is to adopt a stabilized formulation of (92).

We start by introducing the discrete spaces for displacements and pressures

$$V_h = [\mathcal{V}_h]^d \cap [H^1_{\Gamma_D}(\Omega)]^d \tag{94}$$

$$P_h = \mathcal{V}_h \cap H^1(\Omega) \tag{95}$$

Note that we are requiring continuity also on the pressures and, for the moment, we are assuming equal-order displacement and pressure fields. Following [24], [18, 26], and [15] we introduce the following stabilized formulations:

SUPG:

$$\begin{aligned} B^{SUPG}(\mathbf{u}, p; \mathbf{v}, q) = (\boldsymbol{\varepsilon}(\mathbf{u}), \boldsymbol{\varepsilon}(\mathbf{v}))_\Omega - (\boldsymbol{\nabla} \cdot \mathbf{v}, p)_\Omega + (\boldsymbol{\nabla} \cdot \mathbf{u}, q)_\Omega + \varepsilon (p, q)_\Omega \\ + \alpha \sum_{K \in \mathcal{K}_h} h_K^2 (-\boldsymbol{\nabla} \cdot \boldsymbol{\varepsilon}(\mathbf{u}) + \boldsymbol{\nabla} p, \boldsymbol{\nabla} q)_K \end{aligned} \tag{96}$$

$$F^{SUPG}(\mathbf{v}) =< \boldsymbol{\psi}, \mathbf{v} > + \alpha \sum_{K \in \mathcal{K}_h} h_K^2 (\mathbf{f}, \boldsymbol{\nabla} q)_K \tag{97}$$

GLS:

$$B^{GLS}(\mathbf{u},p;\mathbf{v},q) = (\boldsymbol{\varepsilon}(\mathbf{u}),\boldsymbol{\varepsilon}(\mathbf{v}))_\Omega - (\boldsymbol{\nabla}\cdot\mathbf{v},p)_\Omega - (\boldsymbol{\nabla}\cdot\mathbf{u},q)_\Omega - \varepsilon(p,q)_\Omega \\ -\alpha\sum_{K\in\mathcal{K}_h} h_K^2(-\boldsymbol{\nabla}\cdot\boldsymbol{\varepsilon}(\mathbf{u})+\boldsymbol{\nabla}p, -\boldsymbol{\nabla}\cdot\boldsymbol{\varepsilon}(\mathbf{v})+\boldsymbol{\nabla}q)_K \tag{98}$$

$$F^{GLS}(\mathbf{v}) =< \boldsymbol{\psi},\mathbf{v} > -\alpha\sum_{K\in\mathcal{K}_h} h_K^2(\mathbf{f}, -\boldsymbol{\nabla}\cdot\boldsymbol{\varepsilon}(\mathbf{v})+\boldsymbol{\nabla}q)_K \tag{99}$$

DW (Douglas-Wang):

$$B^{DW}(\mathbf{u},p;\mathbf{v},q) = (\boldsymbol{\varepsilon}(\mathbf{u}),\boldsymbol{\varepsilon}(\mathbf{v}))_\Omega - (\boldsymbol{\nabla}\cdot\mathbf{v},p)_\Omega - (\boldsymbol{\nabla}\cdot\mathbf{u},q)_\Omega - \varepsilon(p,q)_\Omega \\ -\alpha\sum_{K\in\mathcal{K}_h} h_K^2(-\boldsymbol{\nabla}\cdot\boldsymbol{\varepsilon}(\mathbf{u})+\boldsymbol{\nabla}p, \boldsymbol{\nabla}\cdot\boldsymbol{\varepsilon}(\mathbf{v})+\boldsymbol{\nabla}q)_K \tag{100}$$

$$F^{DW}(\mathbf{v}) =< \boldsymbol{\psi},\mathbf{v} > -\alpha\sum_{K\in\mathcal{K}_h} h_K^2(\boldsymbol{\psi}, -\boldsymbol{\nabla}\cdot\boldsymbol{\varepsilon}(\mathbf{v})+\boldsymbol{\nabla}q)_K \tag{101}$$

where α is a positive constant at our disposal. The discrete NURBS problem then reads: find $(\mathbf{u}_h,p_h)\in V_h\times P_h$ such that

$$B(\mathbf{u}_h,p_h;\mathbf{v},q) = F(\mathbf{v}) \qquad \forall(\mathbf{v},q)\in V_h\times P_h \tag{102}$$

where the bilinear form $B(\cdot,\cdot)$ and the functional $F(\cdot)$ depend on which of the three methods above is adopted.

For the three methods here presented, there hold optimal and $\varepsilon-$uniform error bounds in the natural norms of the problem. Given the interpolation and inverse inequality results of the previous sections, the proof of this result follows in step-by-step fashion its finite element counterpart. For the SUPG method, see Theorem 4.1 in [24], while for the GLS and DW methods see respectively Theorem 3.1, case (ii), and Theorem 3.2, case (ii), in [18]. For completeness we include, in the next lemma, a very brief sketch of the proof of the stability result for the GLS case, the other two cases being very similar; we will make use of the notation

$$|||(\mathbf{v},q)|||^2 := \|\boldsymbol{\varepsilon}(\mathbf{v})\|^2_{L^2(\Omega)} + (1+\varepsilon)\|q\|^2_{L^2(\Omega)}. \tag{103}$$

We recall the Korn inequality

$$\mathrm{diam}(\Omega)^{-2}\|\mathbf{v}\|^2_{L^2(\Omega)} + |\mathbf{v}|^2_{H^1(\Omega)} \le C_{korn}\|\boldsymbol{\varepsilon}(\mathbf{v})\|^2_{L^2(\Omega)}.$$

Lemma 5.1. *Let the constant $0<\alpha<C_{inv}^{-1}$, where C_{inv} is the (shape dependent) constant of the inverse inequality stated in Lemma 4.1. Then, there exists $C_{shape}>0$, independent of the mesh size, such that*

$$\sup_{(\mathbf{v},q)\in V_h\times P_h} \frac{B^{GLS}(\mathbf{u},p;\mathbf{v},q)}{|||(\mathbf{v},q)|||} \ge C_{shape}|||(\mathbf{u},p)|||. \tag{104}$$

Proof. We follow the approach of [18]. The inf-sup condition (104) is equivalent to the following: given any $(\mathbf{u},p)\in V_h\times P_h$, there exists a $(\mathbf{v},q)\in V_h\times P_h$ and two positive constants C_{shape}, C'_{shape} such that

$$\begin{aligned} B^{GLS}(\mathbf{u},p;\mathbf{v},q) &\ge C_{shape}|||(\mathbf{u},p)|||^2 \\ |||(\mathbf{v},q)|||^2 &\le C'_{shape}|||(\mathbf{u},p)|||^2. \end{aligned} \tag{105}$$

Inequalities (105) allow one to establish the uniform stability condition by selecting the appropriate test function for the bilinear form. We start by recalling an argument given in Verfürth [38] that gives the existence of two positive constants C_{shape} and C'_{shape} such that

$$\sup_{0\neq\mathbf{v}\in V_h} \frac{(\boldsymbol{\nabla}\cdot\mathbf{v},q)_\Omega}{|\mathbf{v}|_{H^1(\Omega)}} \geq C_{shape}\|q\|_{L^2(\Omega)} - C'_{shape}\Big(\sum_{K\in\mathcal{K}_h} h_K^2\|\boldsymbol{\nabla}q\|^2_{L^2(K)}\Big)^{1/2}, \quad \forall q\in P_h. \tag{106}$$

The above inequality relies solely on the interpolation estimate, which for the NURBS approximation space was established in Theorem 3.3. The following bound is immediate, provided the inverse estimate (Theorem 4.2) holds together with the bound on α ($0<\alpha<C_{inv}^{-1}$):

$$\begin{aligned} B^{GLS}(\mathbf{u},p;\mathbf{u},-p) \;&\geq\; C_{shape}\,|\mathbf{u}|^2_{H^1(\Omega)} + \varepsilon\,\|p\|^2_{L^2(\Omega)} \\ &\quad +\alpha\sum_{K\in\mathcal{K}_h} h_K^2\|\boldsymbol{\nabla}p\|^2_{L^2(K)} \qquad \forall(\mathbf{u},p)\in V_h\times P_h, \end{aligned} \tag{107}$$

with $C_{shape}=C_{korn}(1-\alpha C_{inv})$.

Consider $\mathbf{w}\in V_h$ which achieves the supremum in (106) for $q=p$ ($\mathbf{w}$ can be rescaled such that $|\mathbf{w}|_{H^1(\Omega)}=\|p\|_{L^2(\Omega)}$, which is what is assumed in the sequel). Then the following bound holds:

$$\begin{aligned} B^{GLS}(\mathbf{u},p;\mathbf{w},0) \;&\geq\; -C_{shape}\,|\mathbf{u}|^2_{H^1(\Omega)} + C'_{shape}\,\|p\|^2_{L^2(\Omega)} \\ &\quad -C''_{shape}\sum_{K\in\mathcal{K}_h} h_K^2\|\boldsymbol{\nabla}q\|^2_{L^2(K)}, \end{aligned} \tag{108}$$

where C_{shape}, C'_{shape}, and C''_{shape} are positive and $(\mathbf{u},p)\in V_h\times P_h$. Denoting $(\mathbf{v},q)=(\mathbf{u}-\delta\mathbf{w},-p)$ and combining (107) and (108) we arrive at

$$B^{GLS}(\mathbf{u},p;\mathbf{v},q)\geq C_{shape}\,(|\mathbf{u}|^2_{H^1(\Omega)}+(1+\varepsilon)\|p\|^2_{L^2(\Omega)}), \tag{109}$$

with a suitable choice for a positive parameter δ. On the other hand we have

$$|\mathbf{v}|^2_{H^1(\Omega)}+(1+\varepsilon)\|q\|^2_{L^2(\Omega)}\leq C_{shape}\,(|\mathbf{u}|^2_{H^1(\Omega)}+(1+\varepsilon)\|p\|^2_{L^2(\Omega)}). \tag{110}$$

which, in conjunction with (109), completes the proof of the uniform stability (104). □

The uniform stability result of Lemma 5.1 combined with the inverse inequalities of Section 4 and the interpolation estimates of Section 3.3 leads to error estimates which are optimal. Let $k=\min(p_1,p_2,..,p_d)$ where $p_1,p_2,..,p_d$ are as the anisotropic polynomial degrees of $\mathcal{V}_h$. Then, if $\mathbf{u}\in H^{k+1}(\Omega)$ and $p\in H^k(\Omega)$,

$$|\mathbf{u}-\mathbf{u}_h|_{H^1(\Omega)}+\|p-p_h\|_{L^2(\Omega)}\leq C(\mathbf{u},p)\,C_{shape}\,h^k. \tag{111}$$

Moreover, assuming as in Section 5.1 the regularity of the problem and making use of the Aubin-Niestche argument, we get

$$\|\mathbf{u}-\mathbf{u}_h\|_{L^2(\Omega)}\leq C(\mathbf{u},p)\,C_{shape}\,h^{k+1}. \tag{112}$$

Remark 5.1. *Similar results can be obtained for any pair of continuous NURBS spaces V_h, P_h. It is not required that the displacement and pressure spaces be based on the same knot vectors and polynomial degree. If $\mathbf{u}\in H^{s+1}(\Omega)$ and $p\in H^s(\Omega)$, then*

$$|\mathbf{u}-\mathbf{u}_h|_{H^1(\Omega)}+\|p-p_h\|_{L^2(\Omega)}+h^{-1}\|\mathbf{u}-\mathbf{u}_h\|_{L^2(\Omega)}\leq C(\mathbf{u},p)C_{shape}\,h^k, \quad k=\min\{s,k_u,k_p+1\} \tag{113}$$

where k_u and k_p are the minimal anisotropic polynomial degrees used for displacements and pressures, respectively.

5.3 Incompressible and almost incompressible isotropic elasticity – a BB-stable method

In this section we introduce pairs of displacement and pressure NURBS spaces suitable for the approximation of problem (92) without the necessity of adding stabilizing terms. Given a positive isotropic degree k, we introduce the spaces of displacements and pressures

$$V_h = [\mathcal{V}_h(k+1,\ldots,k+1)]^d \cap [H^1_{\Gamma_D}(\Omega)]^d, \tag{114}$$

$$P_h = \mathcal{V}_h(k,\ldots,k) \cap H^1(\Omega), \tag{115}$$

where $\mathcal{V}_h(k+1,\ldots,k+1)$ and $\mathcal{V}_h(k,\ldots,k)$ denote the NURBS spaces introduced in (19), of degree $k+1$ and k, respectively. We assume that in V_h no continuity of derivatives is enforced across the element boundaries, that is, in each coordinate direction, the internal knots are repeated $k+1$ times. By construction, there is a basis function that is interpolatory at each vertex of the mesh. The control point associated with each vertex is physically located at that vertex. These control points are a subset of the control points comprizing the control net. For this subset, the control points are identical to the nodal points of finite elements.

We are now able to introduce the discrete problem: find $(\mathbf{u}_h, p_h) \in V_h \times P_h$ such that

$$\begin{cases} (\boldsymbol{\varepsilon}(\mathbf{u}_h), \boldsymbol{\varepsilon}(\mathbf{v}))_\Omega - (\boldsymbol{\nabla}\cdot\mathbf{v}, p_h)_\Omega = <\boldsymbol{\psi}, \mathbf{v}> & \forall \mathbf{v} \in V_h \\ (\boldsymbol{\nabla}\cdot\mathbf{u}_h, q)_\Omega + \varepsilon(p_h, q)_\Omega = 0 & \forall q \in P_h \end{cases} \tag{116}$$

We recall that

$$h = \max_{Q\in\mathcal{Q}_h} h_Q.$$

Moreover, in what follows we denote by h_{max} a quantity, representing a mesh-size, which depends only on the problem domain, mesh family shape-regularity, and polynomial degree k. We have the following a priori error estimate.

Theorem 5.1. *There exists $h_{max} > 0$ such that for $h \le h_{max}$,*

$$|\mathbf{u}-\mathbf{u}_h|_{H^1(\Omega)} + \|p-p_h\|_{L^2(\Omega)} \le C_{shape}\left(\inf_{\mathbf{v}_h\in V_h}|\mathbf{u}-\mathbf{v}_h|_{H^1(\Omega)} + \inf_{q_h\in P_h}\|p-q_h\|_{L^2(\Omega)}\right). \tag{117}$$

where $(\mathbf{u}, p)$ is the solution of problem (92) and $(\mathbf{u}_h, p_h)$ is the solution of problem (116).

Theorem 5.1 and the interpolation estimates of Section 3.3 lead to error estimates which are optimal: if $\mathbf{u} \in H^{k+1}(\Omega)$ and $p \in H^k(\Omega)$,

$$|\mathbf{u}-\mathbf{u}_h|_{H^1(\Omega)} + \|p-p_h\|_{L^2(\Omega)} \le C(\mathbf{u},p)\, C_{shape}\, h^k. \tag{118}$$

The proof of Theorem 5.1 follows directly from the Babuška-Brezzi inf-sup (stability) condition stated in the next theorem, and the classical theory of mixed finite element methods (see [8]).

Theorem 5.2. *There exists $h_{max} > 0$ and $C_{shape} > 0$ such that the inf-sup condition*

$$\sup_{\mathbf{v}\in V_h} \frac{(\boldsymbol{\nabla}\cdot\mathbf{v}, q)}{|\mathbf{v}|_{H^1(\Omega)}} \ge C_{shape}\|q\|_{L^2(\Omega)}, \qquad \forall q \in P_h, \tag{119}$$

holds provided that

$$h \le h_{max}. \tag{120}$$

The proof of Theorem 5.2 requires some preliminary results and Lemma 3.3. We denote by $\bar{\mathbf{F}}_h$ the (piecewise multilinear) nodal interpolant of $\mathbf{F}$, and by $\bar{\Omega}_h$ the image of $\bar{\mathbf{F}}_h$, that is

$$\bar{\mathbf{F}}_h \ : \ (0,1)^d \longrightarrow \bar{\Omega}_h. \tag{121}$$

Note that the domain $\bar{\Omega}_h$ depends on the mesh $\mathcal{Q}_h$. We also introduce finite-dimensional spaces on the patch $(0,1)^d$,

$$\hat{V}_h = \left\{\hat{\mathbf{v}} : (0,1)^d \to \mathbb{R}^d \mid \hat{\mathbf{v}} = \mathbf{v} \circ \mathbf{F} \ , \ \mathbf{v} \in V_h\right\}, \tag{122}$$

$$\hat{P}_h = \left\{\hat{q} : (0,1)^d \to \mathbb{R} \mid \hat{q} = q \circ \mathbf{F} \ , \ q \in P_h\right\}, \tag{123}$$

and on $\bar{\Omega}_h$:

$$\bar{V}_h = \left\{\bar{\mathbf{v}} : \bar{\Omega}_h \to \mathbb{R}^d \mid \bar{\mathbf{v}} = \hat{\mathbf{v}} \circ \bar{\mathbf{F}}_h^{-1} \ , \ \hat{\mathbf{v}} \in \hat{V}_h\right\}, \tag{124}$$

$$\bar{P}_h = \left\{\bar{q} : \bar{\Omega}_h \to \mathbb{R} \mid \bar{q} = \hat{q} \circ \bar{\mathbf{F}}_h^{-1} \ , \ \hat{q} \in \hat{P}_h\right\}, \tag{125}$$

Given $K \in \mathcal{K}_h$, we define the corresponding *vertex element* $\bar{K}$ as

$$\bar{K} = \bar{\mathbf{F}}_h(\mathbf{F}^{-1}(K)) = \left\{x \in \bar{\Omega}_h | x = \bar{\mathbf{F}}_h(\mathbf{F}^{-1}(y)), \, y \in K\right\} \tag{126}$$

The mesh of all $\bar{K}$'s is referred to as the *vertex mesh* $\bar{\mathcal{K}}_h$. The union of all $\bar{K} \in \bar{\mathcal{K}}_h$ gives $\bar{\Omega}_h$; also note that the $\bar{K}$'s are bilinear quadrilaterals and trilinear hexahedra in $\mathbb{R}^2$ and $\mathbb{R}^3$, respectively. $\bar{\mathcal{K}}_h$ may be thought of as a coarsening of the *control net*, or *control mesh*, in NURBS theory (see [25, 13]). The control net facilitates a geometric interpretation of the control points as it is a piecewise multilinear interpolation of *all* the control points. We recall that $\mathbf{F}_h$ interpolates only a subset of the control points. See Box 1 for a schematic illustration of the setup and the relation between mappings.

Box 1. Geometrical setup.

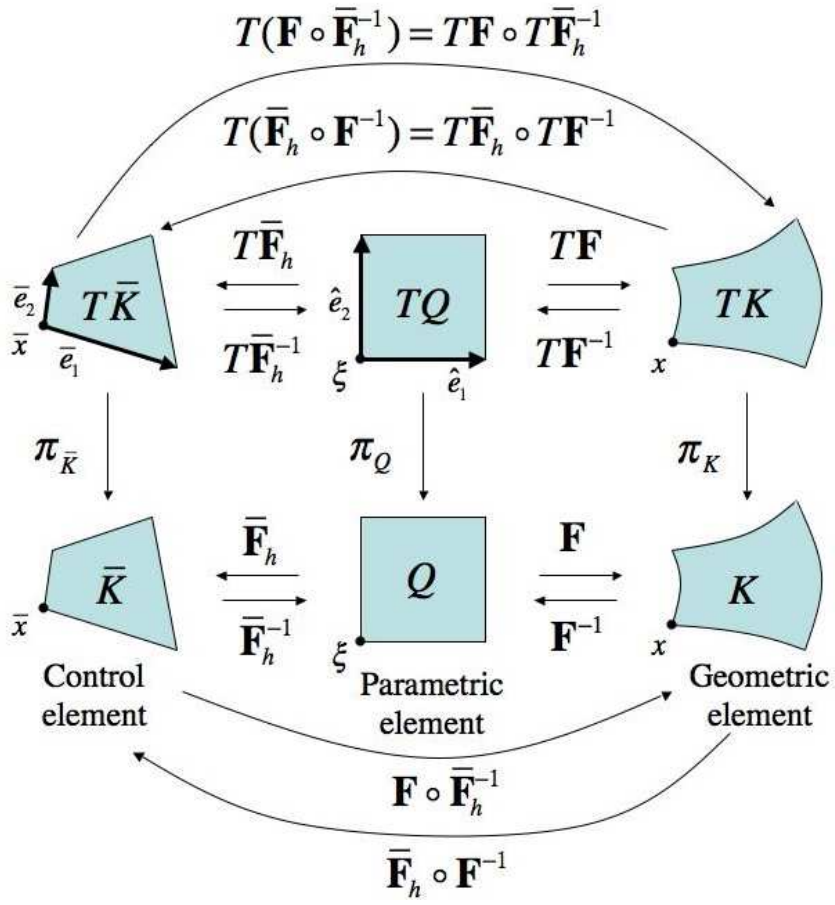

Q is a parametric element, K is a geometric element, and $\bar{K}$ is a vertex element. K and $\bar{K}$ are the images of Q under the mappings $\mathbf{F}$ and $\bar{\mathbf{F}}_h$, respectively. The tangent bundles TQ, TK and $T\bar{K}$ consist of base points and d-dimensional vector spaces emanating from the base points. Corresponding to the mappings $\mathbf{F}$ and $\bar{\mathbf{F}}_h$ are the tangent maps $T\mathbf{F}$ and $T\bar{\mathbf{F}}_h$ (and likewise their inverses). For example, we write $T\mathbf{F} = (\mathbf{F}, \boldsymbol{\nabla}\mathbf{F})$ and thus the tangent maps base points, $\xi \longmapsto \mathbf{F}(\xi)$, and vectors by the linear transformation $\hat{e}(\xi) \longmapsto \boldsymbol{\nabla}\mathbf{F}(\xi)\hat{e}(\xi)$. Composite tangent maps transform by the chain rule, as illustrated in the figure. Vertex elements are multilinear maps of parametric elements. Thus $\bar{\mathbf{F}}_h$ is bilinear in two dimensions and trilinear in three. Geometric elements are portions of the exact geometry defined by NURBS. Under h-refinement, the vertex elements converge to the geometric elements. π_Q, π_K and $\pi_{\bar{K}}$ are the canonical projections onto the base elements.

Taking ξ at a corner of Q, we have $x = \mathbf{F}(\xi)$ and $\bar{x} = \bar{\mathbf{F}}_h(\xi)$, as shown, and $T\bar{\mathbf{F}}_h(\xi) = (\bar{\mathbf{F}}_h(\xi), \boldsymbol{\nabla}\bar{\mathbf{F}}_h(\xi))$ and $T\bar{\mathbf{F}}_h^{-1}(\bar{x}) = (\bar{\mathbf{F}}_h^{-1}(\bar{x}), \boldsymbol{\nabla}\bar{\mathbf{F}}_h^{-1}(\bar{x}))$. The edge lengths are given by $h_{\hat{e}_\alpha} = \|\hat{e}_\alpha\|$ and $h_{\bar{e}_\alpha} = \|\bar{e}_\alpha\|$, $1 \le \alpha \le d$. Furthermore, $\bar{e}_\alpha(\bar{x}) = \boldsymbol{\nabla}\bar{\mathbf{F}}_h(\xi)\hat{e}_\alpha(\xi)$ and $\hat{e}_\alpha(\xi) = \boldsymbol{\nabla}\bar{\mathbf{F}}_h^{-1}(\bar{x})\bar{e}_\alpha(\bar{x})$, from which easily follows $h_{\bar{e}_\alpha} \le \|\boldsymbol{\nabla}\bar{\mathbf{F}}_h\|_{L^\infty(Q)} h_{\hat{e}_\alpha}$ and $h_{\hat{e}_\alpha} \le \|\boldsymbol{\nabla}\bar{\mathbf{F}}_h^{-1}\|_{L^\infty(\bar{K})} h_{\bar{e}_\alpha}$, and in turn (137).

Let $x = \mathbf{F}(\xi)$ where $\xi \in Q$ is arbitrary. Likewise, $\xi = \mathbf{F}^{-1}(x)$. Since $\mathbf{F}\circ\mathbf{F}^{-1}(x) = x$, $\boldsymbol{\nabla}\mathbf{F}(\xi)\boldsymbol{\nabla}\mathbf{F}^{-1}(x) = \mathbf{I}$, the identity matrix, and so $\boldsymbol{\nabla}\mathbf{F}(\xi)^{-1} = \boldsymbol{\nabla}\mathbf{F}^{-1}(x)$. We write this as $(\boldsymbol{\nabla}\mathbf{F})^{-1} = \boldsymbol{\nabla}\mathbf{F}^{-1}\circ\mathbf{F}$. It is necessary to be careful with compositions and base points in the analysis. Similar results may be derived for the other mappings.

Lemma 5.2. *There exists $h'_{max} > 0$ (only dependent on the shape regularity of the mesh $\mathcal{Q}_h$ and on the shape of Ω), such that given $Q \in \mathcal{Q}_h$, $K = \mathbf{F}(Q)$, $\bar{K}$ as in (126) and assuming that $h_Q \leq h'_{max}$, then $\bar{\mathbf{F}}_h$ is a one-to-one mapping from Q into $\bar{K}$ and we have*

$$\|\boldsymbol{\nabla}\bar{\mathbf{F}}_h\|_{L^\infty(Q)} \leq C_{shape}\|\boldsymbol{\nabla}\mathbf{F}\|_{L^\infty(Q)} \tag{127}$$

$$\|\boldsymbol{\nabla}\bar{\mathbf{F}}_h^{-1}\|_{L^\infty(\bar{K})} \leq C_{shape}\|\boldsymbol{\nabla}\mathbf{F}^{-1}\|_{L^\infty(K)} \tag{128}$$

$$\|\det\boldsymbol{\nabla}\bar{\mathbf{F}}_h\|_{L^\infty(Q)} \leq C_{shape}\|\boldsymbol{\nabla}\mathbf{F}\|^d_{L^\infty(Q)} \tag{129}$$

$$\|\det\boldsymbol{\nabla}\bar{\mathbf{F}}_h^{-1}\|_{L^\infty(\bar{K})} \leq C_{shape}\|\boldsymbol{\nabla}\mathbf{F}^{-1}\|^d_{L^\infty(K)} \tag{130}$$

Proof. We introduce the map $\mathbf{E}$ and its derivative[3]

$$\mathbf{E} = \bar{\mathbf{F}}_h - \mathbf{F}, \qquad \boldsymbol{\nabla}\mathbf{E} = \boldsymbol{\nabla}\bar{\mathbf{F}}_h - \boldsymbol{\nabla}\mathbf{F} \tag{131}$$

Note that a classical result gives the estimate for the interpolation error

$$\|\boldsymbol{\nabla}\mathbf{E}\|_{L^\infty(Q)} \leq C_{ie}h_Q\|\boldsymbol{\nabla}^2\mathbf{F}\|_{L^\infty(Q)}; \tag{132}$$

therefore, we have[4]

$$\|\boldsymbol{\nabla}\mathbf{F}^{-1}\boldsymbol{\nabla}\mathbf{E}\|_{L^\infty(Q)} \leq \|\boldsymbol{\nabla}\mathbf{F}^{-1}\|_{L^\infty(Q)}\|\boldsymbol{\nabla}\mathbf{E}\|_{L^\infty(Q)} \leq C_{ie}\|\boldsymbol{\nabla}\mathbf{F}^{-1}\|_{L^\infty(K)}h_Q\|\boldsymbol{\nabla}^2\mathbf{F}\|_{L^\infty(Q)}.$$

In particular, if

$$h_Q\|\boldsymbol{\nabla}^2\mathbf{F}\|_{L^\infty(Q)}\|\boldsymbol{\nabla}\mathbf{F}^{-1}\|_{L^\infty(K)} \leq C_{ie}^{-1}/2, \tag{133}$$

then

$$\|\boldsymbol{\nabla}\mathbf{F}^{-1}\boldsymbol{\nabla}\mathbf{E}\|_{L^\infty(Q)} \leq \frac{1}{2}. \tag{134}$$

We set

$$h'_{max} := \max_{\substack{Q\in\mathcal{Q}_h \\ K=\mathbf{F}(Q)}} \left\{ \frac{C_{ie}^{-1}}{2\|\boldsymbol{\nabla}^2\mathbf{F}\|_{L^\infty(Q)}\|\boldsymbol{\nabla}\mathbf{F}^{-1}\|_{L^\infty(K)}} \right\};$$

condition (133) can be stated as $h \leq h'_{max}$, which we assume in what follows. Observe that

$$\boldsymbol{\nabla}\bar{\mathbf{F}}_h(\xi) = \boldsymbol{\nabla}\mathbf{F}(\xi) + \boldsymbol{\nabla}\mathbf{E}\,(\xi) = \boldsymbol{\nabla}\mathbf{F}(\xi)\left(\mathbf{I} + (\boldsymbol{\nabla}\mathbf{F})^{-1}(\xi)\boldsymbol{\nabla}\mathbf{E}(\xi)\right) \qquad \forall\xi \in Q, \tag{135}$$

whence

$$\|\boldsymbol{\nabla}\bar{\mathbf{F}}_h\|_{L^\infty(Q)} \leq \frac{3}{2}\|\boldsymbol{\nabla}\mathbf{F}\|_{L^\infty(Q)}, \tag{136}$$

that is, $C_{shape} = \frac{3}{2}$ in (127). Furthermore, fixing $\xi \in Q$, the right hand side of (135) is a non-singular matrix, and, in particular,

$$\|\left(\mathbf{I} + (\boldsymbol{\nabla}\mathbf{F})^{-1}(\xi)\boldsymbol{\nabla}\mathbf{E}(\xi)\right)^{-1}\| \leq (1 - \|(\boldsymbol{\nabla}\mathbf{F})^{-1}(\xi)\boldsymbol{\nabla}\mathbf{E}(\xi)\|)^{-1} \leq 2.$$

[3] If linear NURBS are utilized, $\mathbf{F}$ and $\bar{\mathbf{F}}_h$ are the same and thus $\mathbf{E} = \mathbf{0}$.

[4] We need to elaborate on the geometric meaning of $\boldsymbol{\nabla}\mathbf{F}^{-1}\boldsymbol{\nabla}\mathbf{E}$. $\boldsymbol{\nabla}\mathbf{F}^{-1}(x)$ is a linear map from the tangent space T_xK to $T_\xi Q$, where $x = \mathbf{F}(\xi)$. Likewise, $\boldsymbol{\nabla}\mathbf{F}(\xi)$:$T_\xi Q \longrightarrow T_xK$ is its inverse. However, $\boldsymbol{\nabla}\bar{\mathbf{F}}_h(\xi)$:$T_\xi Q \to T_{\bar{x}}\bar{K}$, where $\bar{x} = \bar{\mathbf{F}}_h(\xi)$. Thus, the images of $\boldsymbol{\nabla}\mathbf{F}(\xi)$ and $\boldsymbol{\nabla}\bar{\mathbf{F}}_h(\xi)$ reside in different tangent spaces, namely, T_xK and $T_{\bar{x}}\bar{K}$, respectively. To make sense of $\boldsymbol{\nabla}\mathbf{F}^{-1}\boldsymbol{\nabla}\mathbf{E}$, we need to identify the linear space $T_{\bar{x}}\bar{K}$ with T_xK so that $\boldsymbol{\nabla}\mathbf{E}(\xi) = \boldsymbol{\nabla}\bar{\mathbf{F}}_h(\xi) - \boldsymbol{\nabla}\mathbf{F}(\xi)$ may be viewed as a linear map from $T_\xi Q$ to T_xK. In other words, if $\hat{e}(\xi) \longmapsto \boldsymbol{\nabla}\bar{\mathbf{F}}_h(\xi)\hat{e}(\xi) \in T_{\bar{x}}\bar{K}$, then $\boldsymbol{\nabla}\bar{\mathbf{F}}_h(\xi)\hat{e}(\xi)$ is parallel transported to T_xK.

Therefore, $\boldsymbol{\nabla}\bar{\mathbf{F}}_h$ is nonsingular and

$$\begin{aligned}\|(\boldsymbol{\nabla}\bar{\mathbf{F}}_h)^{-1}\|_{L^\infty(Q)} &= \|\left(\mathbf{I}+(\boldsymbol{\nabla}\mathbf{F})^{-1}\boldsymbol{\nabla}\mathbf{E}\right)^{-1}(\boldsymbol{\nabla}\mathbf{F})^{-1}\|_{L^\infty(Q)}\\ &\le \|\left(\mathbf{I}+(\boldsymbol{\nabla}\mathbf{F})^{-1}\boldsymbol{\nabla}\mathbf{E}\right)^{-1}\|_{L^\infty(Q)}\|(\boldsymbol{\nabla}\mathbf{F})^{-1}\|_{L^\infty(Q)}\\ &\le 2\|\boldsymbol{\nabla}\mathbf{F}^{-1}\|_{L^\infty(K)}.\end{aligned}$$

Since $\|\boldsymbol{\nabla}\bar{\mathbf{F}}_h^{-1}\|_{L^\infty(\bar{K})} = \|(\boldsymbol{\nabla}\bar{\mathbf{F}}_h)^{-1}\|_{L^\infty(Q)}$, we get (128). The estimates (129) and (130) follow easily from (127) and (128), respectively. □

Given an element $Q \in \mathcal{Q}_h$, let $\hat{e}_1$ and $\hat{e}_2$ be tangent vectors associated with any two adjacent edges having lengths $h_{\hat{e}_1} = \|\hat{e}_1\|$ and $h_{\hat{e}_2} = \|\hat{e}_2\|$, respectively. Let $\bar{e}_1$ and $\bar{e}_2$ denote the corresponding edges of $\bar{K}$, of lengths $h_{\bar{e}_1}$ and $h_{\bar{e}_2}$, respectively. Then, we have (see Box 1)

$$\frac{h_{\bar{e}_1}}{h_{\bar{e}_2}} \le \|\boldsymbol{\nabla}\bar{\mathbf{F}}_h^{-1}\|_{L^\infty(\bar{K})}\|\boldsymbol{\nabla}\bar{\mathbf{F}}_h\|_{L^\infty(Q)}\frac{h_{\hat{e}_1}}{h_{\hat{e}_2}} \le C_{shape}\,. \tag{137}$$

where we also used the shape regularity of $\mathcal{Q}_h$ in the last bound.

We have indeed more, as stated in the next result.

Lemma 5.3. *Under the assumption of Lemma 5.2, the family of vertex meshes $\{\bar{\mathcal{K}}_h\}_h$ is shape-regular.*

Proof. Since a uniform bound on the edge lengths ratio follows immediately from (137), we are only left to prove a minimum angle condition for $\{\bar{\mathcal{K}}_h\}_h$. We will start addressing the case $d = 2$. In addiction to the notation introduced above, denote by $\bar{\theta}$ the angle shared by the two adjacent edges $\bar{e}_1$ and $\bar{e}_2$ of $\bar{K}$. We will prove that

$$|\sin\bar{\theta}| \ge C_{shape} > 0. \tag{138}$$

Denoting by $\hat{e}_1$ and $\hat{e}_2$ the two corresponding edges of Q, and $\xi \in Q$ the common vertex, then basic geometrical arguments give

$$|\sin\bar{\theta}| = \frac{\|\bar{e}_1 \times \bar{e}_2\|}{\|\bar{e}_1\|\,\|\bar{e}_2\|} = \frac{\|\boldsymbol{\nabla}\bar{\mathbf{F}}_h(\xi)\hat{e}_1 \times \boldsymbol{\nabla}\bar{\mathbf{F}}_h(\xi)\hat{e}_2\|}{\|\boldsymbol{\nabla}\bar{\mathbf{F}}_h(\xi)\hat{e}_1\|\,\|\boldsymbol{\nabla}\bar{\mathbf{F}}_h(\xi)\hat{e}_2\|} \tag{139}$$

where "$\times$" stands for the cross product. Since $\hat{e}_1$ and $\hat{e}_2$ are orthogonal, then $\|A\hat{e}_1 \times A\hat{e}_2\| = |\det A|\|\hat{e}_1\|\|\hat{e}_2\|$ for all matrices $A \in \mathbb{R}^{2\times 2}$. Therefore, from (139), we have

$$|\sin\bar{\theta}| \ge \frac{|\det\boldsymbol{\nabla}\bar{\mathbf{F}}_h(\xi)|}{\|\boldsymbol{\nabla}\bar{\mathbf{F}}_h(\xi)\|^2}. \tag{140}$$

The uniform lower bound (138) now follows from (140) and Lemma 5.2.

The case $d = 3$ follows similarly, the main difference being that now the inequality

$$|\det A|\|\hat{e}_1\|\|\hat{e}_2\|\|\hat{e}_3\| \;=\; |(A\hat{e}_1 \times A\hat{e}_2)\cdot A\hat{e}_3| \le \|A\hat{e}_1 \times A\hat{e}_2\|\|A\|\|\hat{e}_3\|, \tag{141}$$

which holds for any orthogonal vectors $\hat{e}_1$, $\hat{e}_2$ and $\hat{e}_3$, is used to bound $\|\boldsymbol{\nabla}\bar{\mathbf{F}}_h(\xi)\hat{e}_1 \times \boldsymbol{\nabla}\bar{\mathbf{F}}_h(\xi)\hat{e}_2\|$ from below. □

In order to prove Theorem 5.1 we use a *macroelement* technique (see [36],[35]). A macroelement $\bar{M}$ is a connected set of elements $\bar{K} \in \bar{\mathcal{K}}_h$ (precisely, $\bar{M}$ is the interior of the union of the closure of adjacent elements $\bar{K}$), therefore a subset of $\bar{\Omega}_h$. In two dimensions we consider macroelements made of two quadrilaterals that share an edge, while in three dimensions we consider macroelements made of four adjacent hexahedra such that each shares two faces with other two hexahedra and one edge with the last hexahedron. We denote by $h_{\bar{M}}$ the diameter of $\bar{M}$. We assume that the mesh $\mathcal{Q}_h$ is made at least of 2×1 or of $2 \times 2 \times 1$ elements when $d = 2$ or $d = 3$ respectively, so that a macroelement partitioning $\bar{\mathcal{M}}_h$ of $\bar{\Omega}_h$ can be found (with possibly overlapping macroelements) such that each $\bar{K} \in \bar{\mathcal{K}}_h$ is contained in at least one and no more than two (if $d = 2$) or four (if $d = 3$) macroelements $\bar{M}$ of $\bar{\mathcal{M}}_h$.

We associate to a macroelement $\bar{M} \in \bar{\mathcal{M}}_h$ the set

$$\hat{M} = \bar{\mathbf{F}}_h^{-1}(\bar{M}) = \left\{ \xi \in (0,1)^d \text{ such that } \bar{\mathbf{F}}_h(\xi) \in \bar{M} \right\}.$$

$\hat{M}$ is a macroelement on $(0,1)^d$.

For a macroelement $\bar{M}$ we define the spaces

$$\bar{V}_{0,\bar{M}} = \bar{V}_{h|\bar{M}} \cap H_0^1(\bar{M}), \tag{142}$$

$$\bar{P}_{\bar{M}} = \bar{P}_{h|\bar{M}}; \tag{143}$$

moreover, for brevity we denote by $(\cdot,\cdot)_{\bar{M}}$ the $L^2(\bar{M})$ scalar product.

The next step is to obtain a local inf-sup condition, for the spaces $\bar{V}_{0,\bar{M}}$ and $\bar{P}_{\bar{M}}$.

Lemma 5.4. *Under the assumption of Lemma 5.2, there exists a constant $C_{shape} > 0$ such that, given $\bar{M} \in \bar{\mathcal{M}}_h$ and given any $\bar{q} \in \bar{P}_{\bar{M}}$, there exists a $\bar{\mathbf{v}} \in \bar{V}_{0,\bar{M}}$ for which*

$$\begin{aligned} &(\boldsymbol{\nabla} \cdot \bar{\mathbf{v}}, \bar{q})_{\bar{M}} \geq C_{shape} h_{\bar{M}} |\bar{q}|_{H^1(\bar{M})} - C'_{shape} h_{\bar{M}} \, \|\boldsymbol{\nabla} \bar{\mathbf{F}}_h^{-1}\|_{L^\infty(\bar{M})} \, \|\bar{q}\|_{L^2(\bar{M})}, \\ &|\bar{\mathbf{v}}|_{H^1(\bar{M})} \leq 1. \end{aligned} \tag{144}$$

Proof. In [35], a similar inf-sup condition for quadrilateral Taylor-Hood type elements, which in our context correspond to the case when w is constant and $d = 2$, is proven. The purely polynomial case for $d = 3$ is an easy extension of that result. We take it as a starting point for our analysis: specifically, from [35] one can easily obtain:

$$w = \text{constant} \qquad \Rightarrow \qquad \sup_{\bar{\mathbf{v}} \in \bar{V}_{0,\bar{M}}} \frac{(\boldsymbol{\nabla} \cdot \bar{\mathbf{v}}, \bar{q})_{\bar{M}}}{|\bar{\mathbf{v}}|_{H^1(\bar{M})}} \geq C_{shape} h_{\bar{M}} |\bar{q}|_{H^1(\bar{M})}, \quad \forall \bar{q} \in \bar{P}_{\bar{M}}. \tag{145}$$

Note that a key ingredient of the proof in [35] (and therefore of (145)) is the regularity of the mesh, here given by Lemma 5.3.

The inf-sup condition (145) implies that, when w is not a constant and introducing $\bar{w} = w \circ \bar{\mathbf{F}}_h^{-1}$, we have

$$\sup_{\bar{\mathbf{v}} \in \bar{V}_{0,\bar{M}}} \frac{(\boldsymbol{\nabla} \cdot (\bar{w}\bar{\mathbf{v}}), \bar{w}\bar{q})_{\bar{M}}}{|\bar{w}\bar{\mathbf{v}}|_{H^1(\bar{M})}} \geq C_{shape} h_{\bar{M}} |\bar{w}\bar{q}|_{H^1(\bar{M})}, \qquad \forall \bar{q} \in \bar{P}_{\bar{M}}. \tag{146}$$

Given $\bar{q} \in \bar{P}_{\bar{M}}$, we denote by $\bar{\mathbf{v}}^* \in \bar{V}_{0,\bar{M}}$ a function which realizes maximum of the quantity $(\boldsymbol{\nabla} \cdot (\bar{w}\bar{\mathbf{v}}), \bar{w}\bar{q})_{\bar{M}} / |\bar{w}\bar{\mathbf{v}}|_{H^1(\bar{M})}$. We want to show that

$$\frac{(\boldsymbol{\nabla} \cdot \bar{\mathbf{v}}^*, \bar{q})_{\bar{M}}}{|\bar{\mathbf{v}}^*|_{H^1(\bar{M})}} \geq C_{shape} h_{\bar{M}} |\bar{q}|_{H^1(\bar{M})} - C'_{shape} h_{\bar{M}} \, \|\boldsymbol{\nabla} \bar{\mathbf{F}}_h^{-1}\|_{L^\infty(\bar{M})} \|\bar{q}\|_{L^2(\bar{M})}, \tag{147}$$

which gives (144).

Denoting by $\bar{w}_{mv}$ the mean value of $\bar{w}$ on $\bar{M}$, we have

$$\begin{aligned}(\boldsymbol{\nabla}\cdot(\bar{w}\bar{\mathbf{v}}^*),\bar{w}\bar{q})_{\bar{M}} &= (\bar{w}\boldsymbol{\nabla}\bar{w}\cdot\bar{\mathbf{v}}^*,\bar{q})_{\bar{M}} + (\bar{w}^2\boldsymbol{\nabla}\cdot\bar{\mathbf{v}}^*,\bar{q})_{\bar{M}}\\ &= (\bar{w}\boldsymbol{\nabla}\bar{w}\cdot\bar{\mathbf{v}}^*,\bar{q})_{\bar{M}} + ((\bar{w}^2-\bar{w}_{mv}^2)\boldsymbol{\nabla}\cdot\bar{\mathbf{v}}^*,\bar{q})_{\bar{M}} + (\bar{w}_{mv}^2\boldsymbol{\nabla}\cdot\bar{\mathbf{v}}^*,\bar{q})_{\bar{M}}\\ &= I + II + III.\end{aligned} \tag{148}$$

Recalling that $\bar{\mathbf{F}}_h(\hat{M}) = \bar{M}$ and making use of the chain rule, we have

$$\begin{aligned}\|\bar{w}\|_{L^\infty(\bar{M})} &= \|w\|_{L^\infty(\hat{M})},\\ \|\boldsymbol{\nabla}\bar{w}\|_{L^\infty(\bar{M})} &\le \|\boldsymbol{\nabla}w\|_{L^\infty(\hat{M})}\|\boldsymbol{\nabla}\bar{\mathbf{F}}_h^{-1}\|_{L^\infty(\bar{M})},\end{aligned} \tag{149}$$

while, from the Friedrich-Poincaré inequality,

$$\begin{aligned}\|\bar{w}-\bar{w}_{mv}\|_{L^\infty(\bar{M})} &\le Ch_{\bar{M}}\|\boldsymbol{\nabla}\bar{w}\|_{L^\infty(\bar{M})}\\ &\le Ch_{\bar{M}}\|\boldsymbol{\nabla}w\|_{L^\infty(\hat{M})}\|\boldsymbol{\nabla}\bar{\mathbf{F}}_h^{-1}\|_{L^\infty(\bar{M})}\end{aligned} \tag{150}$$

and

$$\|\bar{\mathbf{v}}^*\|_{L^2(\bar{M})} \le Ch_{\bar{M}}\|\boldsymbol{\nabla}\bar{\mathbf{v}}^*\|_{L^2(\bar{M})}. \tag{151}$$

Notice also that, from the definition of C_{shape} and recalling that $\bar{w}_{mv}$ is positive, we can write

$$\begin{aligned}\|w\|_{L^\infty(\hat{M})} &\le C_{shape}\,\bar{w}_{mv}\\ \|\boldsymbol{\nabla}w\|_{L^\infty(\hat{M})} &\le C_{shape}\,\bar{w}_{mv}.\end{aligned} \tag{152}$$

Therefore, using the Cauchy-Schwarz inequality, (149), (151), and (152), we have

$$\begin{aligned}I &= (\bar{w}\boldsymbol{\nabla}\bar{w}\cdot\bar{\mathbf{v}}^*,\bar{q})_{\bar{M}}\\ &\le \|\bar{w}\|_{L^\infty(\bar{M})}\|\boldsymbol{\nabla}\bar{w}\|_{L^\infty(\bar{M})}\|\bar{\mathbf{v}}^*\|_{L^2(\bar{M})}\|\bar{q}\|_{L^2(\bar{M})}\\ &\le Ch_{\bar{M}}\|w\|_{L^\infty(\hat{M})}\|\boldsymbol{\nabla}w\|_{L^\infty(\hat{M})}\|\boldsymbol{\nabla}\bar{\mathbf{F}}_h^{-1}\|_{L^\infty(\bar{M})}|\bar{\mathbf{v}}^*|_{H^1(\bar{M})}\|\bar{q}\|_{L^2(\bar{M})}\\ &\le h_{\bar{M}}C_{shape}\,\bar{w}_{mv}^2\|\boldsymbol{\nabla}\bar{\mathbf{F}}_h^{-1}\|_{L^\infty(\bar{M})}|\bar{\mathbf{v}}^*|_{H^1(\bar{M})}\|\bar{q}\|_{L^2(\bar{M})}.\end{aligned} \tag{153}$$

Furthermore, using the Cauchy-Schwarz inequality, (149), (150), and (152), we have

$$\begin{aligned}II &= ((\bar{w}^2-\bar{w}_{mv}^2)\boldsymbol{\nabla}\cdot\bar{\mathbf{v}}^*,\bar{q})_{\bar{M}}\\ &\le \|\bar{w}-\bar{w}_{mv}\|_{L^\infty(\bar{M})}\|\bar{w}+\bar{w}_{mv}\|_{L^\infty(\bar{M})}|\bar{\mathbf{v}}^*|_{H^1(\bar{M})}\|\bar{q}\|_{L^2(\bar{M})}\\ &\le Ch_{\bar{M}}\|\boldsymbol{\nabla}w\|_{L^\infty(\hat{M})}\|w\|_{L^\infty(\hat{M})}\|\boldsymbol{\nabla}\bar{\mathbf{F}}_h^{-1}\|_{L^\infty(\bar{M})}|\bar{\mathbf{v}}^*|_{H^1(\bar{M})}\|\bar{q}\|_{L^2(\bar{M})}\\ &\le h_{\bar{M}}C_{shape}\,\bar{w}_{mv}^2\|\boldsymbol{\nabla}\bar{\mathbf{F}}_h^{-1}\|_{L^\infty(\bar{M})}|\bar{\mathbf{v}}^*|_{H^1(\bar{M})}\|\bar{q}\|_{L^2(\bar{M})},\end{aligned} \tag{154}$$

while, of course,

$$III = \bar{w}_{mv}^2(\boldsymbol{\nabla}\cdot\bar{\mathbf{v}}^*,\bar{q})_{\bar{M}}. \tag{155}$$

Using again the chain rule and (149), we have

$$\begin{aligned}|\bar{q}|_{H^1(\bar{M})} &= |\frac{\bar{w}\bar{q}}{\bar{w}}|_{H^1(\bar{M})}\\ &\le \|\frac{\boldsymbol{\nabla}(\bar{w}\bar{q})}{\bar{w}}\|_{L^2(\bar{M})} + \|\bar{w}\bar{q}\boldsymbol{\nabla}\frac{1}{\bar{w}}\|_{L^2(\bar{M})}\\ &\le \|\frac{1}{\bar{w}}\|_{L^\infty(\bar{M})}\|\boldsymbol{\nabla}(\bar{w}\bar{q})\|_{L^2(\bar{M})} + \|\boldsymbol{\nabla}\frac{1}{\bar{w}}\|_{L^\infty(\bar{M})}\|\bar{w}\|_{L^\infty(\bar{M})}\|\bar{q}\|_{L^2(\bar{M})}\\ &\le \|\frac{1}{w}\|_{L^\infty(\hat{M})}|\bar{w}\bar{q}|_{H^1(\bar{M})} + \|\boldsymbol{\nabla}\bar{\mathbf{F}}_h^{-1}\|_{L^\infty(\bar{M})}\|\boldsymbol{\nabla}\frac{1}{w}\|_{L^\infty(\hat{M})}\|w\|_{L^\infty(\hat{M})}\|\bar{q}\|_{L^2(\bar{M})},\end{aligned} \tag{156}$$

which implies, using $\|\frac{1}{w}\|^{-1}_{L^\infty(\bar{M})} \geq C_{shape}\bar{w}_{mv}$, as well as $\|\boldsymbol{\nabla}\frac{1}{w}\|_{L^\infty(\hat{M})}\|w\|_{L^\infty(\hat{M})} \leq C_{shape}$,

$$\begin{aligned}|\bar{w}\bar{q}|_{H^1(\bar{M})} &\geq \|\frac{1}{w}\|^{-1}_{L^\infty(\bar{M})}\left(|\bar{q}|_{H^1(\bar{M})} - \|\boldsymbol{\nabla}\bar{\mathbf{F}}_h^{-1}\|_{L^\infty(\bar{M})}\|\boldsymbol{\nabla}\frac{1}{w}\|_{L^\infty(\hat{M})}\|w\|_{L^\infty(\hat{M})}\|\bar{q}\|_{L^2(\bar{M})}\right)\\ &\geq C_{shape}\bar{w}_{mv}\left(|\bar{q}|_{H^1(\bar{M})} - \|\boldsymbol{\nabla}\bar{\mathbf{F}}_h^{-1}\|_{L^\infty(\bar{M})}\|\bar{q}\|_{L^2(\bar{M})}\right).\end{aligned} \tag{157}$$

In a similar way, using also the Poincaré inequality $\|\bar{w}\bar{\mathbf{v}}^*\|_{L^2(\bar{M})} \leq Ch_{\bar{M}}|\bar{w}\bar{\mathbf{v}}^*|_{H^1(\bar{M})}$, we have

$$\begin{aligned}|\bar{\mathbf{v}}^*|_{H^1(\bar{M})} &\leq \|\frac{1}{w}\|_{L^\infty(\hat{M})}|\bar{w}\bar{\mathbf{v}}^*|_{H^1(\bar{M})} + \|\boldsymbol{\nabla}\bar{\mathbf{F}}_h^{-1}\|_{L^\infty(\bar{M})}\|\boldsymbol{\nabla}\frac{1}{w}\|_{L^\infty(\hat{M})}\|\bar{w}\bar{\mathbf{v}}^*\|_{L^2(\bar{M})}\\ &\leq \left(\|\frac{1}{w}\|_{L^\infty(\hat{M})} + Ch_{\bar{M}}\|\boldsymbol{\nabla}\bar{\mathbf{F}}_h^{-1}\|_{L^\infty(\bar{M})}\|\boldsymbol{\nabla}\frac{1}{w}\|_{L^\infty(\hat{M})}\right)|\bar{w}\bar{\mathbf{v}}^*|_{H^1(\bar{M})}.\end{aligned} \tag{158}$$

Moreover, following the steps as in (156)–(157) and using $h_{\bar{M}} \leq h_{\hat{M}}\|\boldsymbol{\nabla}\bar{\mathbf{F}}_h\|_{L^\infty(\hat{M})} \leq \|\boldsymbol{\nabla}\bar{\mathbf{F}}_h\|_{L^\infty(\hat{M})}$ together with $\|\boldsymbol{\nabla}\bar{\mathbf{F}}_h^{-1}\|_{L^\infty(\bar{M})}\|\boldsymbol{\nabla}\bar{\mathbf{F}}_h\|_{L^\infty(\hat{M})} \leq C_{shape}\|\boldsymbol{\nabla}\mathbf{F}^{-1}\|_{L^\infty(\mathbf{F}(\hat{M}))}\|\boldsymbol{\nabla}\mathbf{F}\|_{L^\infty(\hat{M})} \leq C_{shape}$, we have

$$|\bar{w}\bar{\mathbf{v}}^*|_{H^1(\bar{M})} \geq C_{shape}\bar{w}_{mv}|\bar{\mathbf{v}}^*|_{H^1(\bar{M})} \tag{159}$$

Recalling that $\bar{\mathbf{v}}^*$ attains the supremum in (146), we can now collect the estimates (157), (159) and (153)–(155), getting

$$\begin{aligned}&h_{\bar{M}}\bar{w}_{mv}\left(|\bar{q}|_{H^1(\bar{M})} - \|\boldsymbol{\nabla}\bar{\mathbf{F}}_h^{-1}\|_{L^\infty(\bar{M})}\|\bar{q}\|_{L^2(\bar{M})}\right)\\ &\quad\leq C_{shape}h_{\bar{M}}|\bar{w}\bar{q}|_{H^1(\bar{M})}\\ &\quad\leq C_{shape}\frac{(\boldsymbol{\nabla}\cdot(\bar{w}\bar{\mathbf{v}}^*),\bar{w}\bar{q})}{|\bar{w}\bar{\mathbf{v}}^*|_{H^1(\bar{M})}}\\ &\quad\leq C_{shape}\frac{I+II+III}{\bar{w}_{mv}|\bar{\mathbf{v}}^*|_{H^1(\bar{M})}}\\ &\quad\leq C_{shape}\left(h_{\bar{M}}\bar{w}_{mv}\|\boldsymbol{\nabla}\bar{\mathbf{F}}_h^{-1}\|_{L^\infty(\bar{M})}\|\bar{q}\|_{L^2(\bar{M})} + \frac{\bar{w}_{mv}(\boldsymbol{\nabla}\cdot\bar{\mathbf{v}}^*,\bar{q})}{|\bar{\mathbf{v}}^*|_{H^1(\bar{M})}}\right),\end{aligned} \tag{160}$$

which is, after dividing by $\bar{w}_{mv}$, (147). This concludes the proof. □

We can get now a global inf-sup condition for the spaces $\bar{V}_h \cap H^1_0(\bar{\Omega}_h)$ and $\bar{P}_h$. We set

$$\bar{h} = \max_{\bar{K}\in\bar{\mathcal{K}}_h} h_{\bar{K}}. \tag{161}$$

Lemma 5.5. *Under the assumption of Lemma 5.2, there exists a constant $C_{shape} > 0$ such that, given any $\bar{q} \in \bar{P}_h$, there exists a $\bar{\mathbf{v}} \in \bar{V}_h \cap H^1_0(\bar{\Omega}_h)$ for which*

$$\begin{aligned}&(\boldsymbol{\nabla}\cdot\bar{\mathbf{v}},\bar{q}) \geq C_{shape}\left(\sum_{\bar{K}\in\bar{\mathcal{K}}_h} h^2_{\bar{K}}|\bar{q}|^2_{H^1(\bar{K})}\right)^{1/2} - C'_{shape}\bar{h}\|\boldsymbol{\nabla}\bar{\mathbf{F}}_h^{-1}\|_{L^\infty(\bar{\Omega}_h)}\|\bar{q}\|_{L^2(\bar{\Omega}_h)},\\ &|\bar{\mathbf{v}}|_{H^1(\bar{\Omega}_h)} \leq 1.\end{aligned} \tag{162}$$

Proof. For each macroelement $\bar{M} \in \mathcal{M}_h$, let $\bar{\mathbf{w}}_{\bar{M}} \in \bar{V}_h \cap H^1_0(\bar{\Omega}_h)$ such that $\bar{\mathbf{w}}_{\bar{M}} = 0$ in $\bar{\Omega}_h/\bar{M}$ and, according to Lemma 5.4,

$$\begin{aligned}&(\boldsymbol{\nabla}\cdot\bar{\mathbf{w}}_{\bar{M}},\bar{q})_{\bar{M}} \geq C_{shape}h_{\bar{M}}|\bar{q}|_{H^1(\bar{M})} - C'_{shape}h_{\bar{M}}\,\|\boldsymbol{\nabla}\bar{\mathbf{F}}_h^{-1}\|_{L^\infty(\bar{M})}\,\|\bar{q}\|_{L^2(\bar{M})},\\ &|\bar{\mathbf{w}}_{\bar{M}}|_{H^1(\bar{M})} \leq 1.\end{aligned}$$

Setting

$$\bar{\mathbf{w}} = \sum_{\bar{M}\in\mathcal{M}_h} h_{\bar{M}} |\bar{q}|_{H^1(\bar{M})} \bar{\mathbf{w}}_{\bar{M}},$$

it is easy to see that (162) holds true for the rescaled vector field $\mathbf{v} = \bar{\mathbf{w}}/|\bar{\mathbf{w}}|_{H^1(\bar{\Omega}_h)}$. □

We are now ready to show the following proposition, which is the counterpart of Lemma 5.5 for the NURBS spaces V_h, P_h.

Proposition 5.1. *Under the assumption of Lemma 5.2, there exists a constant $C_{shape} > 0$ such that, given any $q \in P_h$, there exists a $\mathbf{v} \in V_h \cap H^1_0(\Omega)$ for which*

$$\begin{aligned} &(\boldsymbol{\nabla}\cdot\mathbf{v}, q) \geq C_{shape} \left(\sum_{K\in\mathcal{K}_h} h_K^2 |q|^2_{H^1(K)} \right)^{1/2} - C'_{shape} h \|q\|_{L^2(\Omega)}, \\ &|\mathbf{v}|_{H^1(\Omega)} \leq 1. \end{aligned} \tag{163}$$

Proof. Given any function q in P_h, we define $\hat{q} \in \hat{P}_h$ and $\bar{q} \in \bar{P}_h$

$$\hat{q} = q \circ \mathbf{F} \qquad \bar{q} = \hat{q} \circ \bar{\mathbf{F}}_h^{-1} \tag{164}$$

Due to Lemma 5.5, we have the existence of a function $\bar{\mathbf{v}} \in \bar{V}_h$ such that (162) holds true. We introduce the functions $\hat{\mathbf{v}} \in \hat{V}_h$ and $\mathbf{v} \in V_h$ as

$$\hat{\mathbf{v}} = \bar{\mathbf{v}} \circ \bar{\mathbf{F}}_h \qquad \mathbf{v} = \hat{\mathbf{v}} \circ \mathbf{F}^{-1} \tag{165}$$

Recalling Lemma 5.2 and that $\|\boldsymbol{\nabla}\mathbf{F}^{-1}\|_{L^\infty(\Omega)} \|\boldsymbol{\nabla}\mathbf{F}\|_{L^\infty((0,1)^d)} \leq C_{shape}$, change of variables leads to the bounds

$$\|\hat{q}\|_{L^2((0,1)^d)} \leq C_{shape} \|\boldsymbol{\nabla}\mathbf{F}^{-1}\|^{d/2}_{L^\infty(\Omega)} \|q\|_{L^2(\Omega)}, \tag{166}$$

$$|\hat{v}|_{H^1((0,1)^d)} \leq C_{shape} \|\boldsymbol{\nabla}\mathbf{F}^{-1}\|^{d/2-1}_{L^\infty(\Omega)} |\bar{v}|_{H^1(\bar{\Omega}_h)}, \tag{167}$$

$$\|\bar{q}\|_{L^2(\bar{\Omega}_h)} \leq C_{shape} \|q\|_{L^2(\Omega)}, \tag{168}$$

$$h_K |q|_{H^1(K)} \leq C_{shape} h_{\bar{K}} |\bar{q}|_{H^1(\bar{K})} \qquad \forall \bar{K} \in \bar{\mathcal{K}}_h, \tag{169}$$

$$|\mathbf{v}|_{H^1(\Omega)} \leq C_{shape} |\bar{\mathbf{v}}|_{H^1(\bar{\Omega}_h)}. \tag{170}$$

A direct change of variables and simple algebra now give

$$\begin{aligned} (\boldsymbol{\nabla}\cdot\mathbf{v}, q) &= \int_\Omega (\boldsymbol{\nabla}\cdot\mathbf{v}) q \\ &= \int_{(0,1)^d} \mathrm{tr}(|\mathrm{det}\boldsymbol{\nabla}\mathbf{F}| \boldsymbol{\nabla}\mathbf{F}^{-T} \boldsymbol{\nabla}\hat{\mathbf{v}}^T) \hat{q} \\ &= \int_{(0,1)^d} \mathrm{tr}(\, [\, |\mathrm{det}\boldsymbol{\nabla}\mathbf{F}| \boldsymbol{\nabla}\mathbf{F}^{-T} - |\mathrm{det}\boldsymbol{\nabla}\bar{\mathbf{F}}_h| \boldsymbol{\nabla}\bar{\mathbf{F}}_h^{-T} \,] \, \boldsymbol{\nabla}\hat{\mathbf{v}}^T \,) \, \hat{q} \\ &\quad + \int_{(0,1)^d} \mathrm{tr}(|\mathrm{det}\boldsymbol{\nabla}\bar{\mathbf{F}}_h| \boldsymbol{\nabla}\bar{\mathbf{F}}_h^{-T} \boldsymbol{\nabla}\hat{\mathbf{v}}^T) \hat{q} \\ &= I + II. \end{aligned} \tag{171}$$

We now note that

$$(\mathrm{det}A) A^{-T} = \mathrm{Cof}(A) \qquad \forall A \in \mathbb{R}^{d\times d},\ \mathrm{det}\mathbb{A} \neq 0 \tag{172}$$

where $\mathrm{Cof}(\mathbb{A})$ is the cofactor matrix of $\mathbb{A}$. Therefore, from the definition of $\bar{\mathbf{F}}_h$ and classical interpolation results, it follows

$$\| \, |\mathrm{det}\boldsymbol{\nabla}\mathbf{F}|\boldsymbol{\nabla}\mathbf{F}^{-T} - \, |\mathrm{det}\boldsymbol{\nabla}\bar{\mathbf{F}}_h|\boldsymbol{\nabla}\bar{\mathbf{F}}_h^{-T} \, \|_{L^\infty((0,1)^d)} \leq C_{shape} \, \|\boldsymbol{\nabla}\mathbf{F}\|^{d-1}_{L^\infty((0,1)^d)} \, h \tag{173}$$

where a factor $\|\boldsymbol{\nabla}^2\mathbf{F}\|_{L^\infty((0,1)^d)}/\|\boldsymbol{\nabla}\mathbf{F}\|_{L^\infty((0,1)^d)}$ was included in C_{shape}. Note that this estimate requires the use of NURBS of at least quadratic level. If linear NURBS are utilized the actual geometry is the vertex mesh. Inequality (173) is an estimate of the difference between the actual geometry and the corresponding vertex mesh.

As a consequence, using first the Holder inequality and (173), then (167) and (166), and recalling that $|\bar{v}|_{H^1(\bar{\Omega}_h)} \leq 1$ and $\|\boldsymbol{\nabla}\mathbf{F}^{-1}\|_{L^\infty(\Omega)}\|\boldsymbol{\nabla}\mathbf{F}\|_{L^\infty((0,1)^d)} \leq C_{shape}$, we obtain

$$\begin{aligned} I &\geq -C_{shape}\|\boldsymbol{\nabla}\mathbf{F}\|^{d-1}_{L^\infty((0,1)^d)} \, h \, \|\hat{q}\|_{L^2((0,1)^d)}|\hat{\mathbf{v}}|_{H^1((0,1)^d)} \\ &\geq -C_{shape} h\|q\|_{L^2(\Omega)}. \end{aligned} \tag{174}$$

For term II, first a change of variables and then using (162) we get

$$II = \int_{\bar{\Omega}_h} \mathrm{tr}(\boldsymbol{\nabla}\bar{\mathbf{v}})\bar{q} \geq C_{shape} \left(\sum_{\bar{K}\in\bar{\mathcal{K}}_h} h^2_{\bar{K}}|\bar{q}|^2_{H^1(\bar{K})} \right)^{1/2} - C'_{shape}\bar{h}\|\boldsymbol{\nabla}\bar{\mathbf{F}}_h^{-1}\|_{L^\infty(\bar{\Omega}_h)}\|\bar{q}\|_{L^2(\bar{\Omega}_h)} \tag{175}$$

Without showing the details, using the bounds (168), (169), using Lemma 5.2 and recalling that $\bar{h} \leq h\|\boldsymbol{\nabla}\mathbf{F}\|_{L^\infty((0,1)^d)}$, we easily have

$$\begin{aligned} & C_{shape} \left(\sum_{\bar{K}\in\bar{\mathcal{K}}_h} h^2_{\bar{K}}|\bar{q}|^2_{H^1(\bar{K})} \right)^{1/2} - C'_{shape}\bar{h}\|\boldsymbol{\nabla}\bar{\mathbf{F}}_h^{-1}\|_{L^\infty(\bar{\Omega}_h)}\|\bar{q}\|_{L^2(\bar{\Omega}_h)} \\ & \qquad \geq C_{shape} \left(\sum_{K\in\mathcal{K}_h} h^2_K|q|^2_{H^1(K)} \right)^{1/2} - C'_{shape} h\|q\|_{L^2(\Omega)}. \end{aligned} \tag{176}$$

Bounds (175) and (176) now give

$$II \geq C_{shape} \left(\sum_{K\in\mathcal{K}_h} h^2_K|q|^2_{H^1(K)} \right)^{1/2} - C'_{shape} h\|q\|_{L^2(\Omega)}. \tag{177}$$

After rescaling of $\mathbf{v}$, the identity (171) with the bounds (174) and (177), (162) and (170), finally give (163). □

Replacing q with $q - q_{mv}$ in (163), where q_{mv} is the mean value of q on Ω, we get the following obvious corollary.

Corollary 5.1. *As in Proposition 5.1, given any $q \in P_h$, there exists a $\mathbf{v} \in V_h \cap H^1_0(\Omega)$ such that*

$$\begin{aligned} & (\boldsymbol{\nabla}\cdot\mathbf{v}, q) \geq C_{shape} \left(\sum_{K\in\mathcal{K}_h} h^2_K|q|^2_{H^1(K)} \right)^{1/2} - C'_{shape} h\|q\|_{L^2(\Omega)/\mathbb{R}}, \\ & |\mathbf{v}|_{H^1(\Omega)} \leq 1. \end{aligned} \tag{178}$$

We are now able to show the proof of Theorem 5.2.

Proof. (*Theorem* 5.2) We will use an argument from Verfürth (see [38]). Due to the validity of the continuous inf-sup condition on Ω and recalling that $P_h \in L^2(\Omega)$, we have the existence of a fixed positive constant C^*_{shape} such that for all $q \in P_h$ there exists a $\mathbf{w} \in H^1_0(\Omega)$ such that

$$(\boldsymbol{\nabla} \cdot \mathbf{w}, q) \geq C^*_{shape} \|q\|_{L^2(\Omega)/\mathbb{R}} \tag{179}$$

$$|\mathbf{w}|_{H^1(\Omega)} \leq 1 \tag{180}$$

where we introduced the notation C^*_{shape} in order to keep track of the constants in what follows. Using the scaled Poincaré inequality

$$\|\mathbf{w}\|_{L^2(\Omega)} \leq \operatorname{diam}(\Omega) |\mathbf{w}|_{H^1(\Omega)},$$

bound (180) is equivalent to

$$\left(\sum_{K \in \mathcal{K}_h} \|\boldsymbol{\nabla} \mathbf{F}\|^{-2}_{L^\infty(\mathbf{F}^{-1}(K))} \|\mathbf{w}\|^2_{L^2(K)} \right)^{1/2} + |\mathbf{w}|_{H^1(\Omega)} \leq C_{shape} \tag{181}$$

From Theorem 3.3 there exists a NURBS function $\mathbf{w}_I \in H^1_0(\Omega)$ such that, for all $K \in \mathcal{K}_h$,

$$\|\mathbf{w} - \mathbf{w}_I\|^2_{L^2(K)} \leq C_{shape}\, h_K^2 \left(\|\boldsymbol{\nabla} \mathbf{F}\|^{-2}_{L^\infty(\mathbf{F}^{-1}(K))} \|\mathbf{w}\|^2_{L^2(\tilde{K})} + |\mathbf{w}|^2_{H^1(\tilde{K})} \right), \tag{182}$$

and, using also (181)

$$|\mathbf{w}_I|_{H^1(\Omega)} \leq C_{shape} \left[\left(\sum_{K \in \mathcal{K}_h} \|\boldsymbol{\nabla} \mathbf{F}\|^{-2}_{L^\infty(\mathbf{F}^{-1}(K))} \|\mathbf{w}\|^2_{L^2(K)} \right)^{1/2} + |\mathbf{w}|_{H^1(\Omega)} \right] \leq C_{shape}\,. \tag{183}$$

First integrating by parts, then using the Cauchy-Schwarz inequality and (179), finally applying (182) and (181), it follows

$$\begin{aligned}
(\boldsymbol{\nabla} \cdot \mathbf{w}_I, q) &= (\boldsymbol{\nabla} \cdot (\mathbf{w}_I - \mathbf{w}), q) + (\boldsymbol{\nabla} \cdot \mathbf{w}, q) \\
&\geq - \sum_{K \in \mathcal{K}_h} \|\mathbf{w}_I - \mathbf{w}\|_{L^2(K)} |q|_{H^1(K)} + C^*_{shape} \|q\|_{L^2(\Omega)/\mathbb{R}} \\
&\geq -C_{shape} \left(\sum_{K \in \mathcal{K}_h} \|\boldsymbol{\nabla} \mathbf{F}\|^{-2}_{L^\infty(\mathbf{F}^{-1}(K))} \|\mathbf{w}\|^2_{L^2(\tilde{K})} + |\mathbf{w}|^2_{H^1(\tilde{K})} \right)^{1/2} \left(\sum_{K \in \mathcal{K}_h} h_K^2 |q|^2_{H^1(K)} \right)^{1/2} \\
&\quad + C^*_{shape} \|q\|_{L^2(\Omega)/\mathbb{R}} \\
&\geq -C_{shape,1} \left(\sum_{K \in \mathcal{K}_h} h_K^2 |q|^2_{H^1(K)} \right)^{1/2} + C^*_{shape} \|q\|_{L^2(\Omega)/\mathbb{R}}
\end{aligned} \tag{184}$$

Now, due to Corollary 5.1 and integrating by parts, we have the existence of a $\mathbf{v} \in V_h \cap H^1_0(\Omega)$ such that

$$(\boldsymbol{\nabla} \cdot \mathbf{v}, q) \geq C_{shape,2} \left(\sum_{K \in \mathcal{K}_h} h_K^2 |q|^2_{H^1(K)} \right)^{1/2} - C_{shape,3}\, h \|q\|_{L^2(\Omega)/\mathbb{R}} \tag{185}$$

$$|\mathbf{v}|_{H^1(\Omega)} \leq 1 \tag{186}$$

We now introduce $\mathbf{v}' = \mathbf{w}_I + \alpha \mathbf{v}$ with $\alpha = C_{shape,1}/C_{shape,2}$. From (184) and (185) it follows

$$\begin{aligned}(\boldsymbol{\nabla} \cdot \mathbf{v}', q) &\geq (\alpha C_{shape,2} - C_{shape,1}) \left(\sum_{K \in \mathcal{K}_h} h_K^2 |q|^2_{H^1(K)} \right)^{1/2} \\ &\quad + (C^*_{shape} - \alpha C_{shape,3}\, h) \|q\|_{L^2(\Omega)/\mathbb{R}} \\ &= (C^*_{shape} - \frac{C_{shape,1}\, C_{shape,3}}{C_{shape,2}} h) \|q\|_{L^2(\Omega)/\mathbb{R}} \end{aligned} \tag{187}$$

¿From (183) and (186) it is immediate to show that

$$|\mathbf{v}'|_{H^1(\Omega)} \leq C_{shape} \tag{188}$$

Assume now that the mesh $\mathcal{Q}_h$ satisfies

$$h \leq h''_{max} := \frac{1}{2} \frac{C^*_{shape} C_{shape,2}}{C_{shape,1}\, C_{shape,3}} \tag{189}$$

Then from (187) it follows

$$(\boldsymbol{\nabla} \cdot \mathbf{v}', q) \geq \frac{C^*_{shape}}{2} \|q\|_{L^2(\Omega)/\mathbb{R}} \tag{190}$$

for all meshes in the family.

Therefore, joining (190) and (188), we have found a positive constant C^*_{shape} such that for all $q \in P_h$ we have the existence of a $\mathbf{v}' \in V_h$ that satisfies

$$(\boldsymbol{\nabla} \cdot \mathbf{v}', q) \geq \frac{C^*_{shape}}{2} \|q\|_{L^2(\Omega)/\mathbb{R}} \tag{191}$$

$$|\mathbf{v}'|_{H^1(\Omega)} \leq C_{shape} \tag{192}$$

Finally, note that the control on the globally constant pressures follows easily due to the fact that $\Gamma_D \neq \partial\Omega$. The proposition is proved. □

Remark 5.2. *Note that, in order for Theorem 5.1 to be valid, both the bound (189) and the assumptions of Lemma 5.2 must be satisfied. Therefore the h_{max} in Theorem 5.1 is given by*

$$h_{max} = \min\left(h'_{max}, h''_{max}\right)$$

Remark 5.3. *The numerical tests of the last section seem to show that the method is stable and convergent for practical values of the mesh size. Then, the condition $h \leq h_{\max}$, which is needed in the present theoretical analysis, does not seem to be restrictive in the practical case we have considered.*

Remark 5.4. *The analysis of this section can be extended straightforwardly to the anisotropic case where the displacement space is of polynomial degree $p_1 + 1, p_2 + 1, .., p_d + 1$ and the pressure space $p_1, p_2, .., p_d$. The only point which differs is the starting polynomial inf-sup condition (145), while the rest remains identical. The extension of such inf-sup condition to the anisotropic case can be obtained with an easy modification of Lemma 3.2 in [35].*

5.4 Advection-diffusion

As before, let Ω be the physical domain, and let $\Gamma_D \equiv \partial\Omega$. Let $f : \Omega \to \mathbb{R}$ be the given body force; $\boldsymbol{a} : \Omega \to \mathbb{R}^d$ is the spatially varying velocity vector and $\mathbf{K} : \Omega \to \mathbb{R}^{d\times d}$ is the diffusivity tensor, assumed symmetric positive definite; homogeneous Dirichlet boundary conditions on Γ_D are prescribed. The boundary value problem consists of solving the following equation for $u : \overline{\Omega} \to \mathbb{R}$:

$$\mathcal{L}u = f \quad \text{in } \Omega, \tag{193}$$
$$u = 0 \quad \text{on } \Gamma_D, \tag{194}$$

where

$$\mathcal{L}u = \boldsymbol{a}\cdot\boldsymbol{\nabla}u - \boldsymbol{\nabla}\cdot(\mathbf{K}\boldsymbol{\nabla}u). \tag{195}$$

For the purposes of analysis we assume divergence-free advective velocity field and isotropic diffusion:

$$\boldsymbol{\nabla}\cdot\boldsymbol{a} = 0, \tag{196}$$
$$\mathbf{K} = \kappa\mathbf{I}, \tag{197}$$

where κ is a positive constant. The weak formulation of (193) is: find $u \in H^1_{\Gamma_D}(\Omega)$ such that $\forall v \in H^1_{\Gamma_D}(\Omega)$:

$$B(u,v) = F(v) \quad \text{in } \Omega, \tag{198}$$

where

$$B(u,v) = (v, \boldsymbol{a}\cdot\boldsymbol{\nabla}u)_\Omega + (\boldsymbol{\nabla}v, \kappa\boldsymbol{\nabla}u)_\Omega, \tag{199}$$
$$F(v) = (v,f)_\Omega. \tag{200}$$

We wish to approximate (198) numerically in the NURBS space $\mathcal{V}_h$ defined in Section 2 of this document. Galerkin's method is known to be unstable for (198) when advection dominates, so we choose to concentrate on the set of techniques known as "stabilized methods", namely SUPG, GLS and Multiscale (dubbed MS for brevity). The MS version is also referred to as the adjoint, or "unusual," stabilized method in the literature. These methods were designed to enhance stability of Galerkin's approach without compromising its accuracy. For background and early literature on these formulations we refer the reader to [9], while the state-of-the-art literature on the subject may be found in [20, 28, 37, 12, 14, 10, 22, 6, 21, 5, 2, 30]. Defining $\tilde{\Omega} = \cup K, K \in \mathcal{K}_h$ (i.e., the union of element interiors) and $V_h = \mathcal{V}_h \cap H^1_{\Gamma_D}(\Omega)$, stabilized methods are stated as follows:
SUPG: find $u_h \in V_h$ such that $\forall v_h \in V_h$

$$B^{SUPG}(u_h, v_h) = F^{SUPG}(v_h) \quad \text{in } \Omega, \tag{201}$$

with

$$B^{SUPG}(u,v) = B(u,v) + (\boldsymbol{a}\cdot\boldsymbol{\nabla}v\ \tau, \mathcal{L}u)_{\tilde{\Omega}}, \tag{202}$$
$$F^{SUPG}(v) = F(v) + (\boldsymbol{a}\cdot\boldsymbol{\nabla}v\ \tau, f)_{\tilde{\Omega}}. \tag{203}$$

GLS: find $u_h \in V_h$ such that $\forall v_h \in V_h$

$$B^{GLS}(u_h, v_h) = F^{GLS}(v_h) \quad \text{in } \Omega, \tag{204}$$

with

$$B^{GLS}(u,v) = B(u,v) + (\mathcal{L}v\ \tau, \mathcal{L}u)_{\tilde{\Omega}}, \tag{205}$$
$$F^{GLS}(v) = F(v) + (\mathcal{L}v\ \tau, f)_{\tilde{\Omega}}. \tag{206}$$

MS: find $u_h \in V_h$ such that $\forall v_h \in V_h$

$$B^{MS}(u_h, v_h) = F^{MS}(v_h) \quad \text{in } \Omega, \tag{207}$$

with

$$B^{MS}(u,v) = B(u,v) - (\mathcal{L}^*v\ \tau, \mathcal{L}u)_{\tilde{\Omega}}, \tag{208}$$
$$F^{MS}(v) = F(v) - (\mathcal{L}^*v\ \tau, f)_{\tilde{\Omega}}, \tag{209}$$

where $\mathcal{L}^*$ is an adjoint of $\mathcal{L}$ and is given as

$$\mathcal{L}^*v = -\boldsymbol{a}\cdot\boldsymbol{\nabla}v - \kappa\Delta v. \tag{210}$$

In expressions (201)-(207) a stabilization parameter τ appears, its definition is critical for accuracy, stability and convergence characteristics of the above methods. We adopt expressions presented in Franca, Frey and Hughes [17] and give them here for completeness:

$$\tau(x, \mathrm{Pe}_K(x)) = \frac{h_K}{2\|\boldsymbol{a}(x)\|}\xi(\mathrm{Pe}_K(x)) \tag{211}$$
$$\mathrm{Pe}_K(x) = \frac{\|\boldsymbol{a}(x)\|h_K}{2\kappa} \tag{212}$$
$$\xi(\mathrm{Pe}_K(x)) = \min\{m_k\mathrm{Pe}_K(x), 1\} \tag{213}$$
$$m_K = \min\{\frac{1}{3}, \frac{2}{C_{inv}}\} \tag{214}$$

The above expressions are defined from error analysis considerations. K is any element in the partition $\mathcal{K}_h$ of Ω, C_{inv} is the smallest constant satisfying the local inverse estimate of Theorem 4.1 with a corresponding definition of h_K.

We briefly show analysis of stabilized formulations for advection-diffusion employing NURBS approximation spaces. The approach we use is very similar to that of the stabilized formulations of incompressible elasticity. In what follows we concentrate on SUPG, other methods are analyzed in a similar fashion.

Lemma 5.6. *The bilinear form defined in (201) inherits the following stability property:*

$$B^{SUPG}(w,w) \geq C|||w|||^2 \quad \forall w \in V_h, \tag{215}$$

where

$$|||w|||^2 = \kappa\|\boldsymbol{\nabla}w\|^2_{L^2(\Omega)} + \|\tau^{1/2}\boldsymbol{a}\cdot\boldsymbol{\nabla}w\|^2_{L^2(\Omega)}. \tag{216}$$

The above result, which can be easily verified (see, for example, Franca, Frey and Hughes [17]), is a consequence of boundary conditions, definition of the stabilization parameter τ, and the inverse estimate of Theorem 4.1. Continuity properties of $B^{SUPG}(\cdot,\cdot)$ are stated in the following lemma.

Lemma 5.7. *The bilinear form defined in (201) is continuous in the following sense:*

$$B^{SUPG}(w,v) \leq C|||w||| \; ||||v|||| \quad \forall w \in V_h, \;\; \forall v \in H^1_{\Gamma_D}(\Omega) \cap H^2(\tilde{\Omega}), \tag{217}$$

with the norm above is defined as

$$\begin{aligned} ||||v||||^2 &= \kappa \|\boldsymbol{\nabla} v\|^2_{L^2(\Omega)} + \|\tau^{-1/2} v\|^2_{L^2(\Omega)} \\ &+ \|\tau^{1/2} \boldsymbol{a} \cdot \boldsymbol{\nabla} v\|^2_{L^2(\Omega)} + \|\tau^{1/2} \kappa \Delta v\|^2_{L^2(\tilde{\Omega})}. \end{aligned} \tag{218}$$

This result follows by a direct computation. Having established coercivity and continuity, we proceed with the error estimate as follows. Define the following quantities

$$e = u - u_h \quad \text{(numerical error)} \tag{219}$$

$$\eta = u - \Pi^0_{\mathcal{V}_h} u \quad \text{(interpolation error)} \tag{220}$$

$$e_h = \Pi^0_{\mathcal{V}_h} u - u_h = \Pi^0_{\mathcal{V}_h} e \quad \text{(discrete error)}, \tag{221}$$

and compute:

$$\begin{aligned} |||e_h|||^2 &\leq C \; B(e_h, e_h) \quad \text{(coercivity)} \\ &= C \; B(e_h, -\eta) \quad \text{(Galerkin orthogonality)} \\ &\leq C|||e_h||| \; ||||\eta|||| \quad \text{(continuity)}. \end{aligned} \tag{222}$$

Relation (222) combined with the triangle inequality gives a bound on the numerical error in the solution in terms of the interpolation error

$$|||e||| \leq C||||\eta||||. \tag{223}$$

The following theorem establishes convergence rates of the methods in question posed over NURBS spaces.

Theorem 5.3. *Assuming $u \in H^{p+1}$, there exists $C_{shape} > 0$ such that*

$$|||u - u_h|||^2 \leq C \sum_K (\|\boldsymbol{a}\|_{L^\infty(K)} {h_K}^{2p+1} + \kappa {h_K}^{2p}) \sum_{i=0}^{p+1} \|\boldsymbol{\nabla} \mathbf{F}\|^{2(i-p-1)}_{L^\infty(\mathbf{F}^{-1}(K))} |u|^2_{H^i(K)} \tag{224}$$

Proof. Given the definition of τ, the following bounds are easily established (see, for example, Franca, Frey and Hughes [17]):

$$\|\tau^{-1/2}\eta\|^2_{L^2(K)} \leq C(\kappa/h_K^2 + \|\boldsymbol{a}\|_{L^\infty(K)}/h_K)\|\eta\|^2_{L^2(K)}, \tag{225}$$

$$\|\tau^{1/2}\boldsymbol{a} \cdot \boldsymbol{\nabla}\eta\|^2_{L^2(K)} \leq C(\kappa + \|\boldsymbol{a}\|_{L^\infty(K)} h_K)\|\boldsymbol{\nabla}\eta\|^2_{L^2(K)}, \tag{226}$$

$$\|\tau^{1/2}\kappa\Delta\eta\|^2_{L^2(K)} \leq C(\kappa h_K^2 + \|\boldsymbol{a}\|_{L^\infty(K)} h_K^3)\|\Delta\eta\|^2_{L^2(K)}. \tag{227}$$

Using inequality (223) together with the above bounds, the local error estimate (61), and summing over all the elements in $\mathcal{K}_h$ yields the final result. □

6 Numerical Examples

In this section we report on the results of numerical computations performed with NURBS. We consider examples from compressible and incompressible linear elasticity as well as advection-diffusion. The first two examples were already presented in [25], we repeat them here as evidence in support of convergence theory put forth in the preceding sections of this document. On all the convergence plots the error quantity plotted on the ordinate axis is absolute. In all cases computational results are in agreement with the theoretical findings.

6.1 Solid elastic circular cylinder subjected to internal pressure loading

This problem falls within the framework of Section 5.1. The problem specification is shown in Figure 5. It is a simple matter to obtain an exact solution assuming the pressure varies at most circumferentially (see Gould [19], pp. 117-119). The internal pressure was assumed to vary as $\cos(2\theta)$ and the exact solution is thus of class C^∞. Meshes developed from h-refinement are shown in Figure 6. Quadratic, cubic, and quartic NURBS were employed. As in all of the examples considered herein, the exact geometry is incorporated in the coarsest mesh and is maintained throughout the refinement process. A rational quadratic basis is the minimum order capable of exactly representing the cylindrical geometry. The cubic and quartic cases were obtained from the quadratic case by k-refinement [25, 13], in which case the degree of continuity was increased to C^2 and C^3, respectively. The rates of convergence of the error measured in the energy norm (the natural norm for the problem, equivalent to the H^1-norm) are presented in Figure 7. The rates of convergence for quadratic, cubic, and quartic NURBS elements are optimal, that is, 2, 3, and 4, respectively. This problem falls within the hypotheses of our theoretical framework and the optimal convergence rates are consistent with the results of Section 5.1.

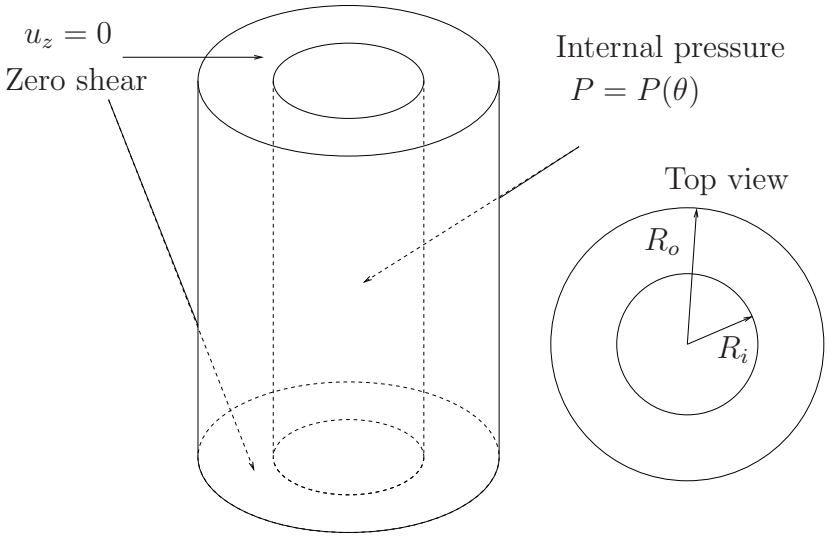

Figure 5: Thick cylinder pressurized internally.

6.2 Infinite elastic plate with circular hole under constant in-plane tension in the x-direction

This is a two-dimensional problem of linear elasticity, falling within the framework of section 5.1. The infinite plate is modeled by a finite quarter plate. The exact solution (Gould [19], pp. 120-123), evaluated at the boundary of the finite quarter plate, is applied as a Neumann boundary condition. The setup is illustrated in Figure 8. T_x is the magnitude of the applied stress at infinity, R is the radius of the traction-free hole, L is the length of the finite quarter plate, E is Young's modulus, and ν is Poisson's ratio. As in the previous example, a rational quadratic basis is the minimum order capable of exactly representing a circle.

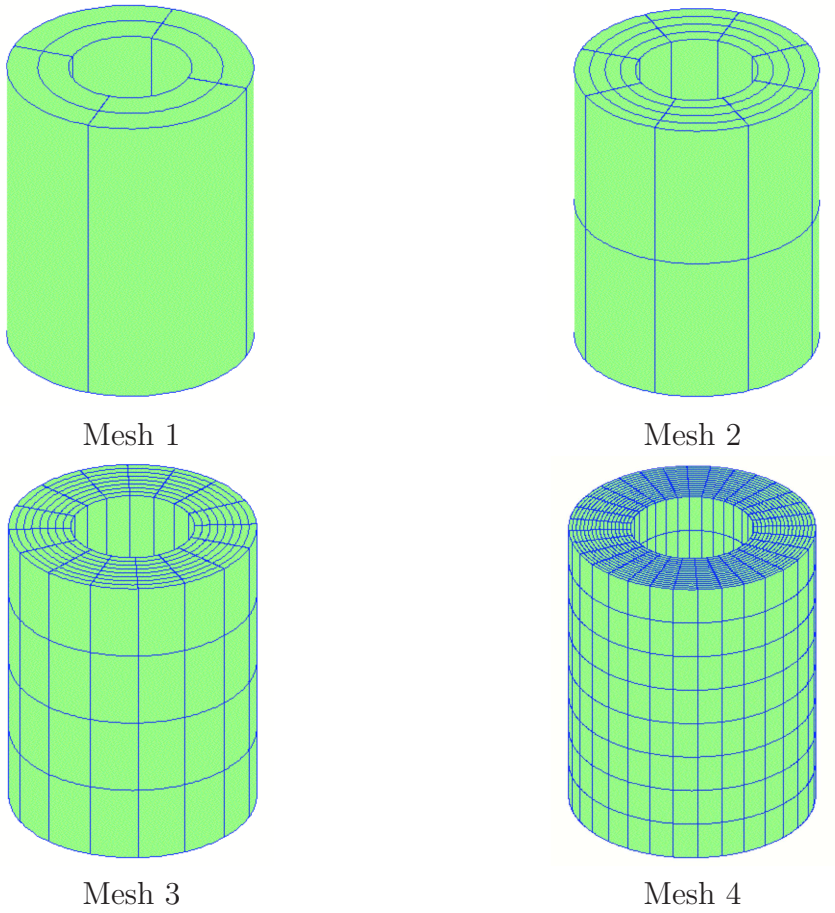

Figure 6: Solid circular cylinder meshes

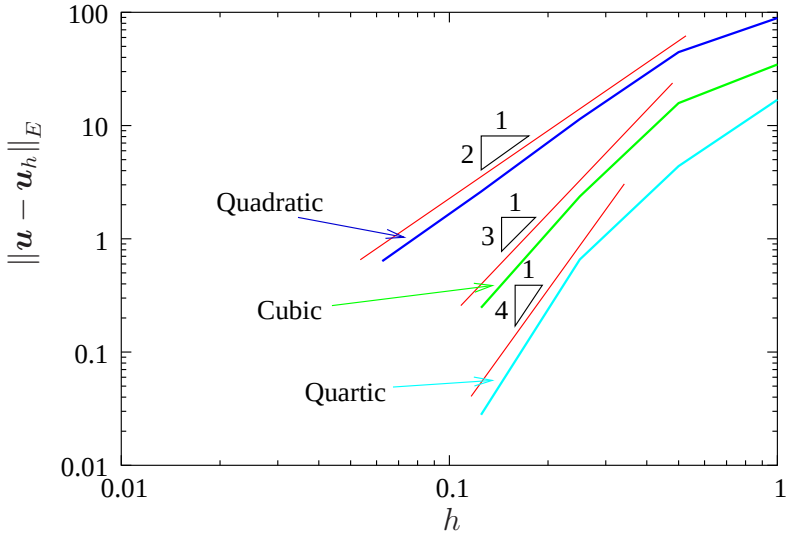

Figure 7: Solid circular cylinder with varying internal pressure. Convergence of the error in the energy norm for quadratic, cubic, and quartic NURBS discretizations.

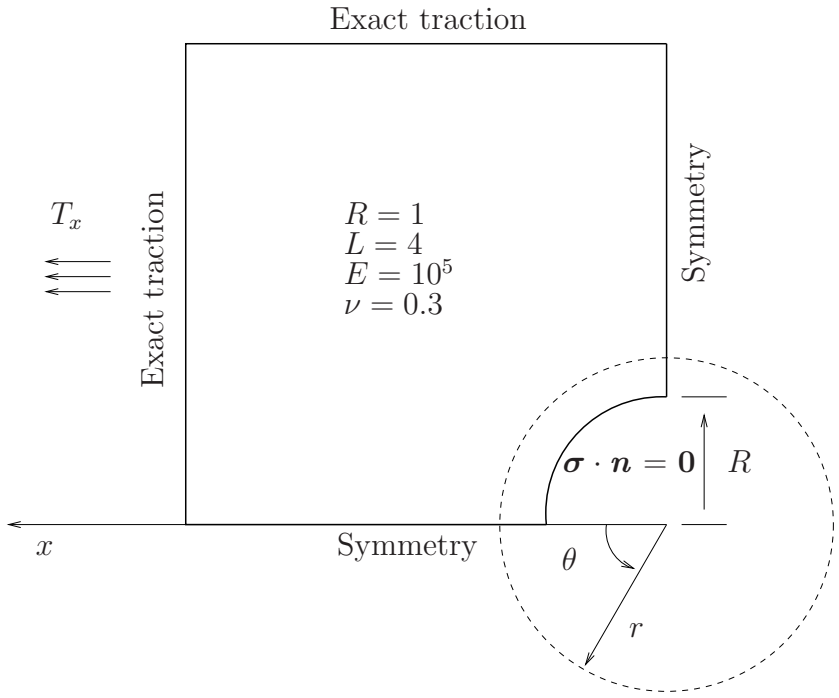

Figure 8: Elastic plate with a circular hole: problem definition.

The first six meshes used in the analysis are shown in Figure 9. The cubic and quartic NURBS are obtained by order elevation of the quadratic NURBS on the coarsest mesh (for details of the geometry and mesh construction, see [25]). Continuity of the basis is C^{p-1} everywhere, except along the line which joins the center of the circular edge with the upper left-hand corner of the domain. There it is C^1 as is dictated by the coarsest mesh employing rational quadratic parameterization. Convergence results in the L^2-norm of stresses (which is equivalent to the H^1-seminorm of the displacements) are shown in Figure 10. As can be seen, the L^2-convergence rates of stress for quadratic, cubic, and quartic NURBS are 2, 3, and 4, respectively. The geometrical mapping used in this example does not conform to the assumptions of the theory, namely, in the elements adjacent to the upper left-hand corner of the domain $\|\boldsymbol{F}^{-1}\|_{W^{1,\infty}}$ is not uniformly bounded. This was a choice, not a neccessity. Nevertheless, optimal convergence rates are still attained.

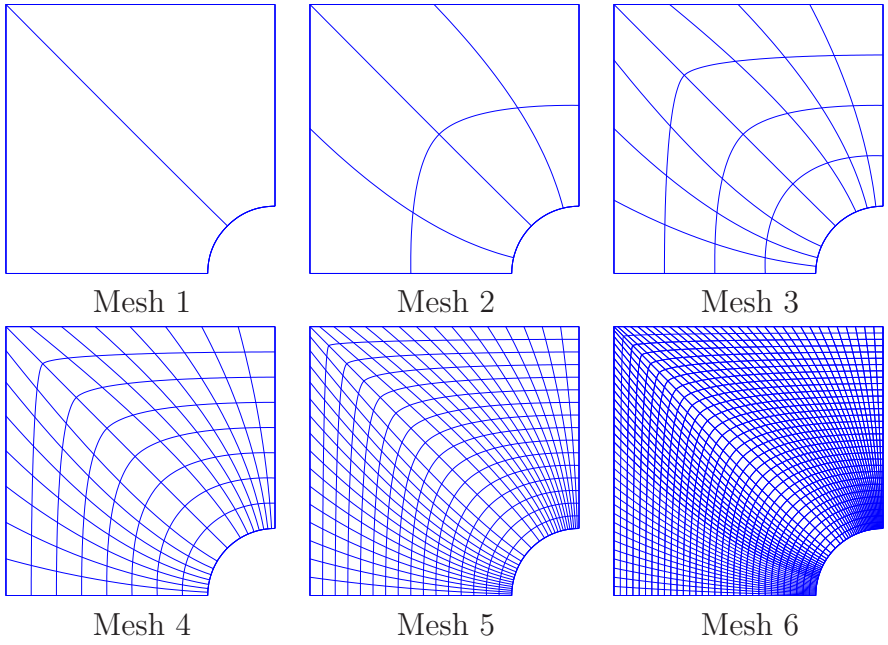

Figure 9: Elastic plate with circular hole. Meshes produced by h-refinement (knot insertion).

6.3 Constrained block subjected to a trigonometric load

In this two-dimensional example we consider a fully constrained square of incompressible elastic material loaded externally. This problem falls within the framework of Sections 5.2 and 5.3. It was designed by Auricchio *et al.* [4], and the setup is illustrated in Figure 11, where $\boldsymbol{u} = (u, v)$ is a displacement vector, μ is the shear modulus and L is the edge half-length. Note that in this case pressure is determined up to an arbitrary constant, so for the purposes of computing an L^2 error of the pressure field, the constant mode is removed from the pressure solution. The load and boundary conditions are selected in such a way that the analytical solution is easily obtained. We give them here for completeness:

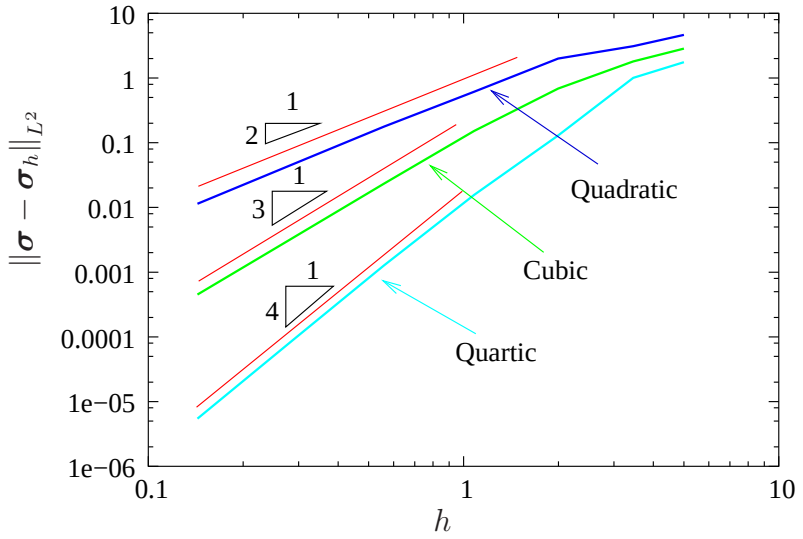

Figure 10: Error measured in the L^2-norm of stress vs. mesh parameter.

$$
\begin{aligned}
u &= -\frac{\cos^2 x \cos y \sin y}{2} \\
v &= \frac{\cos^2 y \cos x \sin x}{2} \\
p &= \sin(x^2 y) \\
f_1 &= \mu \cos y \sin y (1 - 4\cos^2 x) - 2xy \cos(x^2 y) \\
f_2 &= -\mu \cos x \sin x (1 - 4\cos^2 y) - x^2 \cos(x^2 y)
\end{aligned} \tag{228}
$$

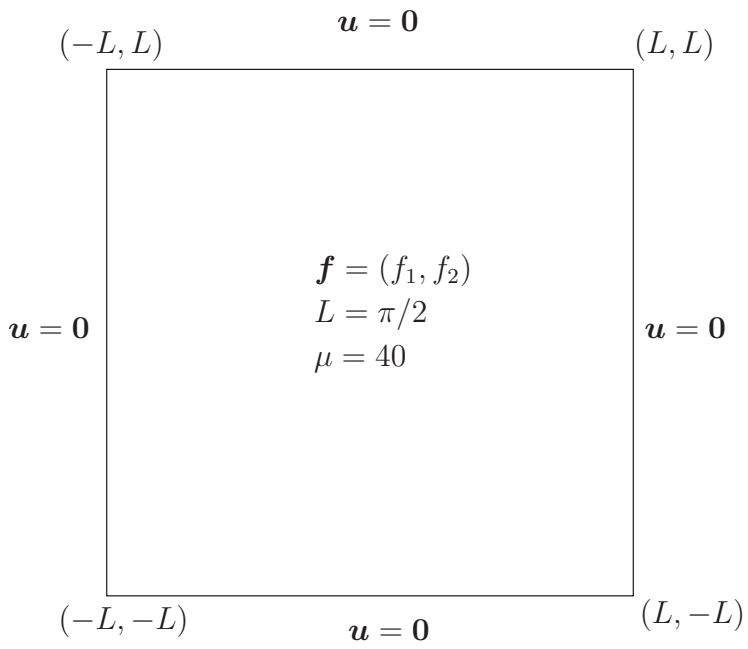

Figure 11: Trigonometric load problem setup.

Meshes 1, 3, and 5 used in the computations are shown in Figure 12. Distortion of the mesh was introduced at the coarsest level of discretization and maintained throughout the refinement. Three studies were performed for this problem. In the first study we used a C^1-continuous rational quadratic basis for both $\mathbf{u}$ and p and employed the Douglas-Wang stabilized formulation. The results of this study are shown on the top plot of Figure 13. The other stabilized methods behaved in the same fashion and thus the results are not shown. Optimal convergence of the L^2-norm and the H^1-seminorm of the displacement error and the L^2-norm of the pressure error is obtained. The results are consistent with the theoretical predictions of Section 5.2. In the second study we used BB-compatible spaces: a C^0 rational quadratic basis for p and C^0 rational cubic basis for $\mathbf{u}$ obtained from the former by degree elevation. These spaces are stable and convergent within Galerkin's method according to the results of Section 5.3. The first four of the five meshes were used in the calculations and the results are presented in the middle plot of Figure 13. All results converge optimally, in agreement with the theory in Section 5.3. In the third study we again used quadratic pressure and cubic displacement, but C^1-continuity was enforced. This case is not covered in the theory of Section 5.3, yet optimal convergence is again obtained, as shown in the bottom plot of Figure 13. We conjecture that this type of discretization is BB-stable.

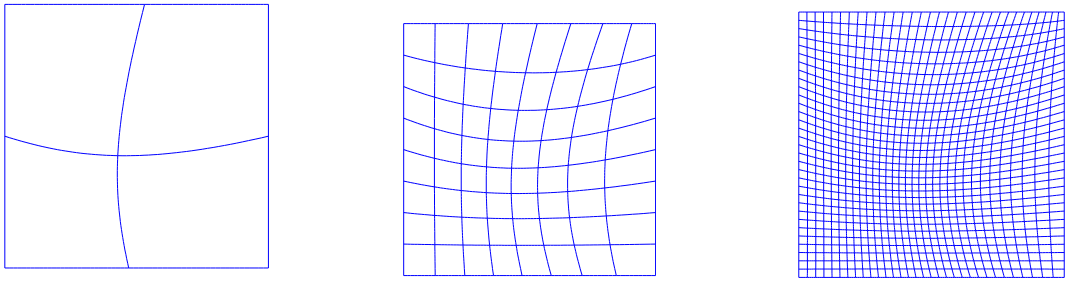

Mesh 1 Mesh 3 Mesh 5

Figure 12: Trigonometric load problem meshes produced by h-refinement (knot insertion).

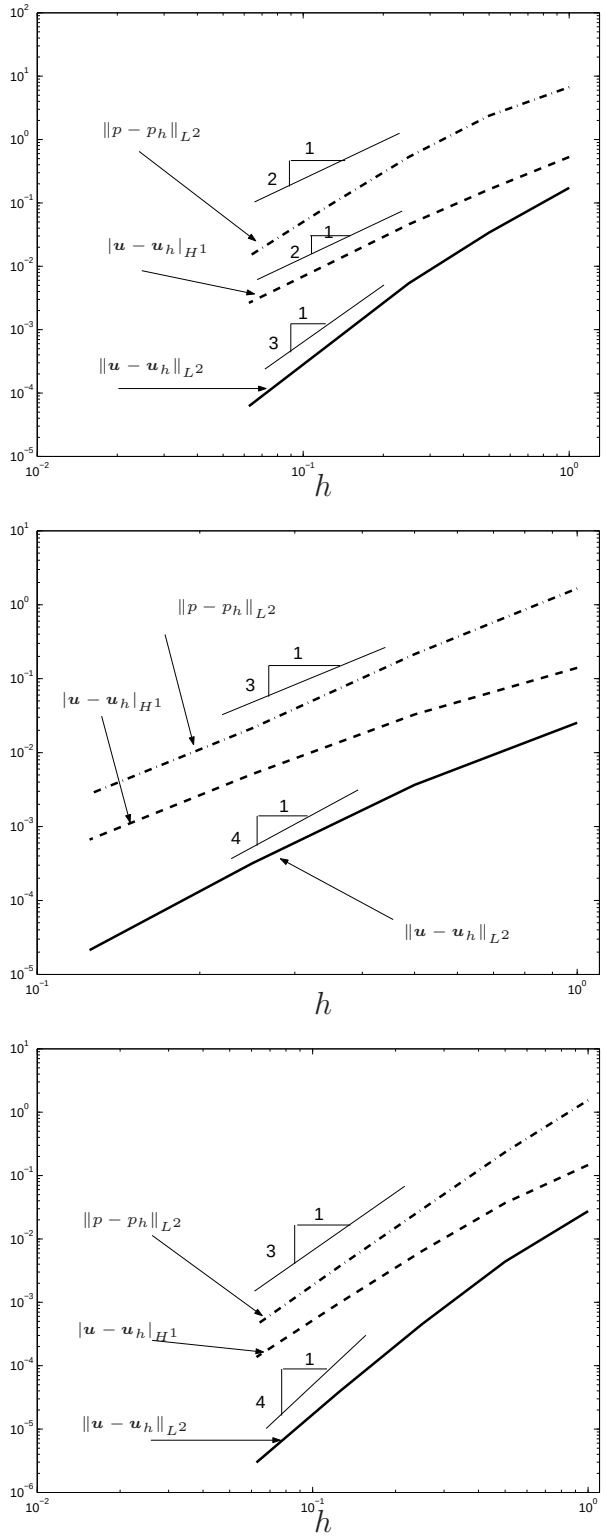

Figure 13: Trigonometric load problem. Convergence to the analytical solution for displacement and pressure. Top: Douglas-Wang stabilization, equal-order, quadratic, C^1-continuous bases. Middle: Galerkin's method, cubic displacement, quadratic pressure, C^0-continuous bases. Bottom: Galerkin's method, cubic displacement, quadratic pressure, C^1-continuous bases.

6.4 Driven cavity problem

The driven cavity problem is a two-dimensional Stokes flow calculation that is often used as a test of numerical stability. The equations of Stokes flow are identical to the equations of linear, isotropic, incompressible elasticity, only the interpretation is different. In Stokes flow $\mathbf{u} = (u, v)$ is the velocity vector and μ is the dynamic viscosity (see, e.g., [23]). In the exact specification of this problem, the velocity boundary condition is discontinuous at the upper two corners, that is, at $(0, L)$ and (L, L); see Figure 14 for the problem setup. This produces singular pressures in both corners which tend to cause unstable formulations to fail in dramatic fashion. The mesh is comprised of 16×16 square elements. In the first two examples, the pressure discretization is taken to be C^1 quadratic splines. The velocity space is the same in the first example and consists of C^1-cubic splines in the second. Figure 15 compares solutions obtained with the Galerkin formulation. As expected, the equal-order combination produces an unstable result, as is especially apparent for pressure, while the mixed interpolation case appears to be quite stable. The solution is very similar to that presented in Franca, Frey and Hughes [17]. Figure 16 shows a stabilized GLS computation for equal-order cases. Both the $p = 2$ and $p = 3$ results appear stable and are again in general agreement with [17]. As may be gleaned from Figures 15 and 16, the velocity at the upper corners is set to $\mathbf{u} = (1, 0)$. This is referred to as the "leaky" boundary condition treatment (see [23] for further elaboration).

Remark 6.1. *Three-dimensional computations of other boundary-value problems (not shown) with the same bases used in this study yielded consistent results, namely, the stabilized methods produced stable calculations with equal-order NURBS whereas the Galerkin formulation did not, and the Galerkin method with velocity one order higher than pressure produced stable results when both velocity and pressure had the same order of continuity across element boundaries. Our theoretical results in Section 5.3 only pertain to C^0-continuous interpolations, but there is considerable evidence that the higher-order uniformly continuous cases are stable as well.*

6.5 Advection-diffusion in a hollow cylinder

The problem geometry and parameters are given on Figure 17. The axisymmetric analytical solution behaves logarithmically in the radial direction and exponentially in the axial direction, viz.,

$$u(r, z) = \frac{(e^{az/\kappa} - e^{aL/\kappa}) \log(r)}{(1 - e^{aL/\kappa}) \log(2)} \tag{229}$$

Four meshes, composed of 32, 256, 2,048 and 16,384 elements, were used. The first three are depicted in Figure 18. The meshes are "biased" toward the outflow where a boundary layer occurs. Two values of the diffusivity were considered. In the first case, κ was chosen to be 0.025, which produces a solution than can be fairly well resolved by meshes 2-4. In the second case, κ was selected to be 0.00625, and the boundary layer is fairly well resolved only by the finest mesh. A rational quadratic basis is employed in each parametric direction and no symmetry was assumed, yet a pointwise axisymmetric response was obtained in all cases as can be seen in Figure 19. All three stabilized formulations were implemented and compared with the Galerkin solution. In the case of the larger value of κ, all methods produced an optimally convergent solution in both the L^2-norm and H^1-seminorm as can be seen in Figure 20. This is consistent with the theory of Section 5.4. The same error norms were computed for the case of smaller diffusivity

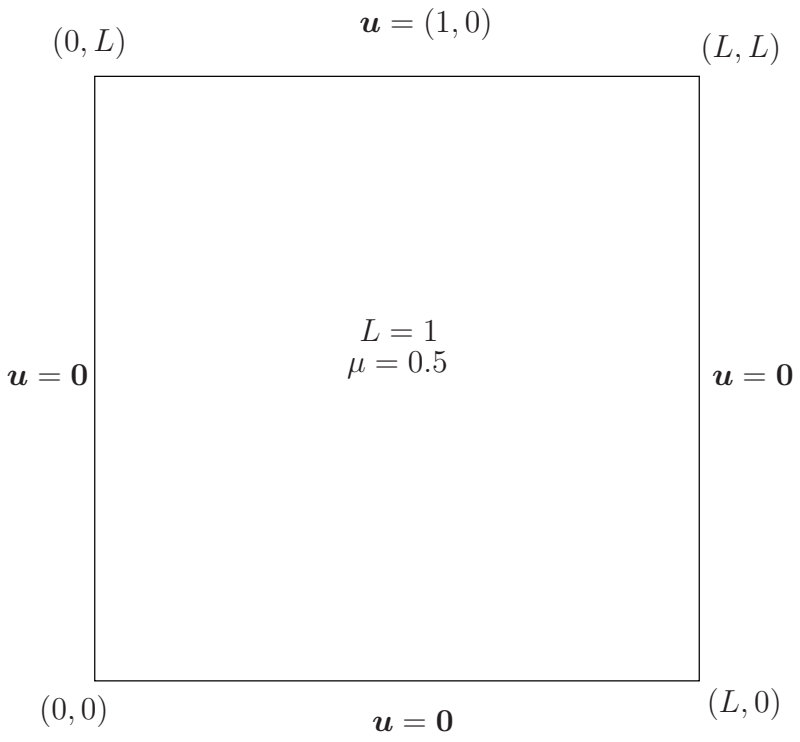

Figure 14: Driven cavity problem setup.

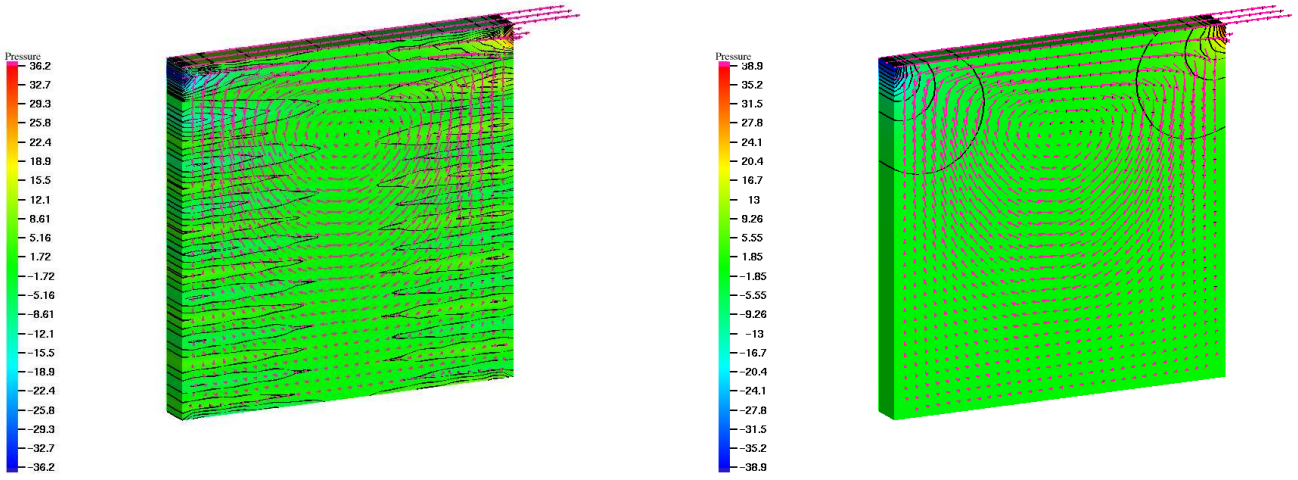

Figure 15: Driven cavity problem. Velocity vectors superposed on pressure contours. Left: Galerkin solution with equal-order discretization ($p = 2$). Right: Galerkin solution with unequal-order discretization ($p = 2$ for the pressure and $p = 3$ for the velocity).

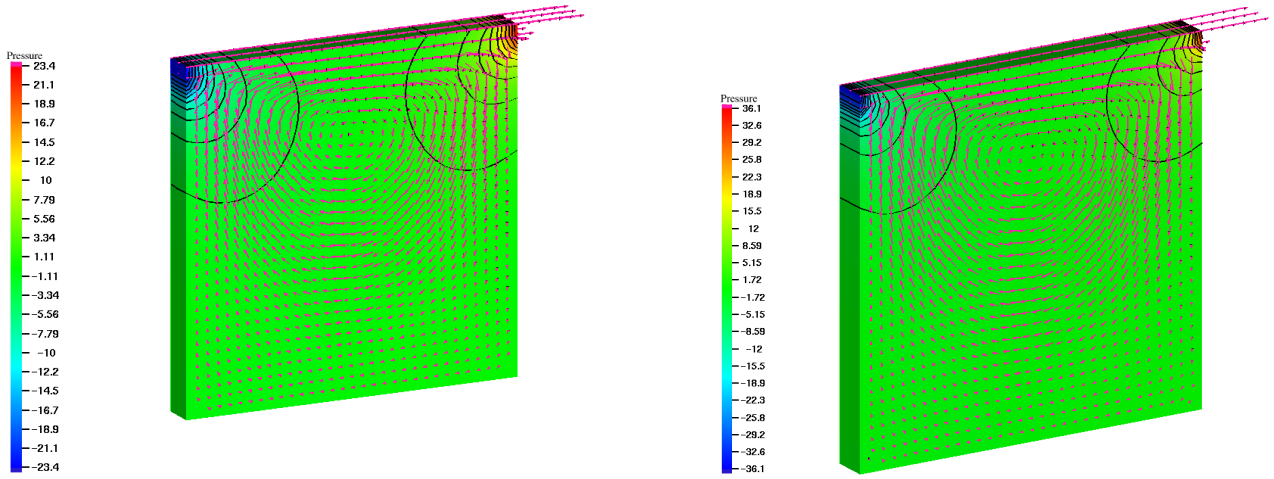

Figure 16: Driven cavity problem. Velocity vectors superposed on pressure contours. GLS solution with equal-order discretization. Left: $p = 2$, Right $p = 3$.

($\kappa = 0.00625$). Galerkin's method produced a globally oscillatory solution on coarser meshes, which resulted in a large global L^2-error compared with the stabilized solutions (see Figure 21). The H^1-error for all methods was suboptimal, which is not surprising, as the major contribution comes from the very thin, unresolved, outflow boundary layer. In order to remove the effect of the boundary layer, we computed the error on the part of the domain which excludes it (i.e., $\{0 < z < 4.95\} \times \{1 < r < 2\}$). The H^1-error is much better behaved for the stabilized methods. The optimal order of convergence is observed for both H^1- and L^2-norms in these cases. The results are typical of stabilized finite element methods in that "localization" or "interior" estimates can be proven (see, e.g., Johnson, Nävert and Pitkäranta [27] and Wahlbin [39]). These estimates are also known *not* to hold for Galerkin finite element methods, for which unresolved layers result in global pollution. This phenomenon is also evident here in Figure 21. On the finest mesh, error measures for the Galerkin and stabilized methods seem to coincide, which suggests that the asymptotic regime has been reached.

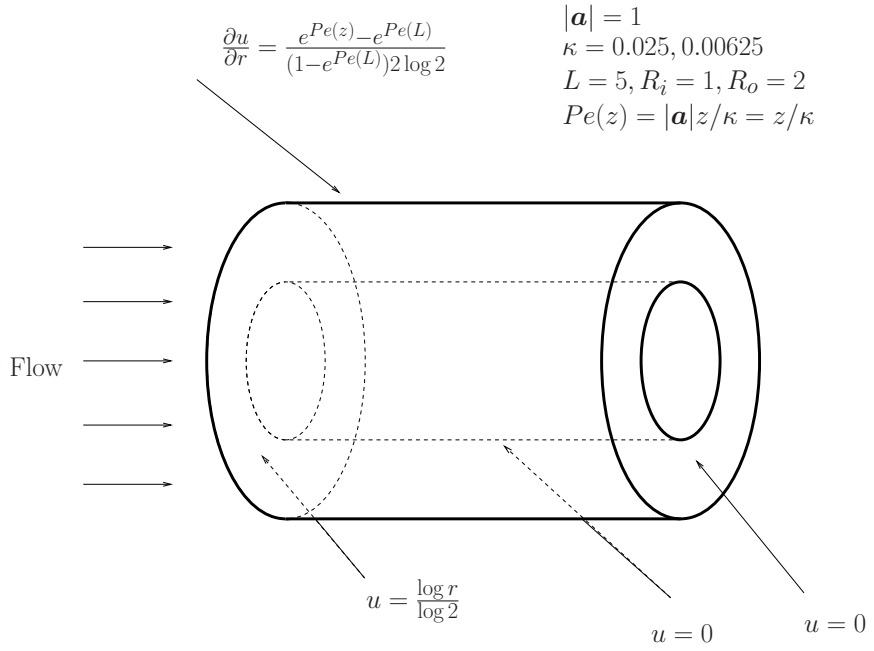

Figure 17: Advection-diffusion in a hollow cylinder. Problem setup.

7 Conclusions

In this paper we initiated the mathematical study of Isogeometric Analysis based on NURBS, an extension of classical finite element analysis. We developed approximation properties based on a new Bramble-Hilbert lemma and new inverse estimates for the cases at hand. Our study focused on h-refinement and did not treat order-elevation methods such as p- or k-refinement. We applied the method to several cases of physical interest, namely, elasticity, isotropic incompressible elasticity and Stokes flow, and advection-diffusion. We considered standard primal and mixed Galerkin methods as well as stabilized methods. All of our numerical results were consistent with our theoretical predictions. We also performed some numerical tests involving singularities and unresolved layers that went beyond the limits of the hypotheses of our mathematical results. These

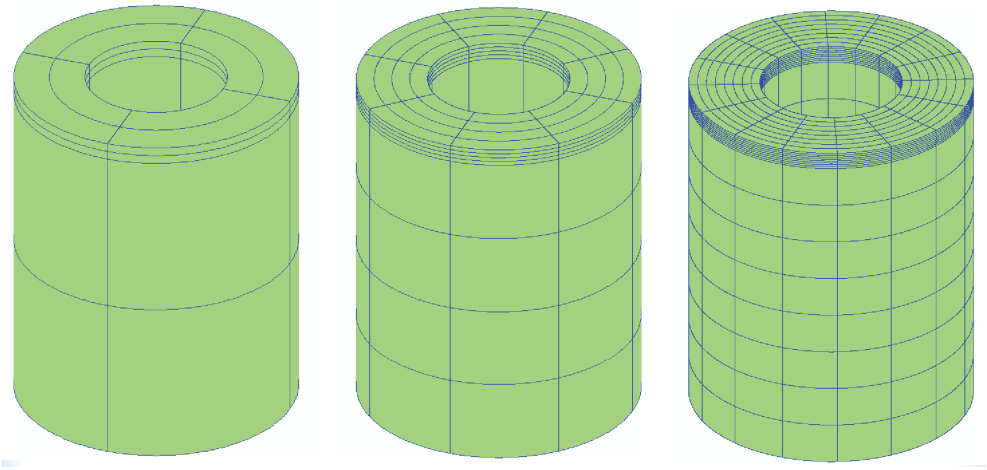

Figure 18: Advection-diffusion in a hollow cylinder. Meshes 1-3.

tests suggest that we have barely scratched the surface in that many other interesting mathematical properties, yet to be rigorously established, are possessed by Isogeometric Analysis.

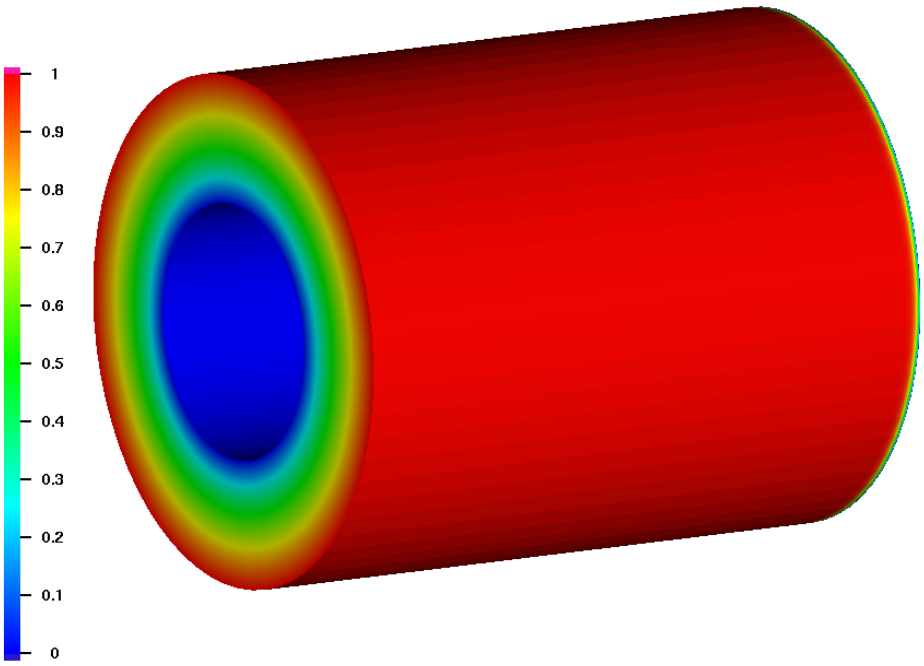

Solution on the whole domain

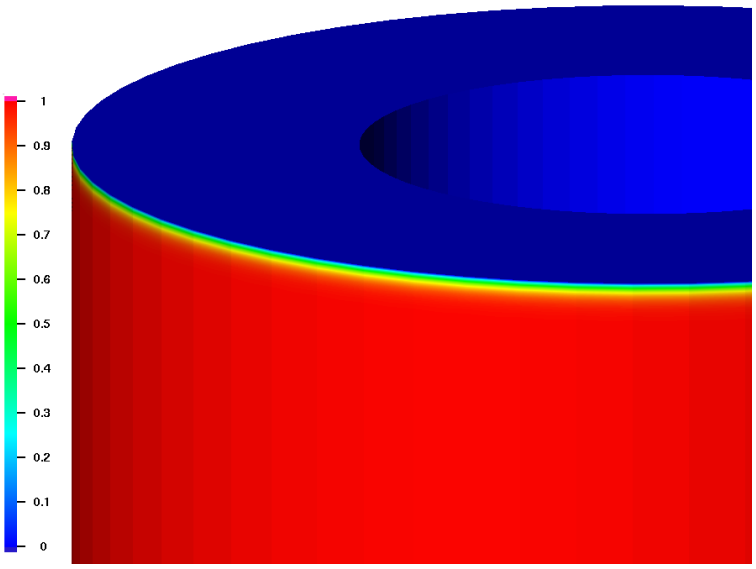

Zoom on the outflow boundary layer

Figure 19: Advection-diffusion in a hollow cylinder. Solution contours on the finest mesh, $\kappa = 0.025$.

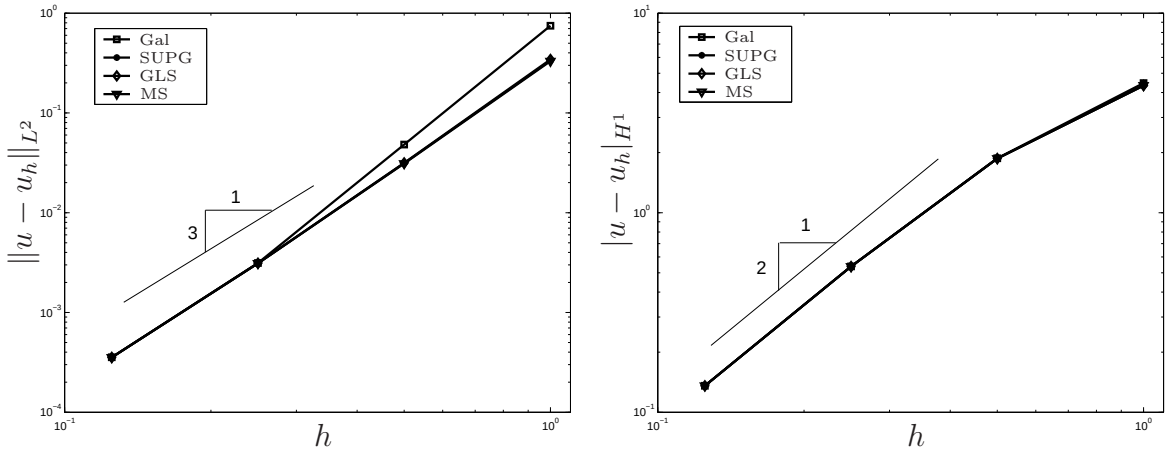

Figure 20: Advection-diffusion in a hollow cylinder, $\kappa = 0.025$. Convergence rates.

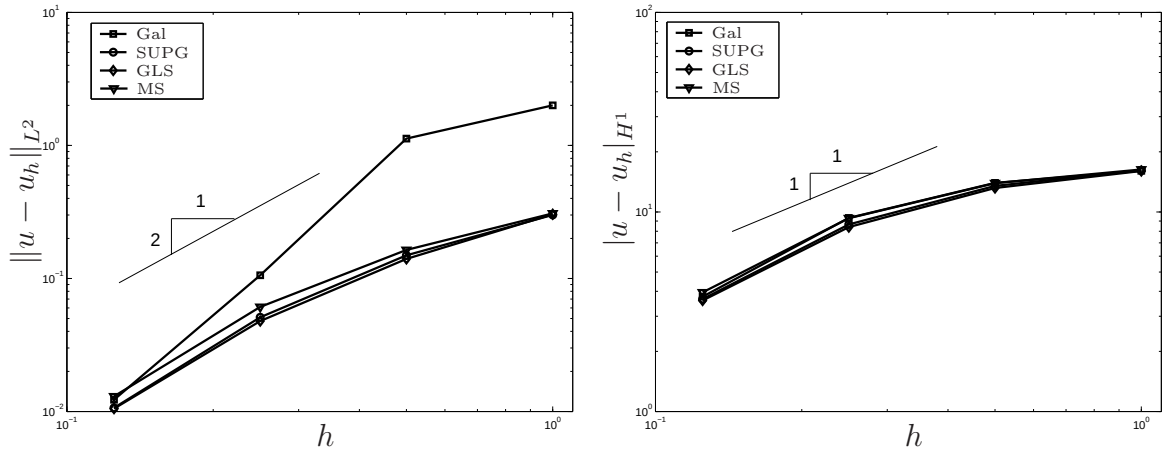

Figure 21: Advection-diffusion in a hollow cylinder, $\kappa = 0.00625$. Convergence rates.

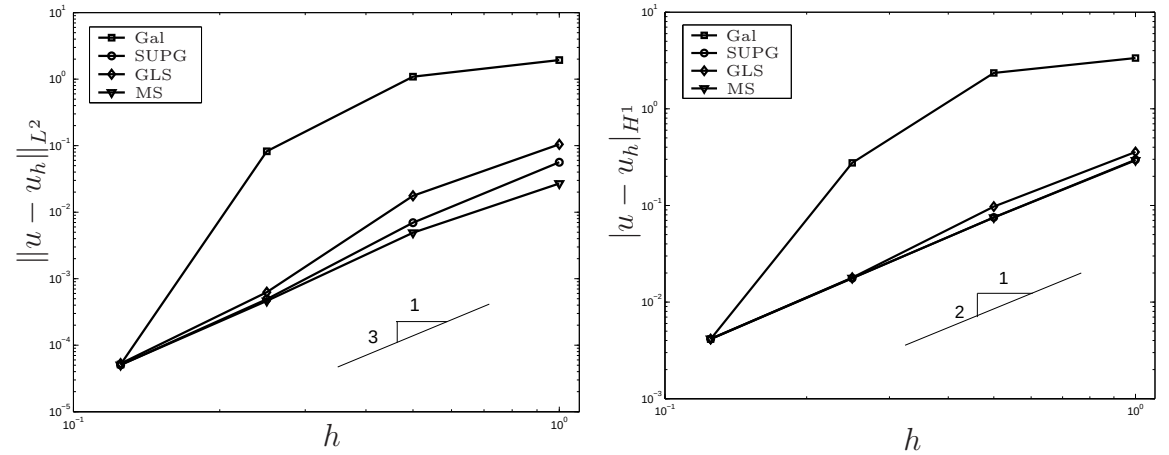

Figure 22: Advection-diffusion in a hollow cylinder, $\kappa = 0.00625$. Convergence rates outside of the boundary layer.

Acknowledgments

Y. Bazilevs, J.A. Cottrell and T.J.R. Hughes were partially supported by Office of Naval Research Contract N00014-03-0263, Dr. Luise Couchman, contract monitor. L. Beirão da Veiga and G. Sangalli were partially supported by the J.T. Oden Faculty Fellowship Research Program at the Institute for Computational Engineering and Sciences during a stay of residence, and by the PRIN 2004 project of the Italian MIUR. This support is gratefully acknowledged.

References

[1] R.A. Adams. *Sobolev Spaces*. Academic Press, New York, 1975.

[2] J. E. Akin and T. E. Tezduyar. Calculation of the advective limit of the SUPG stabilization parameter for linear and higher-order elements. *Computer Methods in Applied Mechanics and Engineering*, 193:1909–1922, 2004.

[3] D.N. Arnold, F. Brezzi, B. Cockburn, and L.D. Marini. Unified analysis of Discontinuous Galerkin methods for elliptic problems. *SIAM Journal of Numerical Analysis*, 39:1749–1779, 2002.

[4] F. Auricchio, L. Beirao da Veiga, C. Lovadina, and A. Reali. Triangular enhanced strain elements for plain linear elasticity. *Computer Methods in Applied Mechanics and Engineering*, to appear, 2005. Preprint IMATI-CNR.

[5] M. Bischoff and K.-U. Bletzinger. Improving stability and accuracy of Reissner-Mindlin plate finite elements via algebraic subgrid scale stabilization. *Computer Methods in Applied Mechanics and Engineering*, 193:1491–1516, 2004.

[6] P. B. Bochev, M. D. Gunzburger, and J. N. Shadid. On inf-sup stabilized finite element methods for transient problems. *Computer Methods in Applied Mechanics and Engineering*, 193:1471–1489, 2004.

[7] J.H. Bramble and S.R. Hilbert. Estimation of linear functionals on Sobolev spaces with application to Fourier transforms and spline interpolation. *SIAM Journal of Numerical Analysis*, 7:112–124, 1970.

[8] F. Brezzi and M. Fortin. *Mixed and Hybrid Finite Element Methods*. Springer-Verlag, Berlin, 1991.

[9] A. N. Brooks and T. J. R. Hughes. Streamline upwind / Petrov-Galerkin formulations for convection dominated flows with particular emphasis on the incompressible Navier-Stokes equations. *Computer Methods in Applied Mechanics and Engineering*, 32:199–259, 1982.

[10] E. Burman and P. Hansbo. Edge stabilization for Galerkin approximations of convection-diffusion-reaction problems. *Computer Methods in Applied Mechanics and Engineering*, 193:1437–1453, 2004.

[11] P.G. Ciarlet and P.A. Raviart. Interpolation theory over curved elements with applications to finite element methods. *Computer Methods in Applied Mechanics and Engineering*, 1:217–249, 1972.

[12] R. Codina and O. Soto. Approximation of the incompressible Navier-Stokes equations using orthogonal subscale stabilization and pressure segregation on anisotropic finite element meshes. *Computer Methods in Applied Mechanics and Engineering*, 193:1403–1419, 2004.

[13] J.A. Cottrell, A. Reali, Y. Bazilevs, and T.J.R. Hughes. Isogeometric analysis of structural vibrations. *Computer Methods in Applied Mechanics and Engineering*, 2005. In press.

[14] A. L. G. A. Coutinho, C. M. Diaz, J. L. D. Alvez, L. Landau, A. F. D. Loula, S. M. C. Malta, R. G. S. Castro, and E. L. M. Garcia. Stabilized methods and post-processing techniques for miscible displacements. *Computer Methods in Applied Mechanics and Engineering*, 193:1421–1436, 2004.

[15] J. Douglas and J. Wang. An absolutely stabilized finite element method for the Stokes problem. *Mathematics of Computation*, 52:495–508, 1989.

[16] G.E. Farin. *NURBS Curves and Surfaces: From Projective Geometry to Practical Use*. A. K. Peters, Ltd., Natick, MA, 1995.

[17] L. P. Franca, S. Frey, and T.J.R. Hughes. Stabilized finite element methods: I. Application to the advective-diffusive model. *Computer Methods in Applied Mechanics and Engineering*, 95:253–276, 1992.

[18] L.P. Franca and R. Stenberg. Error analysis of some galerkin least squares methods for the elasticity problem. *SIAM Journal of Numerical Analysis*, 28(6):1680–1697, 1991.

[19] P. L. Gould. *Introduction to Linear Elasticity*. Springer Verlag, Berlin, 1999.

[20] V. Gravemeier, W. A. Wall, and E. Ramm. A three-level finite element method for the instationary incompressible Navier-Stokes equations. *Computer Methods in Applied Mechanics and Engineering*, 193:1323–1366, 2004.

[21] I. Harari. Stability of semidiscrete formulations for parabolic problems at small time steps. *Computer Methods in Applied Mechanics and Engineering*, 193:1491–1516, 2004.

[22] G. Hauke and L. Valiño. Computing reactive flows with a field Monte Carlo formulation and multi-scale methods. *Computer Methods in Applied Mechanics and Engineering*, 193:1455–1470, 2004.

[23] T. J. R. Hughes. *The Finite Element Method: Linear Static and Dynamic Finite Element Analysis*. Dover Publications, Mineola, NY, 2000.

[24] T. J. R. Hughes, L. P. Franca, and M. Balestra. A new finite element formulation for fluid dynamics: V. A stable Petrov-Galerkin formulation of the Stokes problem accommodating equal-order interpolations. *Computer Methods in Applied Mechanics and Engineering*, 59:85–99, 1986.

[25] T.J.R. Hughes, J.A. Cottrell, and Y. Bazilevs. Isogeometric analysis: CAD, finite elements, NURBS, exact geometry, and mesh refinement. *Computer Methods in Applied Mechanics and Engineering*, 194:4135–4195, 2005.

[26] T.J.R. Hughes and L. P. Franca. A new finite element formulation for fluid dynamics: VII. The Stokes problem with various well-posed boundary conditions: Symmetric formulations that converge for all velocity/pressure spaces. *Computer Methods in Applied Mechanics and Engineering*, 65:85–96, 1987.

[27] C. Johnson, U. Nävert, and J. Pitkäranta. Finite element methods for linear hyperbolic problems. *Computer Methods in Applied Mechanics and Engineering*, 45:285–312, 1984.

[28] B. Koobus and C. Farhat. A variational multiscale method for the large eddy simulation of compressible turbulent flows on unstructured meshes – application to vortex shedding. *Computer Methods in Applied Mechanics and Engineering*, 193:1367–1383, 2004.

[29] Y. Maday, A.T. Patera, and E.M. Ronquist. The $P_N \times P_{N-2}$ method for the approximation of the Stokes problem. Technical report, Department of Mechanical Engineering, Massachusetts Institute of Technology, 1992.

[30] A. Masud and R. A. Khurram. A multiscale/stabilized finite element method for the advection-diffusion equation. *Computer Methods in Applied Mechanics and Engineering*, 193:1997–2018, 2004.

[31] J. T. Oden, I. Babuška, and C. E. Baumann. A discontinuous *hp* finite element method for diffusion problems. *Journal of Computational Physics*, 146:491–519, 1998.

[32] L. Piegl and W. Tiller. *The NURBS Book (Monographs in Visual Communication), 2nd ed.* Springer-Verlag, New York, 1997.

[33] D. F. Rogers. *An Introduction to NURBS With Historical Perspective.* Academic Press, San Diego, CA, 2001.

[34] L.L. Schumaker. *Spline Functions: Basic Theory.* Krieger, 1993.

[35] R. Stenberg. Error analysis of some finite element methods for the stokes problem. *Mathematics of Computation*, 54:495–508, 1990.

[36] R. Stenberg. A technique for analyzing finite element methods for viscous incompressible flow. *International Journal of Numerical Methods in Fluids*, 11:934–948, 1990.

[37] T. E. Tezduyar and S. Sathe. Enhanced-discretization space-time technique (EDSTT). *Computer Methods in Applied Mechanics and Engineering*, 193:1385–1401, 2004.

[38] R. Verfürth. Error estimates for a mixed finite element approximation of the Stokes problem. *RAIRO Anal. Numer.*, 18(175–182), 1984.

[39] L. B. Wahlbin. Local behavior in finite element methods. In P. G. Ciarlet and J. L. Lions, editors, *Finite Element Methods (Part 1)*, volume 2 of *Handbook of Numerical Analysis*, pages 353–522. North-Holland, 1991.